Integrated Heat Pump Thermal Storage and Power Cycle for CSP: Final Technical Report

Joshua D. McTigue,[1] Pau Farres-Antunez,[2] Alexander J. White,[2] Christos N. Markides,[3] Janna Martinek,[1] Jennie Jorgenson,[1] Ty Neises,[1] and Mark Mehos[1]

1 National Renewable Energy Laboratory
2 Cambridge University Engineering Department, UK
3 Clean Energy Processes (CEP) Laboratory, Department of Chemical Engineering, Imperial College London, UK

NREL is a national laboratory of the U.S. Department of Energy
Office of Energy Efficiency & Renewable Energy
Operated by the Alliance for Sustainable Energy, LLC

This report is available at no cost from the National Renewable Energy Laboratory (NREL) at www.nrel.gov/publications.

Contract No. DE-AC36-08GO28308

Technical Report
NREL/TP-5700-79806
March 2022

Integrated Heat Pump Thermal Storage and Power Cycle for CSP: Final Technical Report

Joshua D. McTigue,[1] Pau Farres-Antunez,[2] Alexander J. White,[2] Christos N. Markides,[3] Janna Martinek,[1] Jennie Jorgenson,[1] Ty Neises,[1] and Mark Mehos[1]

1 National Renewable Energy Laboratory
2 Cambridge University Engineering Department, UK
3 Clean Energy Processes (CEP) Laboratory, Department of Chemical Engineering, Imperial College London, UK

Suggested Citation
McTigue, Joshua D., Pau Farres-Antunez, Alexander J. White, Christos N. Markides, Janna Martinek, Jennie Jorgenson, Ty Neises, and Mark Mehos. 2022. *Integrated Heat Pump Thermal Storage and Power Cycle for CSP: Final Technical Report*. Golden, CO: National Renewable Energy Laboratory. NREL/TP-5700-79806.
https://www.nrel.gov/docs/fy22osti/79806.pdf

NREL is a national laboratory of the U.S. Department of Energy
Office of Energy Efficiency & Renewable Energy
Operated by the Alliance for Sustainable Energy, LLC

This report is available at no cost from the National Renewable Energy Laboratory (NREL) at www.nrel.gov/publications.

Contract No. DE-AC36-08GO28308

Technical Report
NREL/TP-5700-79806
March 2022

National Renewable Energy Laboratory
15013 Denver West Parkway
Golden, CO 80401
303-275-3000 • www.nrel.gov

NOTICE

This work was authored in part by the National Renewable Energy Laboratory, operated by Alliance for Sustainable Energy, LLC, for the U.S. Department of Energy (DOE) under Contract No. DE-AC36-08GO28308. Funding provided by U.S. Department of Energy Office of Energy Efficiency and Renewable Energy Solar Energy Technologies Office. The views expressed herein do not necessarily represent the views of the DOE or the U.S. Government.

FINAL TECHNICAL REPORT

Project Title:	Integrated Heat Pump Thermal Storage and Power Cycle for CSP
Project Period:	(10/01/18–09/30/20)
Budget Period:	(10/01/19–09/30/20)
Reporting Period:	(10/01/18–09/30/20)
Reporting Frequency:	Annual
Submission Date:	(12/31/20)
Recipient:	National Renewable Energy Laboratory (NREL)
Address:	15013 Denver West Parkway
	Golden, CO 80401
Website (if available)	www.nrel.gov
Award Number:	#34243
Project Team:	NREL (Cambridge University; Imperial College, London)
Principal Investigator:	Dr. Joshua McTigue
	Phone: 303-275-4682
	Email: JoshuaDominic.McTigue@nrel.gov
Business Contact:	Mark Mehos
	Phone: 303-384-7458
	Email: Mark.Mehos@nrel.gov
HQ Tech Manager:	Matthew Bauer
HQ Project Officer:	Christine Bing
GO Grant Specialist:	N/A
GO Contracting Officer:	N/A

Signature

12/31/2020

Date

Executive Summary

Pumped thermal energy storage (PTES) is a storage system that stores electricity in thermal reservoirs. In this project, methods of integrating PTES with concentrating solar power (CSP) systems were investigated and their feasibility evaluated. Hybrid "solar-PTES" devices can provide both flexible renewable power generation as well as a variety of electricity storage services.

Techno-economic models of PTES and solar-PTES were developed and used to assess their performance, cost, and commercial viability. Systems were optimized using multi-objective optimization techniques. The value that these storage devices provide to the grid was estimated using production cost modeling.

Key advances made in this project include the development of detailed techno-economic models that improve state-of-the-art assessments of these technologies. Off-design models were developed and used in grid-analysis models. This work describes for the first time how PTES and solar-PTES behave over a range of operating points and assesses the value that these systems can provide to the electrical grid. Feedback was obtained from experts in the field, which clarified key technological and economic barriers that must be addressed to improve the feasibility of these devices.

Several PTES and solar-PTES systems were investigated, using a variety of power cycles, working fluids, and storage fluids. The main technologies discussed in this report are (1) a PTES system that uses an ideal-gas Joule-Brayton cycle with nitrate molten salt storage (2) a solar-PTES system where an existing CSP plant is retrofitted with a Joule-Brayton heat pump that can "top up" the shared molten salt storage. Other cycles that use supercritical CO_2 are also discussed and evaluated.

Simple thermodynamic models were first developed of a variety of PTES and solar-PTES concepts. Results were used to determine which systems were the most promising and merited further research. More detailed techno-economic models were then built. The technical models captured the performance of each component in the system. In particular, quality representations of heat exchangers were required, and the models were successfully validated against experimental results taken from the literature. The off-design performance of each component was modeled which enabled evaluation of PTES and solar-PTES performance at variable part load and ambient temperature. The system capital cost and levelized cost of storage (LCOS) were estimated by obtaining cost correlations for each component from the literature. Several correlations were used for each component, which enabled the use of a Monte-Carlo technique to calculate the likely cost and its uncertainty. This analysis emphasized the importance of heat exchanger design on the system performance, and high values of effectiveness (over 90%) are required to achieve reasonable round-trip efficiencies. It was found that this high effectiveness also minimized the lifetime cost (LCOS).

The techno-economic models were integrated with a stochastic multi-objective optimization algorithm that was used to find optimal trade-off surfaces between performance and cost. A "multi-fidelity" modeling methodology was employed to improve the computational runtime of the optimizations. Optimization studies revealed that there were limited benefits to operating

PTES at temperatures over 600°C due to the increased material costs in heat exchangers. PTES using nitrate molten salts as the hot storage fluid can reach round-trip efficiencies over 65% at high cost. Round-trip efficiencies of 62% can be obtained without increasing the LCOS significantly above its minimum value of 0.126±0.03 $/kWh$_e$. Similarly, solar-PTES systems can reach maximum round-trip efficiencies of 62%, but values of 58% can be obtained without increasing the LCOS significantly above its minimum value of 0.11±0.03 $/kWh$_e$.

The off-design models were used to develop simple, but realistic, representations of PTES and solar-PTES that could be integrated with a grid analysis model. Off-design models are necessary to capture the unique features of PTES-type systems as they operate over a range of operational points. It was found that PTES can operate down to 40% part-load without significantly compromising the round-trip efficiency.

A production cost model was implemented, and it optimizes the running cost of an electrical grid with many generation and demand nodes. Adding PTES or solar-PTES to the grid changes the running cost, and a reduction in cost can be interpreted as the *value* that these systems provide. The value of PTES and solar-PTES were investigated under various renewable penetration scenarios in California and Texas. This value was compared to the system cost calculated by the techno-economic model, and a simple pay-back period was estimated.

Pay-back periods for PTES and solar-PTES were found to be long, but could be reduced to more reasonable values (<25 years) by increasing renewable penetration and reducing capital costs. Several other value streams are not included, such as the value derived from providing grid inertia and capacity, and future work should evaluate these factors which will further reduce pay-back periods.

The solar-PTES system was compared to a CSP plant which could use an electrical heater to charge the molten salt storage instead of a heat pump. This system is considerably less efficient than the heat pump system, with round-trip efficiencies of ~40%. However, it is also cheaper and less complex to implement. As a result, payback periods could be around 5-10 years, and this variation may provide the simplest route to demonstrate solar-PTES-type technology. Using electric heaters or heat pumps to charge thermal storage for use in thermal power plants also has interesting applications in retiring fossil fuel plants.

Table of Contents

1 Background

This report concerns an energy storage device known as Pumped Thermal Energy Storage (PTES), and its integration with Concentrating Solar Power (CSP) systems. PTES is a system that allows electrical power to be stored as thermal energy, and later dispatched as electricity [1]. The use of reversible heat pump/power cycle provides relatively high round-trip efficiency. PTES has been investigated (under a variety of names) at research centers globally. However, the field is still relatively new and there is considerable scope for the development of improved designs and novel ideas. While detailed papers on PTES systems have appeared in the literature since the late 2010s, PTES has been re-invented several times since 1924 when one variation was first patented. Subsequently there has been commercial interest from several companies, including ABB, Isentropic Ltd. (whose prototype resides at Newcastle University, UK), Highview Power (who have developed a variation known as Liquid Air Energy Storage), Bright Energy Storage, Echogen Power Systems, Malta, Siemens Gamesa, and WindTP.

The fundamental concept behind PTES is to create a temperature difference between two reservoirs using a heat pump, and then later exploit this temperature difference using a heat engine. Researchers have investigated a range of different power cycles including Joule-Brayton cycles using an ideal gas [2,3], transcritical-CO_2 (t-CO_2) cycles [4], supercritical-CO_2 (s-CO_2) cycles [5], and steam-based cycles [6]. Different cycles typically require different storage media, working fluids and recuperation. For instance, Joule-Brayton cycles typically use air or argon as the working fluid, and store thermal energy in packed pebble-beds [7–9], concrete stores [10], or in liquid tanks (such as molten salts) [11]. Supercritical cycles have a similar shape on the temperature-entropy diagram, and therefore use similar storage media [12], although the working fluid is generally carbon dioxide. Transcritical cycles have a phase change in the cold store, so phase change materials or ice slurries [4,13] are commonly used, while the working fluid may be carbon dioxide, ammonia [14] or steam [6].

If both the heat pump and heat engine obey the Carnot limits then the round-trip efficiency (net work out during discharge divided by net work in during charge) is 100% [15]. However, irreversibilities in the system mean that this is not achievable, and estimates for the round-trip efficiency fall in the region of 40-80% depending on the operating conditions [3]. A lower limit to the round-trip efficiency may be estimated by assuming the heat pump is replaced with an electrical heater, which converts heat directly into electricity and has a Coefficient of Performance (COP) of 1. The stored heat is then converted back into electricity in a conventional heat engine. The round-trip efficiency is then given by the efficiency of the heat engine, which for a conventional steam turbine cycle is around 40%. Using a heat pump increases the round-trip efficiency by a "multiplier" that is effectively equal to the COP.

Recent advances relating to PTES in the literature and industry are occurring in two areas:

1. Integrating PTES with other energy systems
2. Using an electrical resistance heater instead of the heat pump to reduce costs

More recent advances have considered integrating the PTES system into other energy sources, including gas-turbine exhausts [16], waste heat systems [17], and wind turbines [18]. These energy systems provide alternative (and potentially cheap) sources of heat that can be used to charge the thermal storage. Retrofitting an existing thermal power plant with a heat pump and thermal stores was investigated in a study by Vinnemeier et al. [19]. The resulting hybrid plant is able to operate using either the original heat source (e.g., a fossil fuel) or the heat generated by the heat pump during periods of off-peak electrical demand. If the purchased electricity comes from renewable sources, such hybrid plants would represent a cost-effective way to reduce carbon emissions while ensuring security of supply. A similar concept is being developed at the DLR which proposes that existing coal plants are retrofitted with a heat pump and molten salt thermal storage. Heat can then be dispatched through the existing steam turbine. If the existing coal combustion chamber is retained, then the plant would be able to dispatch flexibly and at high availability.

Another area that is gaining traction is to use an electrical resistance heater to charge the hot storage. This has been recently demonstrated by Siemens Gamesa in Hamburg, Germany[1]. Air is heated with a resistance heater, and then travels through a packed bed at 750°C. Later, air is re-heated in the packed bed, and then transfers its heat to steam which drives a steam turbine. Siemens Gamesa predict a round-trip efficiency of 45% once the system has been scaled up. While this is lower than PTES systems with a heat pump, the system has the advantage of using fewer components (no cold storage) and commercialized technologies.

Benato et al. proposed a PTES system that is supplemented with an electric heater [20]. Extra heat is added in the charging phase after the compression stage. The heat pump compression is a potentially challenging area in PTES development as the compressor inlet is at higher temperatures than conventional systems. Using an electrical heater is a simple way to increase the maximum temperature of the system without developing new compressor technology. Benato et al.'s system could also be considered for solar-PTES concepts, except with the solar heat instead of electrical heat. However, this system achieved a very low round-trip efficiency of ~9%. This was a combination of reducing the heat pump COP and also not capturing and exploiting all the available heat in discharge (heat was rejected at quite high temperatures). A similar concept was explored early in the project, and a bottoming Organic Rankine Cycle (ORC) captured the waste heat. This system achieved round-trip efficiencies of 53% and is relatively complex, so has not been explored further.

Electric heater charging systems provide an interesting alternative to heat pump systems. They are relatively simple to model and should be considered along with PTES devices to investigate whether cheaper, simpler approaches can justify lower round-trip efficiencies.

[1] https://www.siemensgamesa.com/en-int/newsroom/2019/06/190612-siemens-gamesa-inauguration-energy-system-thermal [Accessed July 13, 2019]

2 Introduction

This final report describes progress made over two years for a project titled "Integrated heat pump thermal storage and power cycle for CSP". A novel electricity storage device, known under various names such as Pumped Thermal Electricity Storage (PTES), Pumped Heat Electricity Storage (PHES), and Carnot Batteries, uses a heat pump to convert grid electricity into a thermal potential. Energy is stored in hot and cold storage media and can be converted back into electricity using a heat engine. PTES has advantages over other bulk electricity storage systems, such as lithium-ion batteries, pumped-hydro and compressed air energy storage, because it has no geographical restrictions and potentially makes use of cheap, sustainable materials.

PTES involves various flows of heat and electricity, which enable it to integrate with other energy systems. This project focuses on methods of integrating PTES with concentrating solar power (CSP) systems [21], henceforth known as "solar-PTES" devices. The objective of this project is to develop technologies that enable the highly efficient, reliable dispatch of solar energy. This project involves the invention of new power cycles and storage systems, thermo-economic analysis of these systems, and an analysis of integration with the electrical grid.

The objective of this project is to assess the commercial viability of a solar-PTES system. We aim to demonstrate scenarios where solar-PTES provides greater value than CSP with storage. The following milestones were developed to facilitate the technical path to achieve this goal:

Milestone 1: Develop solar-PTES concepts and simple thermodynamic models based on energy balances and system analysis.

Milestone 2: Develop component cost correlations

Milestone 3: Calculate the expected range of net-values that solar-PTES will provide to the grid.

Milestone 4: Generate detailed, transient (time-stepping) thermal storage and power cycle models to minimize exergy losses.

Milestone 5: Optimize system design with respect to efficiency and cost.

Milestone 6: Improve solar-PTES models that can be used in grid analysis models.

Milestone 7: Assess net value of PTES and solar-PTES by undertaking grid analysis studies using updated system performance curves and cost correlations.

Milestone 8: Assess the commercial viability of solar-PTES concept.

Work was divided into four tasks which will be described in detail in this report. The requirements of each milestone, and the progress towards its completion, will be discussed more fully under the relevant sections.

3 Public Output Arising From This Project

Several journal articles, book chapters, conference papers and presentations were produced as a result of this project:

Journal articles:

[1] J. D. McTigue, P. Farres-Antunez, K. Sundarnath, C. N. Markides, A. J. White, "Techno-economic analysis of recuperated Joule-Brayton pumped thermal energy storage systems", *Energy Conversion & Management*, vol. 252, 115016, 2022 (link)

[2] A. Olympios, J. D. McTigue, P. Farres-Antunez, A. Romagnoli, W-D. Steinmann, A. Thess, L. Wang. H. Chen, Y. Li, Y. Ding, C. Markides, "Progress and prospects of thermo-mechanical energy storage – a critical review," *IOP Progress in Energy*, Vol. 3, 022001, 2021 (link)

[3] J. Martinek, J. Jorgenson, J. D. McTigue, "On the operational characteristics and economic value of pumped thermal energy storage," manuscript submitted to *Journal of Energy Storage*

[4] P. Farres-Antunez, A. J. White, C. Markides, J. D. McTigue, "Energy storage in steam power plants retrofitted with Brayton heat pumps," manuscript in preparation

Book chapters:

[5] S. Freund, M. Abarr, J. D. McTigue, K. Frick, A. Mathur, D. Reindl, A. van Asselt, "Thermal Energy Storage" chapter for the book *Thermal, Mechanical, and Hybrid Chemical Energy Storage Systems*, edited by K. Brun, T. Allison, R. Dennis. Elsevier, 2020 (link)

[6] J. Moore et al., "Heat engine based storage systems," chapter for the book *Thermal, Mechanical, and Hybrid Chemical Energy Storage Systems*, edited by K. Brun, T. Allison, R. Dennis. Elsevier, 2020 (link)

[7] J. D. McTigue, P. Farres-Antunez, C. N. Markides, A. J. White, "Integration of heat pumps with solar thermal systems for energy storage", chapter in *Encyclopedia of Energy Storage,* Elsevier, 2022 (link)

[8] J. D. McTigue, P. Farres-Antunez, C. N. Markides, A. J. White, "Pumped thermal energy storage with liquid storage", chapter in *Encyclopedia of Energy Storage,* Elsevier, 2021 (link)

[9] A. V. Olympios, J. D. McTigue, P. Sapin, C. N. Markides, "Pumped-thermal electricity storage based on Brayton cycles", chapter in *Encyclopedia of Energy Storage,* Elsevier, 2021 (link)

[10] P. Farres-Antunez, J. D. McTigue, R. Morgan, A. J. White, "Integrated Pumped Thermal and Liquid Air Energy Storage", chapter in *Encyclopedia of Energy Storage,* Elsevier, 2022 (link)

Conference papers:

[11] J. D. McTigue, P. Farres-Antunez, T. Neises, A. J. White, "Supercritical CO_2 heat pumps and power cycles for concentrating solar power," SolarPACES conference, virtual conference, October 2020 (link)

[12] J. D. McTigue, P. Farres-Antunez, K. Ellingwood, T. Neises, A. J. White, "Pumped Thermal Electricity Storage with Supercritical CO_2 Cycles and Solar Heat Input," SolarPACES conference, Daegu, South Korea, October 2019 (link, OSTI)

[13] P. Farres-Antunez, J. D. McTigue, A. J. White, "A pumped thermal energy storage cycle with capacity for concentrated solar power integration," Offshore Energy and Storage Summit, Brest, France, July 2019 (link, OSTI)

Presentations[2]:

[14] J. D. McTigue, P. Farres-Antunez, A. J. White, "Pumped Thermal Energy Storage: Thermodynamics and Economics," Concentrating Solar-Thermal Power Research and Development Virtual Workshop Series: Pumped Thermal Energy Storage Innovations, 17 November 2020 (link, OSTI)

[15] P. Farres-Antunez, J. D. McTigue, A. J. White, "High performance Carnot Batteries based on hybrid cycles," International Workshop on Carnot Batteries, Virtual (Germany), September 2020

[16] J. D. McTigue, "Carnot Batteries for electricity storage," Yale Center for Business and the Environment BluePrint Webinars, Webinar, December 2019, (link, OSTI)

[17] J. D. McTigue, P. Farres-Antunez, A. J. White, "Techno-economic modelling of pumped thermal electricity storage," ASME Energy Sustainability, Virtual (USA), June 2019

[18] J. D. McTigue, P. Farres-Antunez, A. J. White, "Integrating pumped thermal electricity storage (PTES) with a concentrating solar power plant," ASME Energy Sustainability, Bellevue, Washington, USA, July 2019

[19] J.D. McTigue, "Integrated heat pump thermal storage and power cycle for CSP," SETO CSP Program Summit, Oakland, California, March 2019

Posters:

[20] J.D. McTigue, T. Neises, P. Farres-Antunez, A. J. White, "Integrating pumped thermal energy storage with concentrating solar power," SolarPACES conference, virtual conference, October 2020

[21] J. D. McTigue, "Integrated heat pump thermal storage and power cycle for CSP," SETO Program Summit, February 2020

[22] J. D. McTigue, "Integrated heat pump thermal storage and power cycle for CSP," SETO CSP Program Summit, Oakland, California, March 2019

Other activities:

[23] Antoine Koen, Pau Farres-Antunez, "How heat can be used to store renewable energy," *The Conversation*, February 2020 (link)

[24] Contributions to the International Energy Agency (IEA) Annex 36 on Carnot Batteries.

[25] Committee member for the 1st and 2nd Thermo-Mechanical-Chemical Electricity Storage Workshops, held at Southwest Research Institute, Texas in January 2019 and Pittsburg, February 2020

[2] The conference papers listed above also had presentations associated with them.

Software:

[26] J. D. McTigue, P. Farres-Antunez, “Solar-PTES Software Project,” National Renewable Energy Laboratory, 2020 https://github.com/NREL/solar-PTES

4 Project Team Members

National Renewable Energy Laboratory, USA: Josh McTigue, Janna Martinek, Jennie Jorgenson, Ty Neises, Craig Turchi, Guangdong Zhu, Mark Mehos, Kevin Ellingwood, Jason Schirck, Kavin Sundarnath

University of Cambridge, UK: Pau Farres-Antunez, Alexander White

Imperial College, London, UK: Christos N. Markides

5 Project Results and Discussion

5.1 Task 1: Simplified Thermodynamic Analysis of Solar-PTES System

The objective of Task 1 was to develop preliminary solar-PTES concepts that achieve high net efficiencies and have simple system designs. The design space of potential cycles is effectively infinite, so the aim of this task was to reduce the size of this space so that future work can concentrate on the most promising designs. Simple thermodynamic models were developed and capture the influence of the most important parameters on the system performance. This approach allowed a range of cycles to be evaluated relatively quickly.

A wide variety of concepts and system configurations were explored, and included a range of working fluids such as CO_2, steam, ammonia, air, and argon. Cycles considered included Joule-Brayton cycles, (sub-critical) Rankine cycles, supercritical cycles, and transcritical cycles (or supercritical Rankine cycles). Several of the most promising candidates are discussed in this section.

Solar-PTES may be used for different applications and operate in different markets. Three broad categories are defined as:

1. Stand-alone PTES: These are storage systems that provide energy storage services by exchanging electricity with the grid and have no solar heat input
2. CSP retrofitted with PTES: These are CSP power cycles that have additional components added to them which enable the storage of electricity. The stored energy is then dispatched through the original CSP equipment. These are electricity storage devices, although the heat pump may be able to improve the dispatch of solar energy.
3. Integrated solar-PTES: These systems provide both electricity storage and generation services. A heat pump takes electricity from the grid and creates hot and/or cold thermal stores, and solar heat is also stored. This heat is dispatched through a heat engine that can combine the different thermal stores.

Each category of solar-PTES should be evaluated with appropriate metrics. Categories 1 and 2 are primarily electricity storage devices, and the round-trip efficiency is a suitable metric:

$$\eta_{rt} = \frac{\dot{W}_{\text{dis}}^{\text{net}}}{\dot{W}_{\text{chg}}^{\text{net}}} \tag{1}$$

Where, $\dot{W}_{\text{dis}}^{\text{net}}$ is the net work output in discharge, and $\dot{W}_{\text{chg}}^{\text{net}}$ is the net work input during charge.

In some concepts, electricity may be stored in thermal storage, and then upgraded with solar heat before being converted back to electricity. In this case, the additional energy input from the solar heat leads to round-trip efficiencies (as defined above) greater than 100%. This is somewhat misleading, and the metric can be improved by considering the maximum work that could be extracted from the solar heat. The exergetic round-trip efficiency $\eta_{rt,x}$ of a solar-PTES device is given by:

$$\eta_{rt,x} = \frac{\dot{W}_{\text{dis}}^{\text{net}}}{\dot{W}_{\text{chg}}^{\text{net}} + \Delta\text{Ex}_{\text{solar}}} \tag{2}$$

where $\Delta\text{Ex}_{\text{solar}} = \dot{m}\left(h_{in} - h_{out} - T_o(s_{in} - s_{out})\right)$ is the maximum work that could be extracted from the solar heat input.

For category 3 concepts, the system performance can be evaluated by considering that the conventional use of solar heat is to generate work in a heat engine. Solar-PTES systems use grid electricity to charge one or more storage units. From a thermodynamic perspective, to be competitive with power generation technologies, the solar-PTES system should provide more electricity to the grid than it consumes in charging. Solar-PTES can be compared to the equivalent solar heat engine with the net efficiency η_{net}:

$$\eta_{\text{net}} = \frac{\dot{W}_{\text{dis}}^{\text{net}} - \dot{W}_{\text{chg}}^{\text{net}}}{\dot{Q}_{\text{solar}}} \tag{3}$$

where $\dot{Q}_{\text{solar}}$ is the solar heat added to the system. However, it should also be considered that these systems provide additional advantages. Firstly, they can take excess electricity off the grid if required. Secondly, the stored energy is used to improve the performance of the discharging heat engine. Therefore, the discharging heat engine is more efficient than a conventional solar heat engine – i.e., for a unit of solar heat, a larger quantity of work (electricity) is dispatched to the grid when it is needed. This is important, because even if a solar-PTES system has a lower net efficiency than a conventional CSP plant, it may still be able to provide a larger quantity of power to the grid *when it is required and valuable* for a given solar field size. Thus, category 3 systems should not be evaluated on the basis of the net efficiency alone as it does not account for the electricity storage services provided, or the high availability and dispatchability of these solar-PTES systems.

In Task 1 it was assumed that all compressors and expanders have isentropic efficiencies of 90%, and that there is no heat loss from storage systems. Each heat exchanger incurs a 1% pressure loss, and a temperature difference is assumed to occur between the two fluids. This temperature difference is at least 5°C, but in some cases may be increased to facilitate heat transfer. The modeling methodology was substantially improved under Task 3.

Results for several interesting and promising cycles are now presented.

5.1.1 Stand-Alone PTES Systems

These systems are electricity storage devices that typically use a heat pump to convert electricity into a temperature difference, thereby creating hot storage and cold storage. To discharge the system, the cycle is reversed and a heat engine is run between the thermal potential. While these systems do not make use of solar mirror technology, they may leverage advances in hot thermal storage systems that have been developed by the CSP industry. Several power cycles are available:

5.1.1.1 Joule-Brayton Cycles

This cycle is similar to that in Ref. [12] and currently being developed by Malta Inc. It is a recuperated Joule-Brayton cycle using air as the working fluid, see Figure 1. During charge, air is first compressed from 278˚C (1) to 565˚C (2) through a pressure ratio of 4. The low-pressure is taken as 25 bar, following Ref. [22], in order to reduce the size of the machinery. Molten salts are used for the hot store, which cools the working fluid down to 278˚C (3). The hot working fluid enters the hot side of a recuperator and is cooled to ambient temperatures (4), at which point it is expanded to -71˚C (5). Methanol is used as the cold storage fluid which transfers heat to the power cycle fluid, warming it back to ambient temperature (6). The power cycle fluid is then heated up to the compressor inlet temperature in the cold side of the recuperator (1).

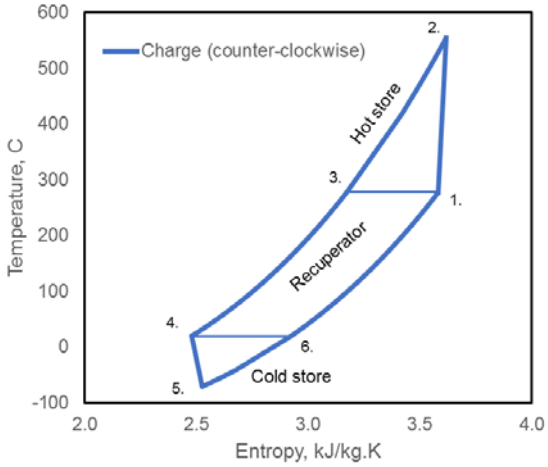

Figure 1: Recuperated air Joule-Brayton PTES cycle.

This cycle has a round-trip efficiency of 64.9% and requires an air mass flow rate of 66.8 kg/s to produce a net power output of 10 MW_e during discharge.

5.1.1.2 sCO_2 Cycles

The layout of this cycle is similar to the air Joule-Brayton cycle. However, the recuperator is removed due to the large density and heat capacity variations that CO_2 exhibits near the critical point. The hot storage temperature affects the choice of storage fluid. Three variations are considered, with hot store temperatures of 212˚C, 388˚C and 503˚C chosen to illustrate the concept. The lowest temperature and highest temperature options are shown in Figure 2.

The low-temperature option compresses sCO_2 from 100˚C (1) to 212˚C (2). These low temperatures enable the use of mineral oil for the hot storage and water for the cold storage. This cycle has a similar round-trip efficiency to the Joule-Brayton cycle. Despite the relatively cheap storage media, the low temperatures lead to low specific work outputs. Furthermore, larger stores are required for a given energy capacity because the temperature difference between the stores is low.

Increasing the hot storage temperature increases the specific work output, reduces the mass flow rates and reduces storage volumes. The round-trip efficiency also increases. However, as

indicated by Figure 2b, higher temperature cycles are more complicated. In this case, the hot store inlet temperature is 503˚C (too high for mineral oils) and the outlet temperature is 30˚C (too low for molten salts). Therefore, two different storage materials are required for the hot storage system. This doubles the number of hot heat exchangers and storage vessels. The "cold" storage is also relatively hot, and thus requires the use of a mineral oil. However, the round-trip efficiency is 12% points greater than the ideal-gas Joule-Brayton cycle, see Table 1.

These results appear to be very promising. However, the simple modeling methodology is inadequate to properly assess these systems since it is challenging to achieve the very good heat transfer needed. The improved methodology in Section 5.3 indicates that sCO_2-PTES systems will have lower efficiencies than ideal-gas PTES systems.

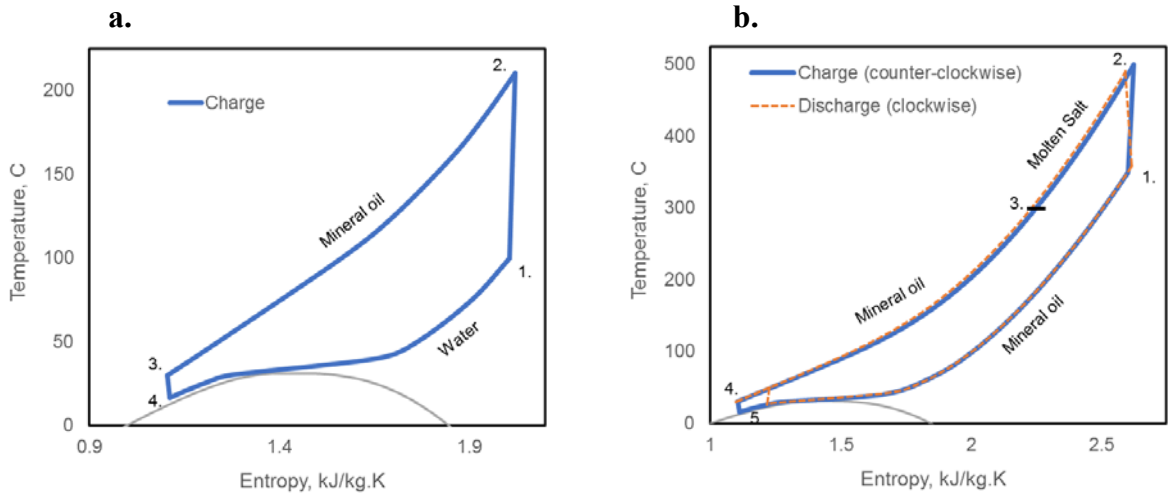

Figure 2: Temperature-entropy diagrams for sCO_2 based PTES cycles. (a) Low-temperature hot store enables the use of water for the cold store. (b) High-temperature hot storage requires two hot storage materials, and a more expensive cold store.

Table 1: Performance of Several Stand-Alone PTES Systems

	Round-trip efficiency, %	Specific discharge net work, kJ/kg	Mass flow rate, kg/s
Ideal Joule-Brayton-TT	64.9	149.7	66.8
Low-temp sCO_2	63.0	41.9	238.7
Mid-temp sCO_2	73.4	86.6	115.5
High-temp sCO_2	77.0	113.4	88.2

5.1.1.3 Electric Heater Based Systems

The heat pump in the above systems may be replaced with an electrical resistive heater which is used to charge the hot storage. Such a system is potentially more cost effective as the charging turbomachinery and generator is removed, as is the cold storage. Furthermore, a conventional heat engine (such as a steam turbine, or combined cycle gas turbine (CCGT)) can be used to dispatch the heat. One concept recently deployed by Siemens Gamesa uses electricity to heat air which then heats up packed bed of rocks to 750°C. To discharge, heat is transferred back into the

air, which then generates steam and drives a steam turbine. Siemens Gamesa project a round-trip efficiency of 45% once the technology is scaled up.

Electric heater systems achieve lower costs at the expense of performance. Electric heaters convert work directly into heat; thus, the coefficient of performance is 1. Additionally, a cold store is not created, meaning that the round-trip efficiency of an electric heater based system is lower than a heat pump based system, as illustrated in Figure 3. Further work is required to establish the operational characteristics of electric heaters. Factors such as power ratings, cost, and compatibility with storage materials should be explored.

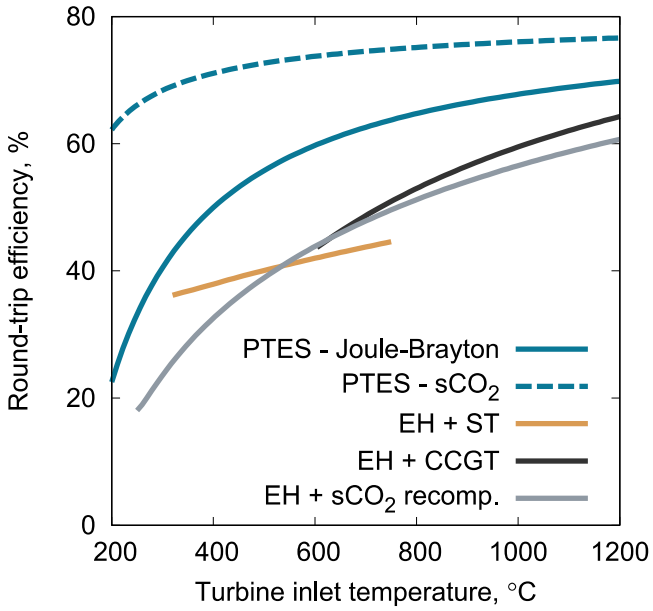

Figure 3: Comparison of heat pump thermal storage systems with electric heater-based storage as a function of turbine inlet temperature. ST: steam turbine. CCGT: combined cycle gas turbine. EH: electric heater.

5.1.2 Solar-PTES Retrofit

In this section, various options for retrofitting a CSP power cycle with a heat pump are explored. The heat pump provides electricity storage services, and in some cases may improve the efficiency at which solar heat is converted to electricity.

5.1.2.1 Joule-Brayton Heat Pump With a Steam Turbine

A conventional CSP system that uses a steam cycle and molten salt storage is retrofitted with a Joule-Brayton heat pump, as shown in Figure 4. The ability to charge the hot storage with a heat pump means that the power cycle is independent of the solar resource, and that electricity can be dispatched year-round (if the storage has been charged at some point). For a CSP retrofit the only additional components required are the machinery for the charging compression and expansion, and a cold storage tank. This may be a relatively cost-effective way to demonstrate PTES technology.

The heat pump cycle creates sub-ambient temperatures after the expansion which can either be stored in a cold store or heated up with the environment or an electrical heater. The cold store could be used in the heat rejection system of the discharging cycle and therefore improve the efficiency and protect against detrimental variations in ambient temperature. Suitable cold storage materials include water/ice, glycol or methanol.

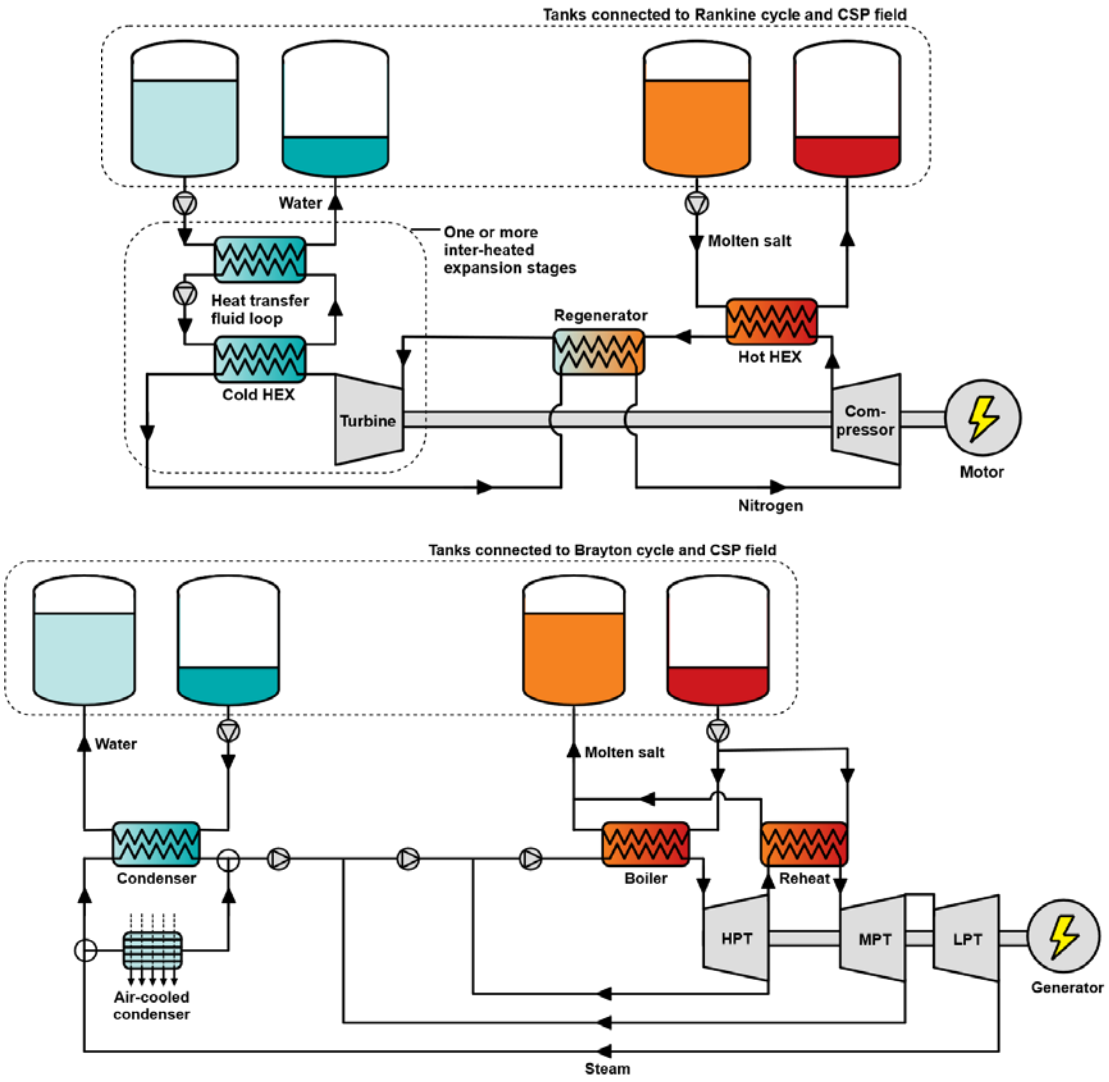

Figure 4: Schematic diagram illustrating how an existing CSP steam cycle with storage may be retrofitted with a Joule-Brayton heat pump. The top figure shows the charging heat pump which creates hot and cold storage which are shared with the discharging steam cycle, shown in the bottom figure.

A Joule-Brayton cycle with an ideal gas is the most suitable power cycle choice for the heat pump, as large temperature ratios can be achieved with modest pressure ratios in the compressor. The number of expansion stages were varied, with inter-stage heating occurring between each expansion stage, as shown in Figure 5 (the inter-stage heating is provided by the cold storage). Increasing the number of expansion stages increases the work output, therefore reducing the net work input to the heat pump and increasing the coefficient of performance (COP), as shown in Figure 6. Adding more expansion stages raises the minimum temperature of the cycle. Therefore, coolants with higher freezing points can be used as storage media in the cold tanks. This is important because there are limited liquids available for these applications, and coolants with higher freezing points tend to be safer and/or more widely available.

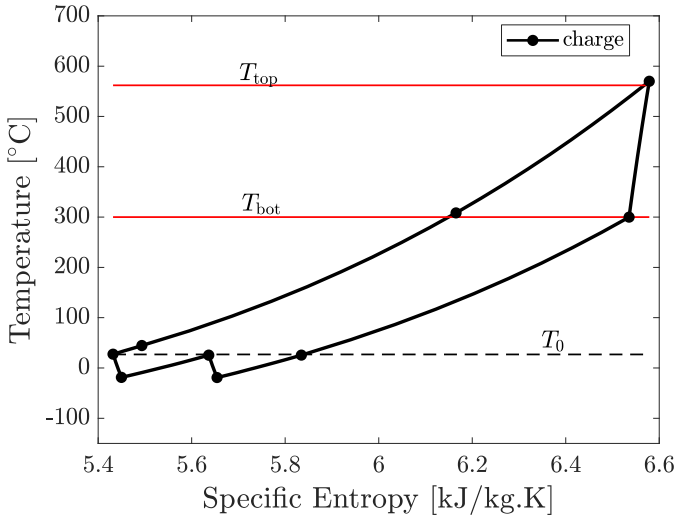

Figure 5: Temperature-entropy diagram of a recuperated Joule-Brayton heat pump with two stages of expansion that are "inter-heated" by the cold storage.

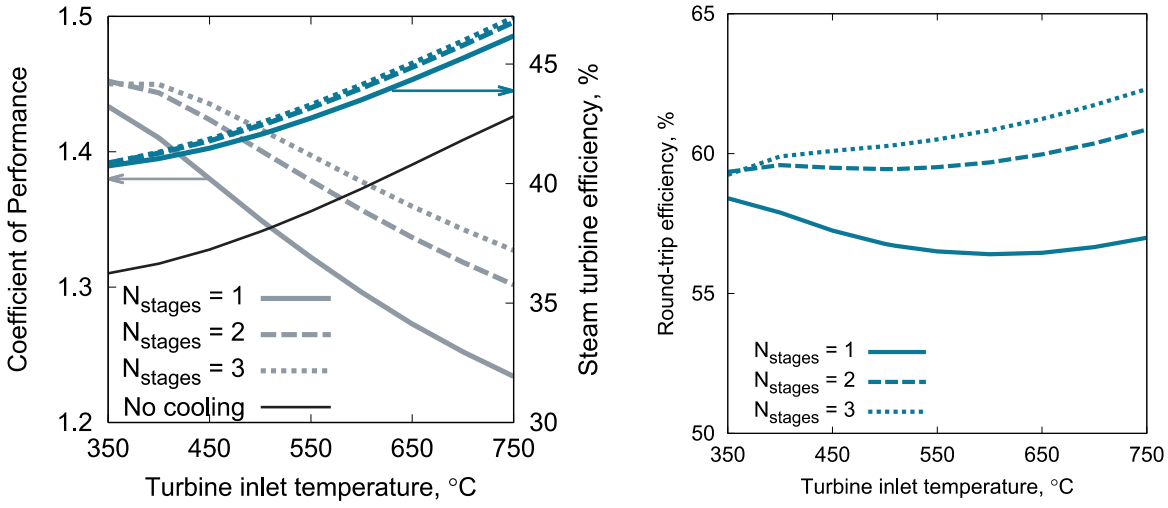

Figure 6: Effect of turbine inlet temperature. Left: Joule-Brayton heat pump COP and steam turbine efficiency. Steam turbine behavior with no cooling from the heat pump is also shown. Right: Round-trip efficiency of the combined system.

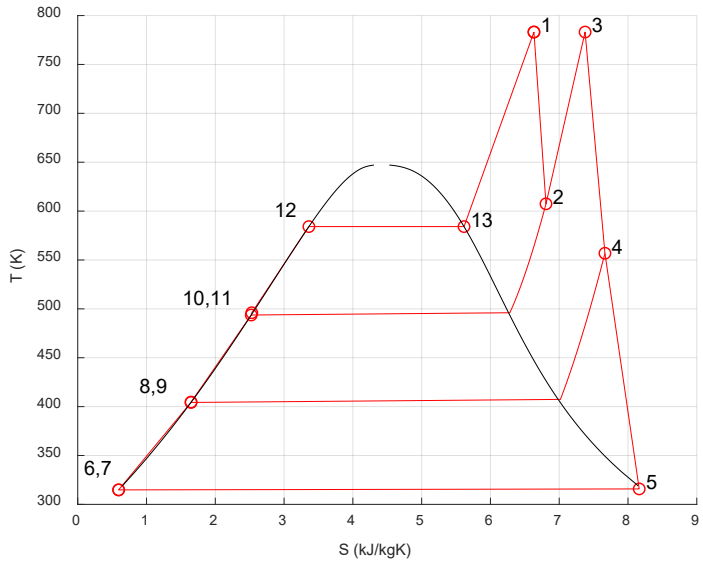

Figure 7: Temperature-entropy diagram of a steam cycle with three expansions, one reheat, and two feedwater heaters.

The temperatures into and out of the hot storage are likely to be fixed by the current operating temperatures of the hot storage in the CSP plant. However, Figure 6 explores the impact of changing the maximum temperature around the cycle. As would be expected, higher maximum temperatures lead to more efficient heat engines, but lower COP heat pumps, and the opposite occurs as the maximum temperature is decreased. This trade-off results in a minimum round-trip efficiency, which can be avoided by having either a very effective heat pump, or a high-efficiency heat engine.

The heat pump creates a cold store during charge, and this source of cooling could be used to assist the heat rejection in the steam turbine system. A model of a steam turbine with three stages of expansion, one reheat, and feedwater heating after the first and second expansions was developed, and a temperature-entropy diagram is shown in Figure 7. Additional cooling reduces the condenser temperature and therefore pressure. This affects the total pressure ratio across the steam turbine and the mass flow rate, and therefore the efficiency. A simple off-design model of the steam turbine was developed, which was validated against existing steam turbine models developed in the flow-sheeting software tool, IPSEpro [23]. It was assumed that the steam turbine inlet pressure and temperature were held constant meaning that the overall pressure ratio across the steam turbine increases. However, the pressure ratios in the first and second stages were also fixed, so only the final stage pressure ratio increased. Off-design isentropic efficiencies were obtained from correlations by Patnode [24] and from a turbine manufacturer [25]. Both correlations exhibit very similar behavior near the design point.

The additional cooling load that can be provided by the cold store to the steam turbine is calculated by requiring the cold store to be discharged in the same amount of time as the hot store. This cooling rate is applied to the condenser and the reduction in condenser temperature is found. The steam turbine efficiency (and work output) therefore increases as heat is rejected at lower temperatures. Figure 6 shows that the steam turbine efficiency increases by up to 2% when

cooling is provided. Increasing the number of heat pump expansion stages has a small benefit on the steam turbine efficiency.

The overall effect is to achieve round-trip efficiencies in the region of 55-62%. For conventional CSP steam turbines with a storage temperature of 565°C, the roundtrip efficiency is 56.6% with one heat pump expansion stage, which increases to 60.5% if three expansion stages are used. It should be noted that although respectable, the round-trip efficiency of these cycles is lower than a system that uses the same type of power cycle in charge and discharge because the cold store is not effectively exploited by the solar power cycles.

Further research is required to determine whether these benefits can be realized in practice. (For instance, reducing the condenser pressure below its design value may lead to more complicated behavior in the steam turbine). Another area for research is to understand how the cold store may be used to overcome the detrimental impact of high ambient temperatures. CSP plants are often dry-cooled, meaning that if ambient temperatures increase above the design value the work output is reduced. The cold storage may provide a method to buffer against these effects. Furthermore, if a new CSP plant is built with an integrated heat pump, the condenser could be designed for a lower condenser temperature than if only heat rejection to the atmosphere was available. Quantifying this benefit requires annual calculations of CSP power block performance with and without cooling.

5.1.2.2 Supercritical CO_2 Cycles With Storage of Recompression Heat

Supercritical CO_2 cycles are considered by some to be the next generation of CSP power cycles, due to high efficiencies, compact machinery, and compatibility with dry cooling. These cycles require a recompression stage due to large variations in real gas heat capacities. The recompression accounts for nearly 40% of the total work input. If the solar heat could be dispatched without requiring the recompression, then the specific electricity output would increase. In Figure 8, a heat pump is used to generate heat at the same temperature as the recompressor. This heat is stored, and a cold store is also generated. Discharging the system requires solar heat to be available at higher temperatures. During discharge, the recompressor is not required as the low temperature heat is provided by the hot storage.

Effectively, the recompressor still operates albeit it at a low-value time rather than a high value time. As a result, this cycle is referred to as the "time-shifted recompression" sCO_2 cycle.

The cold storage can also provide some cooling and reduce the temperature of heat rejection slightly. This also leads to lower pump inlet temperatures and work input. Since only a fraction of the flow (around 25%) goes through the recompressor in a conventional cycle, the mass flow rate of the charging cycle is lower than the discharging cycle. Therefore, the cold storage cannot cool the fluid flow all the way down to the minimum temperature (if the cold storage is discharged over the same time period as the hot storage). However, it can provide a couple of degrees of cooling which has a noticeable impact.

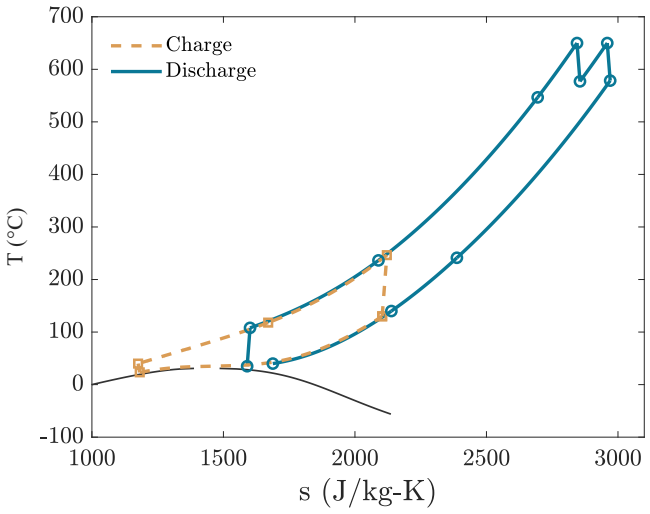

Figure 8: Temperature-entropy diagram of an sCO_2 cycle where a heat pump creates a hot storage to replace the recompression stage of an sCO_2 cycle.

Table 2 compares the proposed heat pump cycle to a conventional sCO_2 cycle for several turbine inlet temperatures. Results are shown for cases with and without additional cooling from the cold cycle. By removing the recompression stage from the discharging part of the cycle, the discharging work output increases by around 9-13%, and exergetic round-trip efficiencies are high – 67-73% – compared to Joule-Brayton cycle heat pumps. (Higher turbine inlet temperatures lead to better performance). The net efficiency is a little lower than the sCO_2 recompression cycle efficiency due to the extra heat transfer processes in the storage systems.

Using the cold store to cool the inlet to the discharging compressor further increases the work output during discharge, which is around 15-23% higher than the conventional sCO_2 cycle. However, the net efficiency decreases by around 0.5%. This is because reducing the compressor inlet temperature decreases the compressor outlet temperature (for a given pressure ratio), which means that more heat must be added to the sCO_2 in the recuperator. As a result, the mass flow rate in the charging cycle increases, which increases the net work input. This illustrates why the net efficiency should be considered in conjunction with other system metrics. A lower net efficiency means that cooling the compressor inlet reduces the net electrical energy delivered to the grid. However, cooling leads to a more efficient storage system that can absorb and dispatch more power (for a given solar field and power plant size) at the times when these services are required.

Table 2: Comparison of Conventional sCO_2 Cycles With Heat Pump Systems That Replace the Recompressor

		TIT – 550°C			TIT – 650°C			TIT - 750°C		
		sCO_2	No cooling	With cooling	sCO_2	No cooling	With cooling	sCO_2	No cooling	With cooling
CIT	°C	40.0	40.0	35.0	40.0	40.0	35.0	40.0	40.0	35.0
$\dot{W}_{\text{net}}^{\text{chg}}$	kJ/kg	-	26.5	36.2	-	26.5	36.2	-	26.5	36.2
$\dot{W}_{\text{comp}}^{\text{dis}}$	kJ/kg	61.9	50.0	41.6	61.4	50.0	41.6	61.0	50.0	41.6
$\dot{W}_{\text{net}}^{\text{dis}}$	kJ/kg	87.8	99.6	108.1	108.1	119.4	127.9	127.9	138.8	147.3
COP		-	2.2	2.7	-	2.2	2.7	-	2.2	2.7
η_{HE}	%	43.9	49.6	53.8	48.7	54.1	58.0	52.7	57.8	61.4
η_{rt}	%	-	375.2	298.8	-	449.9	353.5	-	523.0	407.2
$\eta_{rt,x}$	%	-	66.9	68.1	-	70.1	71.0	-	72.5	73.3
η_{net}	%	43.9	36.4	35.8	48.7	42.1	41.6	52.7	46.8	46.3
Mass flow fraction		0.24	0.35	0.48	0.24	0.33	0.48	0.24	0.35	0.48

5.1.2.3 Transcritical CO_2 Cycles With Storage of Recompression Heat

A similar concept to the one described above may be developed with a transcritical CO_2 cycle as the charging heat pump cycle, as illustrated in Figure 9. By using subcritical pressures, lower temperature cold storage may be achieved. These systems exhibit similar trends as discussed in the previous section: using colder storage significantly increases the work output during discharge – for a turbine inlet temperature of 650°C, the work output is 33% higher than the conventional recompression cycle. However, the heat pump requries a larger work input which decreases the net efficiency to 36%. The t-CO_2 heat pump cycle is also more complex than the s-CO_2 heat pump as it requires a phase change material in the cold store. In addition, the s-CO_2 heat pump can potentially use the existing recompressor from the s-CO_2 cycle, whereas the t-CO_2 cycle requires an additional component.

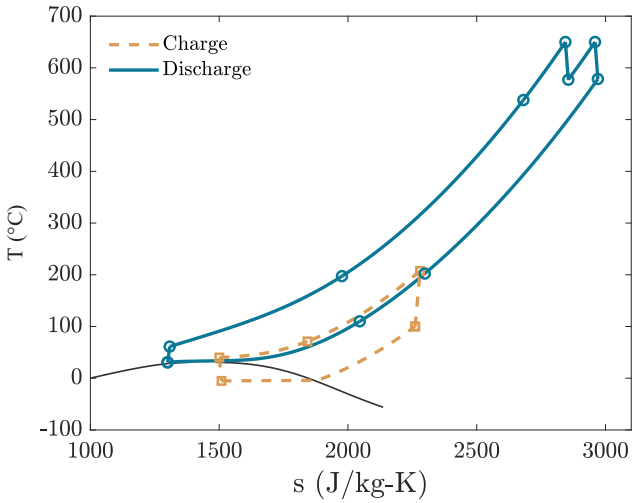

Figure 9: Temperature-entropy diagram of a transcritical-CO_2 heat pump that is used to replace the re-compressor in an s-CO_2 discharging heat engine.

5.1.3 New Build Solar-PTES Systems

PTES achieves highest round-trip efficiencies when both the heat pump and heat engine are based on the same power cycles. This provides a better temperature match in the heat exchangers. Therefore, a new installation that integrates both CSP and PTES may use a power cycle other than the steam cycles and sCO_2 cycles discussed above. (Alternatively, heat pumps using steam could be investigated. These cycles would be similar to the CHEST concept [6] although steam compression requires many compressor stages [11]). The integrated solar-PTES cycles below use a Joule-Brayton cycle in both charge and discharge.

5.1.3.1 Dual-Mode Solar-PTES System

In this design, both the charge and discharge cycles are based on the Joule-Brayton cycle, as shown in Figure 10. The solar-PTES plant has both hot and cold stores and two different modes of operation: a PTES mode, where the hot and the cold storage tanks are charged and discharged via the Joule-Brayton cycle, and a CSP mode, where the hot stores are charged by the solar field and discharged via the Joule-Brayton cycle (but the cold stores are not used).

A temperature entropy-diagram for PTES mode and CSP mode are shown in Figure 11. The CSP mode uses the same compressors as the PTES discharge mode, but they now operate at higher temperatures. The number of heat pump expansion stages is varied, and the impact on round-trip efficiency displayed in Figure 12. For the PTES mode, fewer expansion stages is better, as more expansions reduce the work ratio and make the cycle more susceptible to compression and expansion losses. In CSP mode, there is a benefit to having more than one compression stage, as the compression work decreases. Increasing the low temperature of the hot storage (T_{bot}) is also advantageous as the required heat input decreases. The CSP mode Joule-Brayton cycle achieves efficiencies in the range of 38-42% (for turbine inlet temperatures of 565°C) which is comparable with conventional steam turbines. Choosing the optimal number of heat pump expansion stages (or heat engine compression stages) is a balance between maximizing PTES-mode performance and CSP-mode performance.

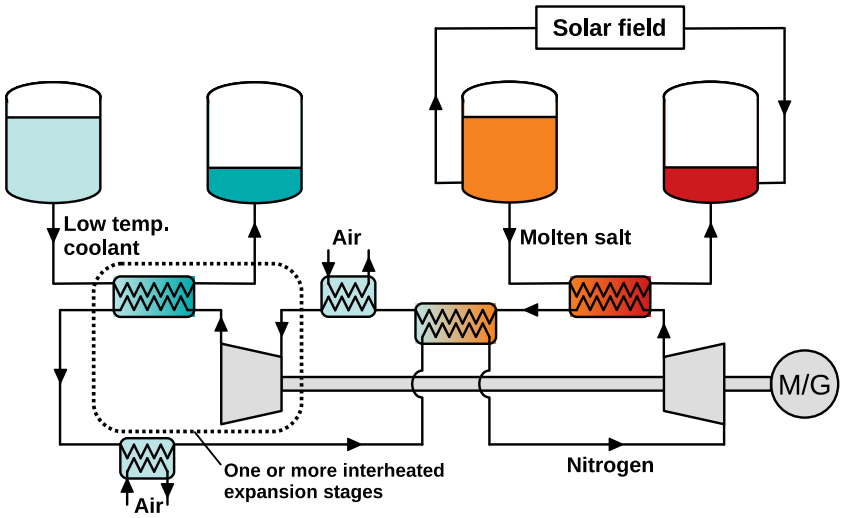

Figure 10: A schematic diagram of a dual-mode solar-PTES system. A heat pump charges hot and cold stores, which are then discharged through a Joule-Brayton cycle. Solar heat can also be discharged through the same cycle, except without the use of the cold stores.

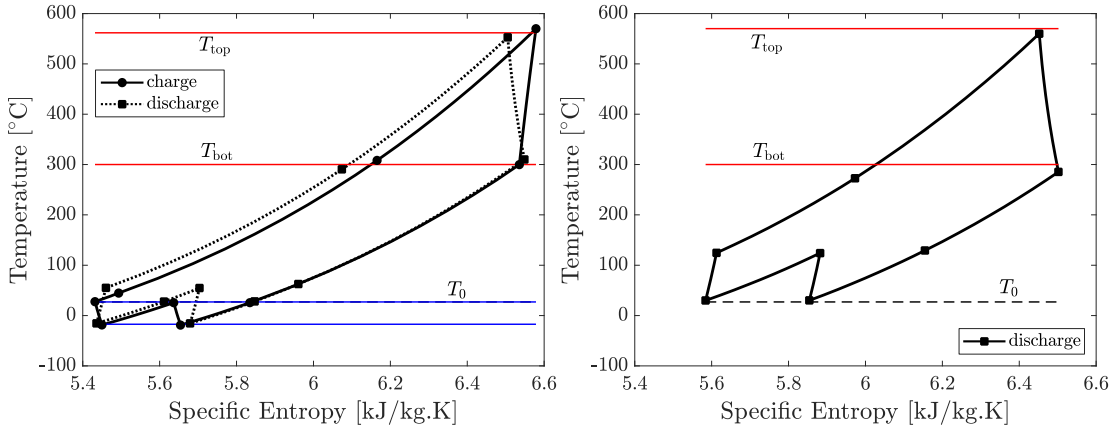

Figure 11: Temperature-entropy diagrams for a dual-mode system. Left: PTES mode with a heat pump and heat engine. Right: CSP mode with no sub-ambient heat rejection.

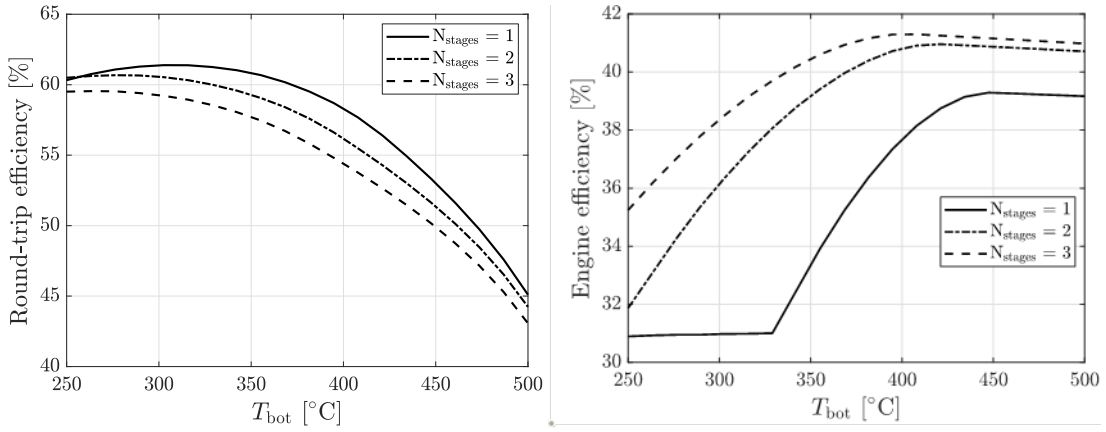

Figure 12: Effect of hot storage low temperature on number of stages Left: Variation in PTES-mode efficiency. Right: Variation in CSP mode efficiency.

5.1.3.2 Joule-Brayton CSP Cycle With Refrigeration

This cycle directly integrates the heat pump mode and the solar heat availability. The heat pump (or refrigerator) creates only a cold store, while a hot store is charged with solar heat. In discharge, a heat engine runs between these two stores, as illustrated in Figure 13. The heat pump can have several compression stages which are intercooled with the environment – i.e., the generated heat is not stored. As a result, increasing the number of compression stages reduces the wasted energy. A single expansion then creates sub-ambient temperatures and this energy is stored.

The discharge cycle is based on a Joule-Brayton cycle which operates between the solar hot storage and the heat pump cold storage. There is flexibility to increase the number of charging compression stages and discharging expansion stages. The former increases the heat pump coefficient of performance, while the latter improves the heat engine efficiency. The pressure ratio was varied while keeping the turbine inlet temperature fixed at 565°C. Figure 14 indicates that an optimal pressure ratio exists, since larger pressure ratios improve heat engine performance at the expense of heat pump performance. Optimal pressure ratios are reasonably low at around 2. The optimal net efficiency for this cycle is around 35% which is lower than a conventional steam cycle operating at this temperature (~42%). However, the discharging efficiency is 53%, and a value should be placed on delivering more power at times it is required.

If the cold storage has not been charged (if prices are not favorable, for example), but solar heat is to be discharged, it is possible to run the cycle with the existing components between the solar hot storage and the environment. This heat engine mode is clearly less efficient than if the cold storage was available. However, having several intercooled compressors enables heat engine efficiencies of around 42% for systems with two compressors and two expanders.

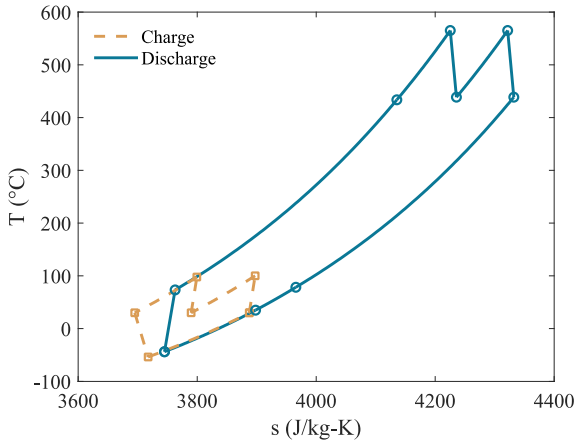

Figure 13: Temperature-entropy diagram of an intercooled Joule-Brayton heat pump that creates only a cold storage. The discharge cycle is a Joule-Brayton cycle operating between solar hot storage and heat pump cold storage.

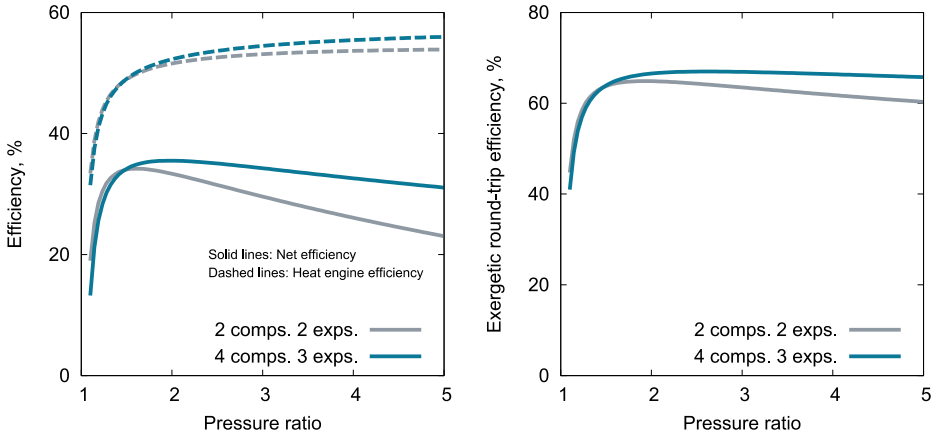

Figure 14: Variation in efficiencies with pressure ratio for a Joule-Brayton refrigeration cycle with Joule-Brayton heat engine. The hot storage temperature is fixed at 565°C. The system has either two intercooled compressions in charge and two expansions in discharge, or four compressions in charge and three expansions in discharge.

5.1.4 Task Milestone

Milestone 1: Develop solar-PTES concepts and simple thermodynamic models based on energy balances and system analysis.

The figure of merit (FOM) for this milestone was to identify solar-PTES cycles where the net efficiency η_{net} was greater than the efficiency of a conventional CSP plant η_{CSP}, which may be approximated as 40%. Thus,

$$\text{FOM} = \frac{\eta_{\text{net}}}{\eta_{\text{CSP}}} \geq 1 \tag{4}$$

This FOM was developed before the design space of solar-PTES systems was fully explored, and this metric is therefore does not adequately assess stand-alone PTES systems or some retrofitted solar-PTES systems: for instance, Category 2 cycles do not have a solar heat input and therefore cannot be described by a net efficiency.

For stand-alone PTES cycles it was decided to continue investigating ideal-gas and sCO_2 PTES cycles. These both achieved promising round-trip efficiencies compared to other thermo-mechanical storage systems. Furthermore, the solar-PTES systems of interest required the same models, meaning that these systems could be investigated without much additional overhead.

For Category 2 cycles, retrofitting the conventional steam CSP plant with a Joule-Brayton cycle was deemed the most practical, as well as apparently achieving reasonably good round-trip efficiencies.

The Time-Shifted Recompression cycle achieved an FOM just under 1. However, it was decided to continue researching this cycle since the performance was still good. The TSRC cycle with a transcritical heat pump was not considered further due to a low net efficiency.

The Joule-Brayton CSP cycle with refrigeration also achieved an FOM under 1. This cycle was also reasonably complex and required several reheated expansions and intercooled compressions to achieve good net efficiencies.

The Dual-Mode Solar-PTES system achieved very good round-trip efficiencies when in electricity storage mode, and also reached heat engine efficiencies comparable with a conventional CSP plant when in CSP mode. This cycle would require the development of a closed Joule-Brayton cycle for CSP applications, and developing machinery that could operate in two modes is likely to be complex. This concept merits further investigation, although this was not possible within the resources of this project.

5.2 Task 2: Develop Economic Cost Models and Define Performance Targets That Are Required for the System To Provide Value

The objective of Task 2 was to develop economic models of the system components, and to use grid integration models to determine the cost and performance required for a solar-PTES system to provide value to the grid.

5.2.1 Subtask 2.1: Develop Capital Cost Correlations

The objective of this task was to estimate the total capital cost of solar-PTES systems. Evaluating the economic cost and value of PTES and solar-PTES systems is a critical step in determining the potential of these devices to provide renewable power and energy storage services. This requires cost estimates for each component. Due to uncertainty in costing systems, several cost correlations were obtained with at least two data sources required. Cost correlations have been obtained for compressors, turbines, motor-generators, heat exchangers (primary heat exchangers, recuperators, and air coolers), storage tanks, pressure vessels, and various hot and cold storage media. These correlations are used to calculate the capital cost and also the lifetime cost of the system – i.e., the levelized cost of storage (LCOS).

Cost correlations for components (such as compressors and heat exchangers) can vary widely (sometimes more than an order of magnitude). Therefore, cost estimates are highly dependent on which cost correlation is chosen for each component. It can be challenging to ascertain which correlations are more suitable than others, which makes it difficult for the designer to choose the "right" correlation. Thus, the result is susceptible to bias as the designer is probably inclined to choose correlations that lead to lower costs.

An economic methodology which also evaluates the total capital cost, the LCOS and the uncertainty was devised with the aim of reducing this bias. In this methodology, several correlations are chosen for each component. This allows the designer to choose several correlations which appear suitable for the application but may differ substantially in the estimated values. A Monte-Carlo simulation is then performed whereby a correlation is randomly picked for each component from the suggested list. Repeating this hundreds or thousands of times leads to a probability distribution of system cost and LCOS from which the average values and uncertainty may be extracted. By allowing multiple cost correlations for each component, the bias from the designer is reduced, and a broader, fairer picture of the cost uncertainty may be developed. (The Monte-Carlo simulation also allows a range of electricity prices, system lifetimes, operations and maintenance costs, and contingency costs to be entered which are then used in the LCOS calculation). As an example, Figure 15 illustrates a histogram of capital cost and LCOS for a Joule-Brayton PTES cycle. Figure 16 shows a box-and-whisker plot which shows the median value, the interquartile range, and the extreme values of cost for each component. This analysis is useful as it indicates which components contribute most significantly to the cost and the uncertainty.

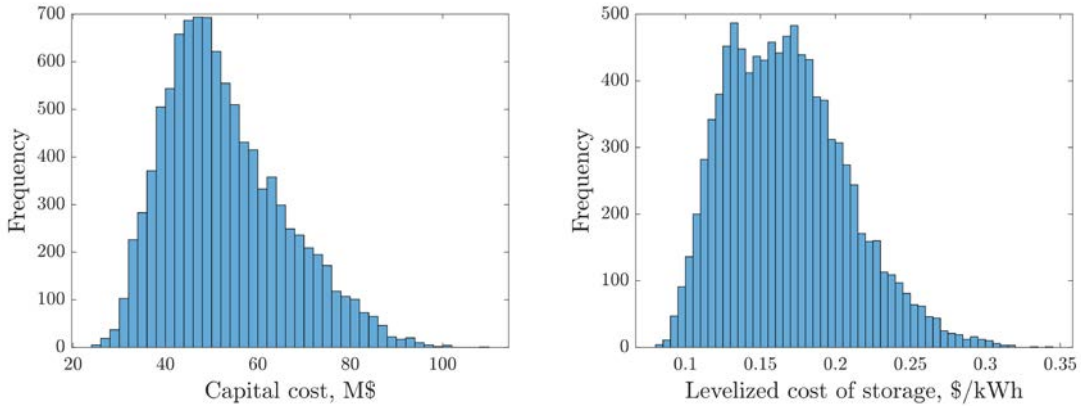

Figure 15: Histograms showing the distribution of capital cost (left) and LCOS (right) for a 15 MW Joule-Brayton PTES system with 10 hours of storage.

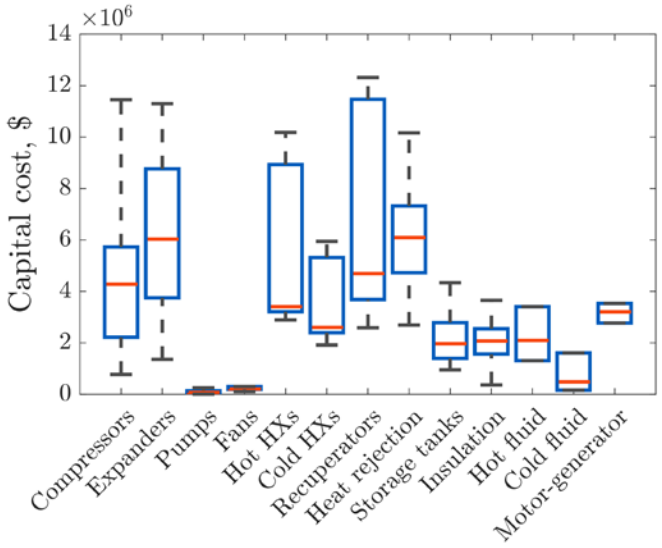

Figure 16: Box-and-whisker plot indicating the capital cost of components for a 15 MW Joule-Brayton PTES cycle with 10 hours of storage.

Correlations were obtained from numerous sources in the literature, such as [26–30]. A full list of correlations is provided in the Appendix. Further modifications were made since most correlations do not include a temperature dependence term. For example, heat exchanger cost correlations are commonly expressed in terms of heat transfer area or conductance. However, operating at higher temperatures will require the use of more expensive materials such as stainless steels or nickel alloys. Therefore, heat exchanger costs are multiplied by a "material factor" depending on the maximum temperature that the heat exchanger operates at, as indicated in Table 3.

Table 3: Cost Factors for Heat Exchanger Materials

Temperature, °C	Material	Cost factor
$T \leq 400$	Carbon steel	1
$400 \leq T \leq 600$	Stainless steel	2
$T > 600$	Nickel alloy	5

5.2.2 Task Milestone

Milestone 2: Develop component cost correlations

This milestone required that at least two sources of data were obtained for each component that accounted for at least 5% of the total system cost. Multiple cost correlations for each component are detailed in the Appendix.

5.2.3 Subtask 2.2: Evaluate Net Value of Solar-PTES

Estimating the cost of solar-PTES provides one perspective on whether it is a worthwhile investment. A second aspect may be achieved by estimating the value that solar-PTES could provide to the electrical grid. A commercial production cost modeling software (PLEXOS) is used to determine the value of a CSP, CSP-PTES or stand-alone PTES system to the grid. Production cost models solve an optimization problem that minimizes the total cost of satisfying electricity demand and ancillary services requirements by controlling commitment and dispatch schedules of an entire fleet of generators while adhering to system-level constraints on transmission capacity and generator physical or operational limitations.

In this task, simple representations of PTES and solar-PTES were implemented in PLEXOS. The storage systems were located in California on the Western Interconnection. The operational value of a CSP, CSP-PTES or stand-alone PTES resource can be determined from avoided generation costs and was evaluated from the change in production costs between the base case grid scenario and the same scenario with an added CSP, CSP-PTES or stand-alone PTES generator. The sensitivity to various factors, such as efficiency, storage duration, solar field size, and energy mix were investigated.

The work completed in this subtask provided preliminary results that indicated whether PTES provided value to the grid, and whether solar-PTES provided more value than a stand-alone CSP plant. More detailed representations and analysis were undertaken in Subtask 5.1. Further details of the modeling methodology and results are provided in Section 5.5.

5.2.4 Task Milestone

Milestone 3: Calculate the expected range of net-values that solar-PTES will provide to the grid.

This milestone required that the solar-PTES system provided more net value than a conventional CSP plant. The PTES value should be greater than 0 – i.e., PTES should have a positive impact on the grid. The full results are not presented here, since results using more detailed models are presented later in this report. However, to demonstrate that the milestone was met, two graphs showing these *preliminary* results are shown in Figure 17 and Figure 18. As can be seen, increasing the efficiency of PTES increases the value to the grid, as would be expected. At all points, PTES has a positive impact on the grid.

The solar-PTES system implemented in PLEXOS was a CSP plant that was retrofitted with a Joule-Brayton heat pump. Figure 18 shows the value provided by the solar-PTES system at two locations, Santa Barbara, CA which is relatively cloudy, and Ivanpah, CA which has a favorable solar resource. The heat pump increases the annual dispatch of electricity to the grid in both locations, but the increase is more substantial in Santa Barbara. If more than 10h storage is installed, then the Santa Barbara plant with a heat pump can dispatch more electricity than the stand-alone CSP plant in Ivanpah. Similarly, the heat pump increases the value provided by the CSP plant, and this increase is larger in an area with lower solar resource. This suggests that, if the heat pump is sufficiently cost-effective, CSP technologies may be deployed in a greater range of locations. These results also indicate that the solar-PTES system provides more value to the grid than the conventional CSP plant, thus satisfying the milestone.

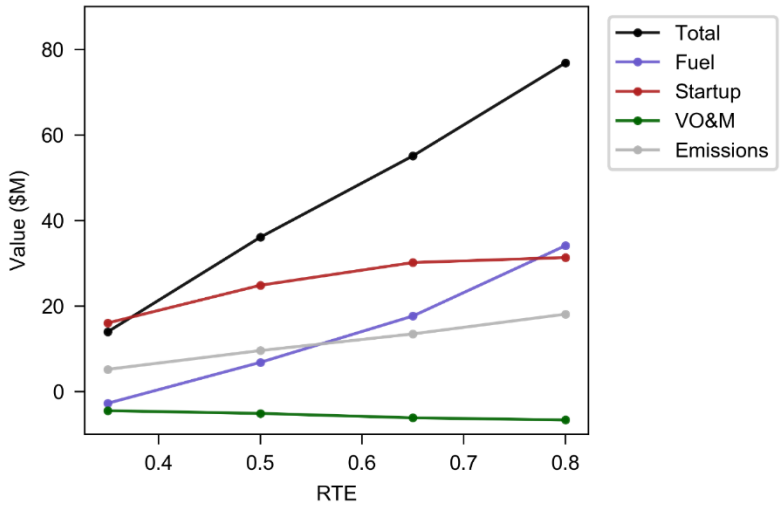

Figure 17: Effect of PTES round-trip efficiency on the value provided to the grid.

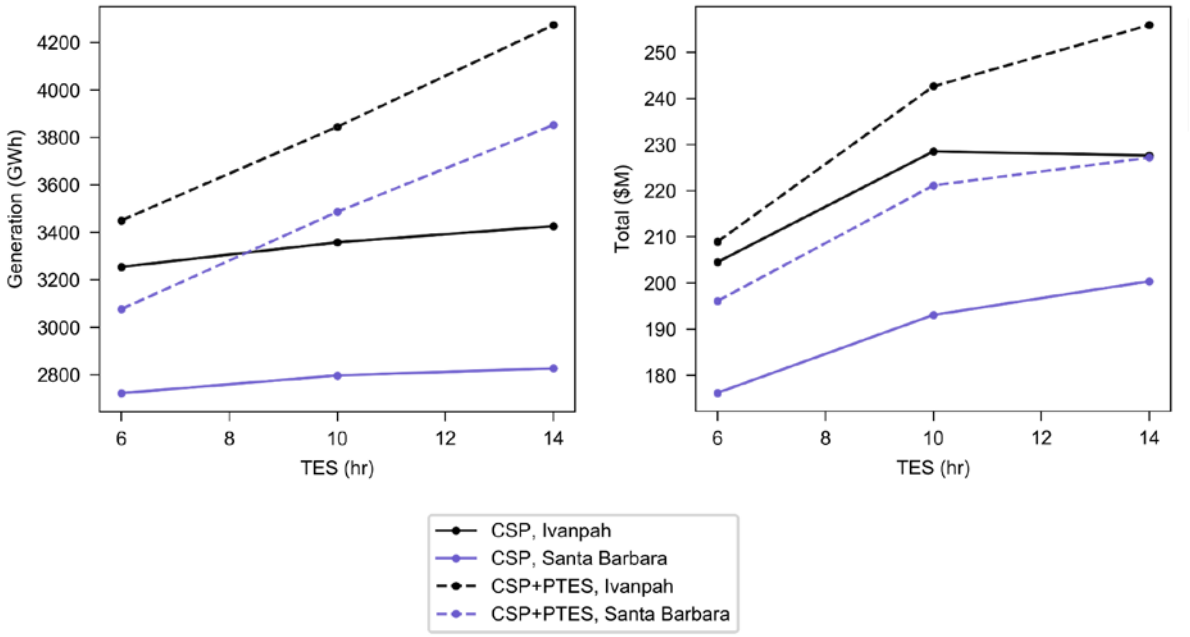

Figure 18: Generation and value provided by CSP and CSP-PTES plants in Ivanpah and Santa Barbara.

In section 5.5, the PTES and solar-PTES models are refined, and a variety of studies are described. The estimated cost is also compared to the value to determine a pay-back period.

5.3 Task 3: Develop Detailed Techno-Economic Models of Solar-PTES

The objective of Task 3 was to generate detailed, transient (time-stepping) thermal storage and power cycle models to minimize exergy losses. Design and off-design models of components were developed, and these were integrated into full system models and combined with economic calculations. By improving the technical models, this Task improved the accuracy of performance and cost estimates.

5.3.1 Subtask 3.1: Develop Component Models

Solar-PTES systems have numerous components, including compressors, expanders, pumps, fans, heat exchangers, storage tanks, motors and generators.

5.3.1.1 Compressor, Expanders, Fans

Compressors and expanders are modeled with polytropic efficiencies, η_p, and for an infinitesimal compression process, the work input is

$$dw = dh = \frac{dp}{\eta\rho} \tag{5}$$

For an ideal-gas compressor, this expression can be integrated to give a relationship between the temperature and pressure ratio:

$$\frac{T_2}{T_1} = \left(\frac{P_2}{P_1}\right)^{\frac{\gamma-1}{\gamma\eta_p}} \tag{6}$$

A similar expression can be derived for an expander. For non-ideal gases, such as supercritical carbon dioxide, the first equation must be integrated numerically while considering the real-gas thermal properties.

The work input to air fans is also calculated using Eq. 6, and the required pressure ratio is given by noting that the fans must overcome a pressure loss in the heat rejection equipment.

5.3.1.2 Pumps

Pumps are required to move the storage liquids between tanks and through the heat exchangers. The parasitic pump work is calculated with an isentropic efficiency η_i, and assuming that the fluid is incompressible and must overcome a pressure drop ΔP

$$\dot{W}_{\text{pump}} = \frac{\dot{m}\Delta P}{\rho\eta_i} \tag{7}$$

5.3.1.3 Motor-Generators

The motor-generator is assumed to be a permanent magnet synchronous machine, which has a design efficiency of 98%. For PTES systems, it is assumed that the same machine is used as the charging motor and discharging generator. Part-load performance of such a machine was obtained from Ref. [31] which indicates that the machine operates close to its design efficiency until about 50% part-load, below which point there is a rapid decrease in efficiency.

5.3.1.4 Storage Tanks

Storage tanks are assumed to be internally insulated and are therefore constructed from carbon steel. The insulation thickness is calculated assuming that there is a 0.5% energy loss from the tanks per day. The storage fluid mass is calculated by finding the required mass flow rate to provide a certain power output and multiplying this by the discharging duration. The internal volume of each tank is oversized by 10% compared to the fluid volume.

5.3.1.5 Fluids

Thermal properties, such as the variation of heat capacity, density, enthalpy, and entropy with temperature are required for each of the fluids. Where possible, fluid properties are obtained from CoolProp Ref. [32], which is used for nitrogen, carbon dioxide, argon, water/steam, and organic fluids, such as methanol. Thermal properties for other fluids are obtained from manufacturer's data sheets and are tabulated. Data sheets typically provide heat capacity variation with temperature, from which the enthalpy and entropy can be calculated. The data tables are then interpolated to find the necessary properties. This approach is used for mineral oils, synthetic fluids, nitrate and chloride molten salts, and glycols.

5.3.1.6 Heat Exchanger Models

Heat exchangers are used to transfer heat in/out of storage, recuperate heat within power cycles, and reject heat to the environment. For PTES systems, the heat exchangers that transfer thermal energy between the power cycles and thermal storage systems are particularly important. In some cases, such as with ideal gases that have constant heat capacities, heat exchanger behavior is relatively straightforward, and simple assumptions (such as a constant temperature difference between the two fluids) are satisfactory.

Some of the solar-PTES cycles use real fluids such as supercritical carbon dioxide or steam. These fluids show large variations in heat capacity (and other properties), especially near the critical point. These variations can lead to pinch points in heat exchangers. Pinch points limit the maximum heat that can be transferred between two fluids and impact the entropy generation. This effect is compounded in PTES systems where the direction of heat transfer reverses between charge and discharge.

Heat exchanger models that capture real fluid behavior were developed [33]. As an example, consider heat transfer between supercritical CO_2 and a mineral oil in the cold storage system of an sCO_2 PTES cycle, see Figure 2 for reference. In the charging process, cold CO_2 cools down the mineral oil. The cold CO_2 is near the critical point and has a large heat capacity. The temperature profile in Figure 19 indicates that the CO_2 behaves almost as if it is undergoing a phase change. The mineral oil, on the other hand, has a fairly constant heat capacity and the temperature profile is almost a straight line. This creates a pinch point at the cold end of the heat exchanger and leads to quite large temperature differences in the middle of the exchanger. The mineral oil is cooled down to just over 300 K in charging.

The heat transfer direction reverses in discharge, and the 300 K mineral oil is used to cool down the hot supercritical CO_2. In the discharging process, a pinch point occurs near the middle of the heat exchanger. This leads to large temperature differences at both ends of the heat exchanger, and it can be seen that the mineral oil is not heated up to its original temperature. Furthermore, the CO_2 is cooled to 325 K, whereas in discharge it was originally at 290 K.

These detailed heat exchanger models allow these effects to be more accurately captured, and their impact on the solar-PTES performance quantified. In addition, this modeling will assist the improved design of solar-PTES systems. For instance, in the illustrated case, heat transfer could be improved by using two or more heat exchangers which match the temperature profiles more closely. The heat exchanger models also calculate the total heat transfer area which is necessary to estimate the exchanger cost.

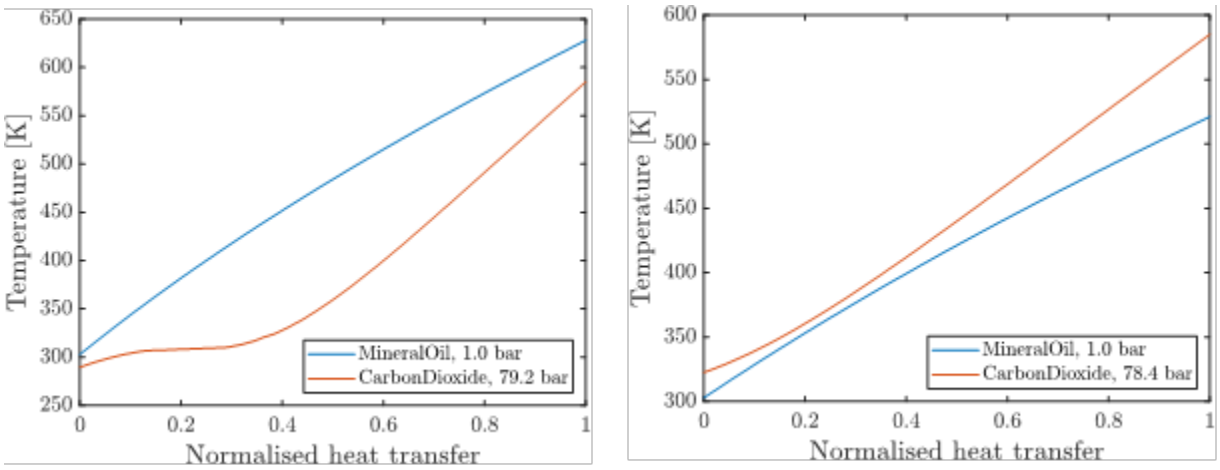

Figure 19: Temperature profiles between mineral oil and supercritical CO_2 in counter-flow heat exchangers. Left: Charging process: heat transfer from oil to CO_2. Right: Discharging process: heat transfer from CO_2 to mineral oil.

5.3.1.7 Packed Bed Modeling

A packed bed is a thermal energy storage system which uses a single container of rocks rather than two tanks of liquid. A heat transfer fluid (HTF) flows through a container which is packed with a filler material. Heat is transferred to or from the filler material from the HTF to charge or discharge the storage. The filler may be a solid such as rocks or gravel (referred to as sensible heat storage), or it may be a phase change material (PCM) such as paraffin wax which undergoes a phase change and stores energy in its latent heat. PCMs must be encapsulated in a solid material. The HTF may be a gas such as air, a liquid such as molten salt or thermal oil, or even a phase change material such as condensing steam.

These systems are of interest because they potentially reduce the required volume of containment and fluid, and therefore cost. However, direct heat transfer between the power cycle fluid and the packing medium means that the containment vessel may have to be pressurized. Furthermore, a thermal gradient exists along the length of the packed bed, and the behavior of this gradient should be accurately captured in order to evaluate the energy stored and the exergetic losses. In addition, for a hot packed bed during charge, the thermal gradient moves along the packed bed and eventually reaches the end. At this point, the temperature of the fluid leaving the storage begins to increase. This represents a waste of energy, and there may also be constraints set by the rest of the system on how much this temperature can change.

A numerical scheme was developed based on Ref. [34] and Ref. [35] to model packed-bed thermal storage. This one-dimensional scheme can model packed beds with sensible and latent packing, and with gaseous and liquid heat transfer fluids. This model was validated against experimental data obtained from the literature. Examples are shown in Figure 20 and Figure 21. In Figure 20 a sensible heat packed bed with air as the working fluid and alumina as the solid filler is validated against data from [36]. Results are shown for the discharging phase in terms of non-dimensional parameters. The thermal gradients predicted by the numerical model show a good agreement with the experimental results. At each time, the energy stored within the packed bed is calculated and numerical and experimental results are presented in Table 4 which demonstrates that the numerical model predicts the energy density to within a 5% error.

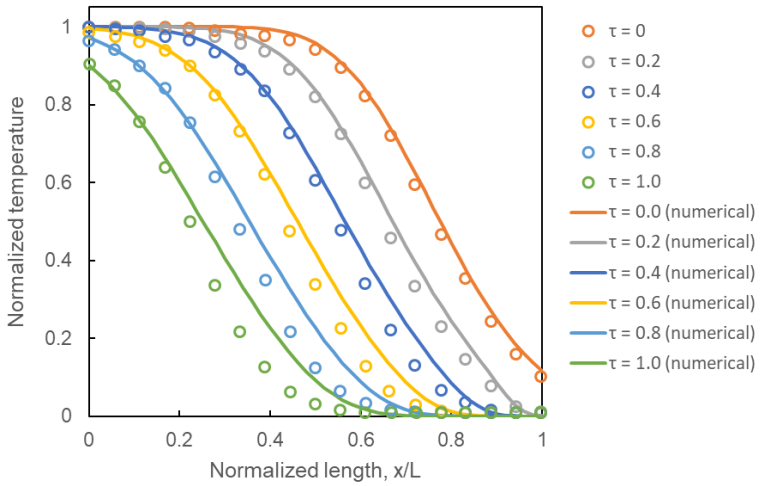

Figure 20: Validation of numerical results against Cascetta et al.'s experimental results for a discharging sensible heat packed bed.

Table 4: Energy Density at Each Time Point for Experimental and Numerical Results

		Energy density, kWh / m³					
Cascetta et al. [36]		$\tau = 0.0$	$\tau = 0.2$	$\tau = 0.4$	$\tau = 0.6$	$\tau = 0.8$	$\tau = 1.0$
Experimental	kWh / m³	84.1	72.0	60.5	48.8	37.6	26.6
Numerical	kWh / m³	83.7	72.4	61.1	49.8	38.7	28.4
Difference	%	0.4	-0.7	-1.1	-2.1	-2.9	-6.5

Loem et al. [37] presented experimental results for a latent heat packed bed with air as the working fluid and a commercial paraffin as the storage media. Numerical and experimental results, and the percentage error at each location are shown in Figure 21. The results show a good agreement with errors typically less than 5%, with the exception of the sensible heating of liquid (melted) media where the errors increase up to 10-15 %.

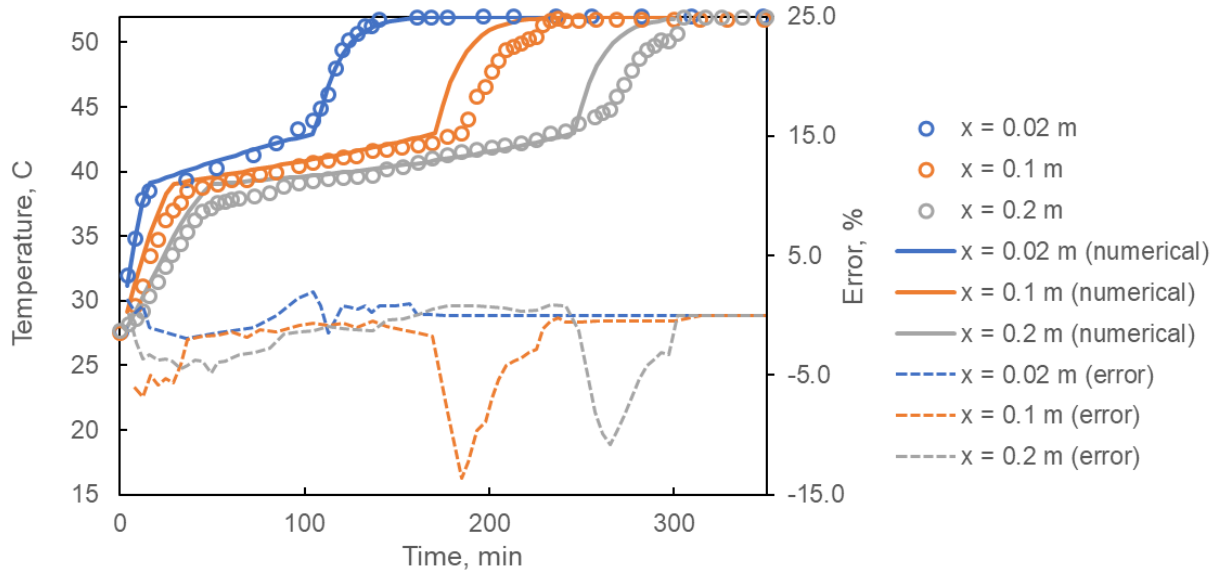

Figure 21: Validation of numerical results against Loem et al.'s experimental results for a charging latent heat packed bed. The percentage error between the experimental and numerical temperatures are also shown.

These packed bed models were not ultimately integrated into solar-PTES power cycle models in this project, although they remain a promising storage technology that should be considered in future work.

5.3.2 Subtask 3.2: Off-Design Models of Components

Off-design models of each component and the full cycle were developed. Energy storage systems are likely to operate over a range of operating conditions, and it is important to evaluate their performance at part-loads and to understand any constraints the technology may have. Off-design behavior is incorporated into the grid analysis models in subsequent tasks which improves the estimates of the system value.

5.3.2.1 Methodology for Off-Design Heat Exchangers

The off-design model is a one-dimensional model of a counter-flow shell-and-tube heat exchanger, which employs the geometry of the device to compute the heat transfer and friction coefficients along the heat exchanger longitudinal axis. The iteration procedure follows a common approach (e.g., see Ref. [38]):

i. An initial value of the overall heat transfer, $\dot{Q}$, is assumed. This fixes the outlet enthalpies (and temperatures) of each fluid.

ii. The heat exchanger is discretized into a number of sections of equal heat duty. This determines the full $T(\dot{Q})$ distribution.

iii. At each section, the geometry of the heat exchanger (i.e., the hydraulic diameter and cross-sectional area of each side) is used to determine the Reynolds numbers of each fluid. Once the Reynolds numbers are known, the heat transfer coefficients and friction factors become determined. These are obtained using standard correlations for fully developed flow in pipes (e.g., see Ref. [39]).

iv. The heat transfer coefficient of each fluid is employed to obtain the overall heat transfer coefficient of each heat exchanger subsection, U_i.

v. The $T(\dot{Q})$ distribution of each fluid, together with the overall heat transfer coefficient, gives the required heat transfer area at each section, $\mathrm{d}A_i = \mathrm{d}\dot{Q}_i \ / U_i \Delta T_\mathrm{i}$, and the total required heat transfer area. The latter is compared to the pre-specified heat transfer area of the heat exchanger, and the initial value of $\dot{Q}$ is updated until both areas are the same (i.e., the iteration procedure has converged).

vi. At each iteration, the computed heat transfer area is used to compute the pressure losses at each section. Since temperature is a function of both enthalpy and pressure for real fluids, $T(h,p)$, this requires the $T(\dot{Q})$ distribution to be updated, which has an impact on the computed heat transfer area itself. However, the pressure dependence is normally weak and pressure losses are typically small, meaning that this internal sub-iteration process converges in a small number of steps.

The above iteration procedure allows one to study how a given geometry performs under varying conditions. Furthermore, details about the variation of different properties along the heat exchanger become readily available. For example, Figure 22 shows how the temperature and the Reynolds numbers vary along the longitudinal axis for an exchanger operating with CO_2 and H_2O.

5.3.2.2 Validation of Heat Exchanger Models

The off-design heat exchanger model was subjected to two validation studies. A study against analytical solutions, valid for fluids with constant properties, and a study against a similar off-design model from another research group, featuring a CO_2 recuperator.

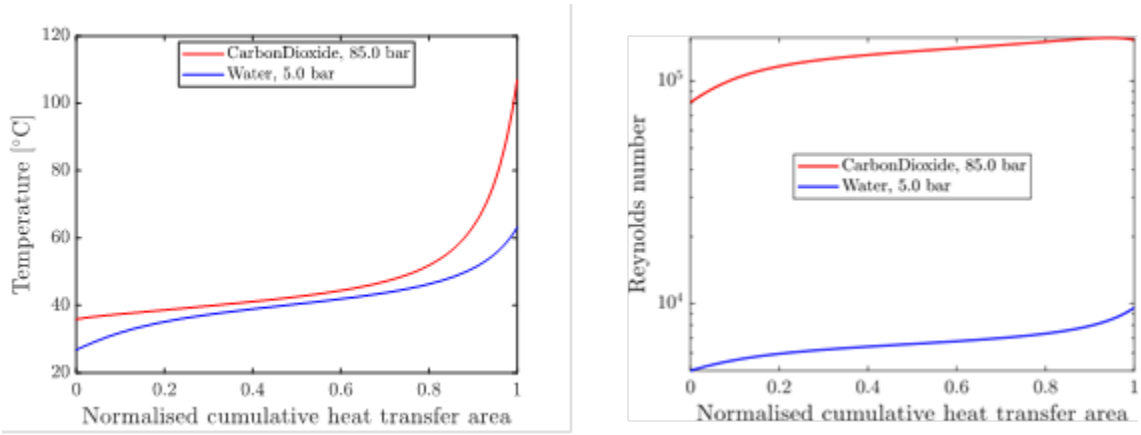

Figure 22: T(A) (left) and Re(A) (right) diagrams of a heat exchange process between supercritical carbon dioxide and liquid water.

The results from the analytical validation study, applied to a helium recuperator are presented in Figure 23. The analytical solutions correspond to the standard effectiveness-NTU (number of transfer units) method [39]. As can be seen in the figure, there is a very good match between analytical and numerical results (the maximum error is below 0.003%), which can be explained by the well-behaved thermophysical properties of helium (in particular, its almost-constant specific heat capacity).

For real fluids with strong non-linear variation of properties, however, analytical solutions significantly deviate from numerical results. It is then necessary to validate the model against other models or, ideally, experimental data. While a validation against experimental data has not yet been performed, here a preliminary validation against the results from an independent numerical model is presented. Data for this validation is taken from Hoopes et al. [40], who present an off-design model of a PCHE (based on a similar discretization scheme) operating as a CO_2 recuperator. The validation here is considered "preliminary" because the comparison is not strictly valid, since the model presented here is of a shell-and-tube geometry, which has a different ratio of cross-sectional flow areas than a PCHE. Nevertheless, very similar results can still be replicated with the shell-and-tube model when employing channels with an equivalent hydraulic diameter. In the near future, the model will be adapted to be able to simulate a PCHE and/or validated against experimental data.

The results from the second validation study are presented in Figure 24. As can be seen, the match between the results from our model and the results from Hoopes et al. are satisfactory, except for the computed pressure losses on the cold channel, which are too large. However, this is explained from the different ratio of cross-sectional areas for the shell-and-tube and the PCHE geometries, as mentioned above.

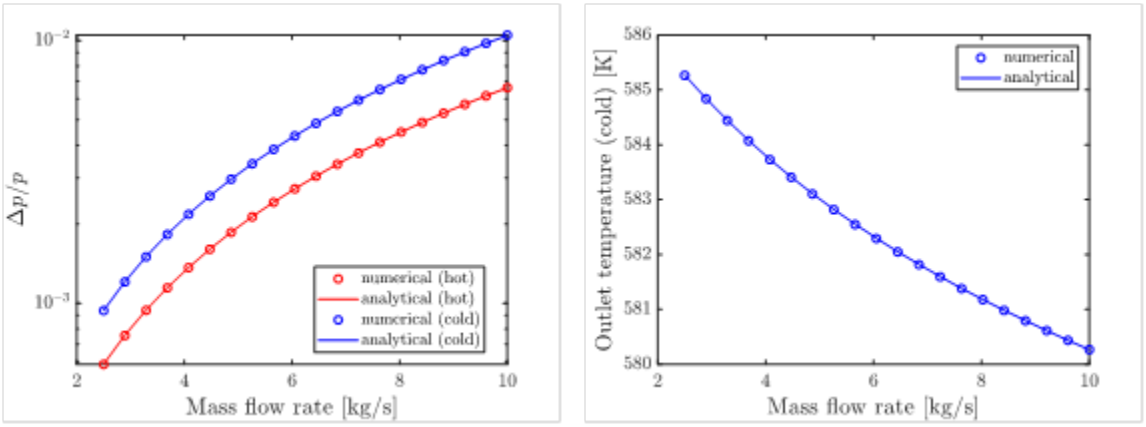

Figure 23: Results from the first validation study. Numerical results are plotted together with analytical solutions for a helium regenerator.

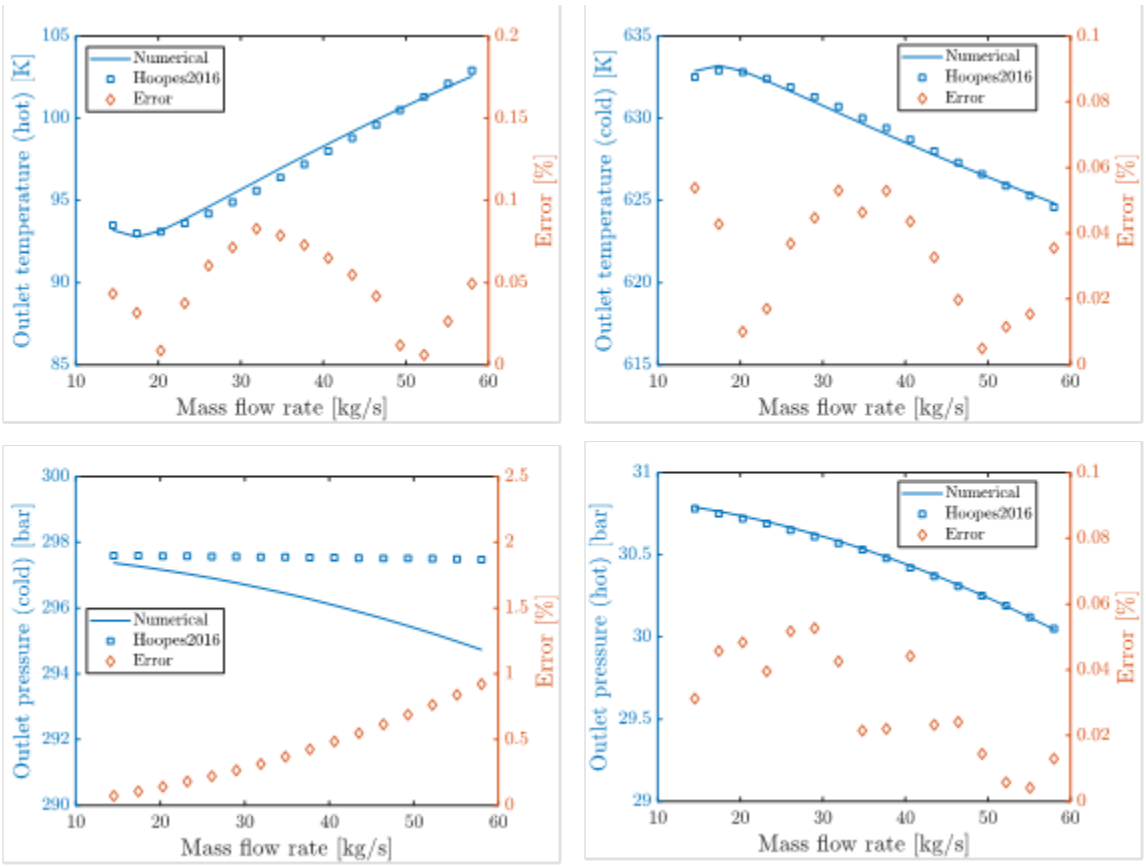

Figure 24: Results from the second validation study. Numerical results from the off-design model are compared to results from Hoopes et al. [40].

5.3.2.3 Compressor and Expander Characteristics

For an electricity storage device to be able to flexibly respond to the supply and demand needs of the electrical grid and variable renewable generators it should be capable of operating over a range of part-load conditions. The part-load behavior of PTES and solar-PTES systems is currently not well understood. Part-load operation of PTES components leads to them operating away from their design point. Compressors and expanders follow characteristic curves, such as those illustrated in Figure 25 and Figure 26, whereby varying the inlet conditions (such as temperature, pressure, mass flow rate, or shaft speed) leads to variations in pressure ratio and efficiency.

The form of these curves were obtained for air-based turbomachinery from Refs. [41–43] and are in the process of being integrated with full cycle models. Expressions that generate similar curves for sCO_2 machinery may be obtained from Ref. [44]. Implementing such off-design curves into full cycle models requires a control strategy: PTES uses closed cycles for the charging and discharging process. Therefore, moving along the characteristic curve of the compressor will affect the inlet conditions and off-design performance of the turbine. Furthermore, the impact on the heat exchangers and storage systems also has to be considered. Off-design analysis of PTES and solar-PTES systems is therefore a valuable area for investigation since part-load operation during charge may have long-term implications by affecting discharge.

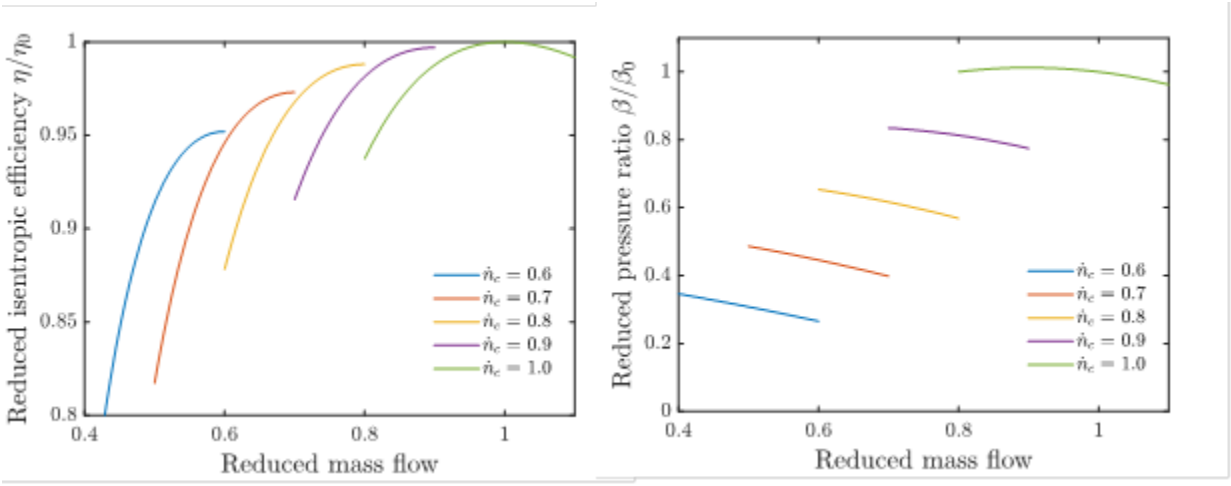

Figure 25: Characteristic curves for compressors.

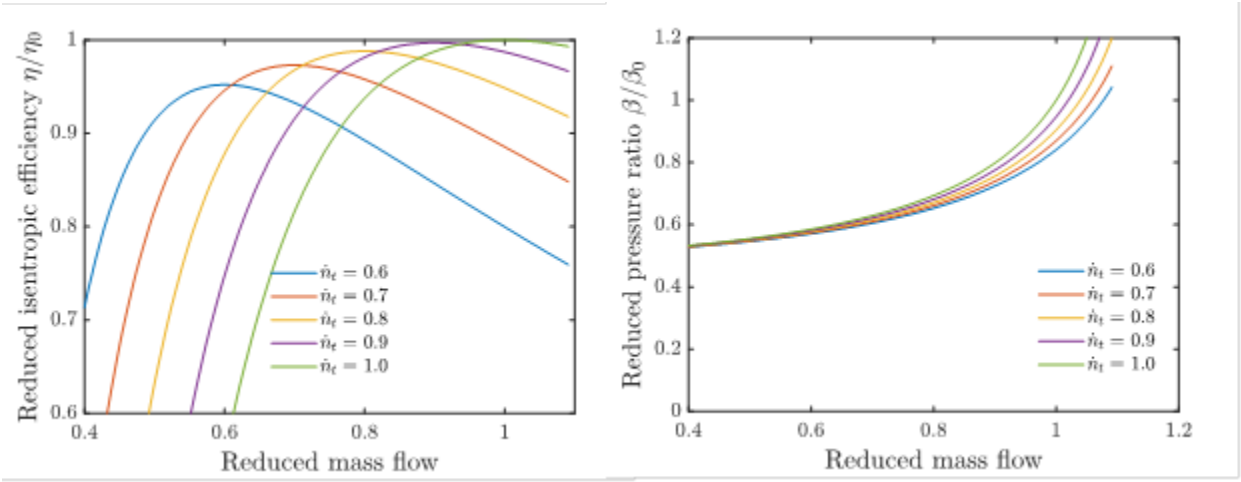

Figure 26: Characteristic curves for turbines.

5.3.2.4 Control Strategies for Ideal-Gas PTES Systems

One control strategy that works particularly well for ideal gas power cycles is known as "inventory control." The aim of this method is to keep the volumetric flow rate through the compressors and turbines constant. A useful quantity, sometimes known as the "swallowing capacity" or mass flow coefficient, is:

$$\dot{m}_c = \frac{\dot{m}\sqrt{T}}{p} = \text{constant} \tag{8}$$

The aim is to keep the swallowing capacity constant. Non-dimensionalizing this term by the design quantities (denoted by subscript 0) gives

$$\frac{\dot{m}}{\dot{m}_0}\frac{p_0}{p}\sqrt{\frac{T}{T_0}} = 1 \tag{9}$$

Thus, it can be seen how the inlet parameters to each compressor and expander may be varied in order to keep this quantity equal to one. Figure 25 and Figure 26 indicates that keeping the mass flow coefficient constant means that the pressure ratios and efficiency of each machine also remains constant, even if the cycle is operating at part-load. Another advantage of this approach is that the rotational speed of the machines can be kept constant, and the compressor and expander can potentially be placed on the same shaft.

Part-load performance may be achieved by reducing the mass flow rate around the cycle. Referring to Eq. 9, the swallowing capacity may be kept constant by either reducing the inlet pressure to each machine or increasing the inlet temperature. Both actions reduce the density which therefore keeps the volumetric flow rate through the machine constant. The inventory control method varies the inlet pressures in proportion to the mass flow rate. This is achieved by varying the mass of working fluid in the system. Therefore, an additional buffer tank is required to add and remove mass from the system in order to adjust the system pressure as necessary.

A significant advantage of using inventory control in ideal gas power cycles is that by keeping the volumetric flows constant, the pressure ratios and efficiencies of the turbomachinery remain constant. As a result, the outlet temperature from each machine also remains at its design value. This is particularly important for PTES systems: if off-design temperatures were created during the charging phase, the thermal storage would be charged to these temperatures and additional mixing losses would occur. The subsequent discharge cycle would discharge from the off-design temperatures which would further reduce the system efficiency. Therefore, inventory control in ideal gas PTES systems therefore allows the device to operate over a range of part-load conditions at efficiencies that are similar to the design point efficiency. Furthermore, the PTES device can operate over part-load operating points without compromising system performance in the future.

The temperature-entropy diagram of a charging PTES cycle is shown in Figure 27, which demonstrates how inventory control keeps pressure ratios and temperature ratios constant.

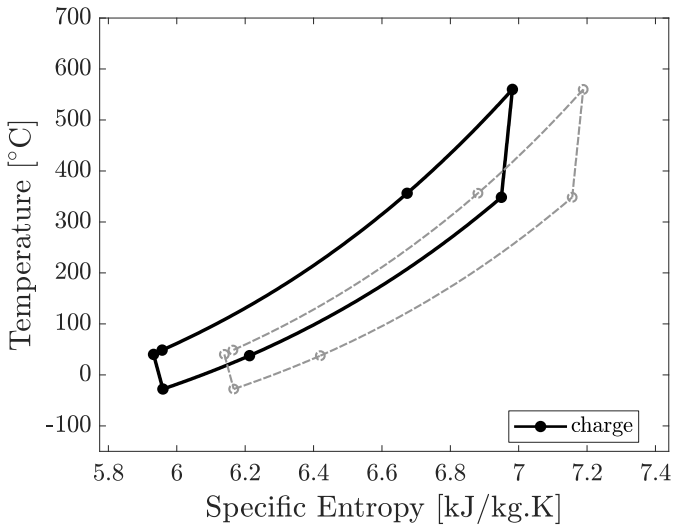

Figure 27: Temperature-entropy diagram of PTES system during charge. The black, solid lines show the design case. The grey, dashed lines show part-load operation with inventory control: the power cycle operates at lower pressures, but pressure ratios and temperature ratios remain constant.

5.3.2.5 Off-Design Results for PTES Cycles

In this section, results for PTES cycles operated at part-load and off-design conditions are presented.

The part-load performance of PTES cycles as described above is somewhat simplified. In practice, changing the working fluid mass flow rate also affects the heat exchanger performance. Typically, lower mass flow rates in a heat exchanger with a fixed geometry lead to lower pressure losses and improved heat transfer. As a result, when operating at part-load, the pressures around the cycle do not scale exactly in proportion with the change in mass flow rate. Instead, the variations in pressure drops and temperature approaches must be accounted for, and several iterations are required in order to find suitable conditions that enable the cycle to be closed. Suitable schemes were developed which find converged solutions with only a few iterations.

The off-design performance of an ideal-gas PTES system is shown in Figure 28 and Figure 29 which show how the power output and round-trip efficiency are affected by part-load operating points and changes in ambient temperatures. The mass flow rate of nitrogen is decreased compared to the design point which reduces the power input and output of the charging and discharging cycles, respectively. The power output scales proportionally with the reduction in mass flow rate. Reducing the ambient temperature below the design value leads to an increased power output.

Notably, the round-trip efficiency remains almost constant across part-load operating points. This is because, even accounting for variations in the heat exchangers, the compressors and expanders remain very close to their design points as a result of the inventory control method. The round-trip efficiency begins to reduce more significantly once the system operates below 40% part-load. Again, low ambient temperatures correlate to improved round-trip efficiencies.

Therefore, inventory control in ideal gas PTES systems allows the device to operate over a range of part-load conditions at efficiencies that are similar to the design point efficiency. Furthermore, the PTES device can operate over part-load operating points without compromising system performance in the future.

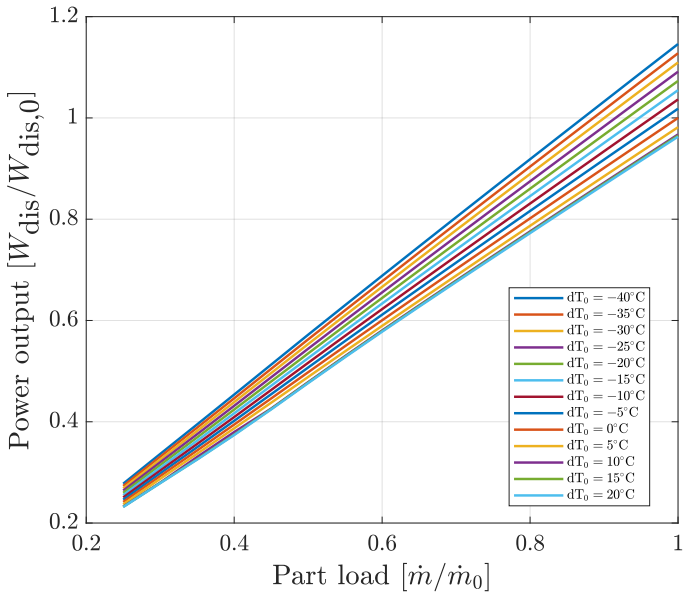

Figure 28: Power output of a discharging PTES cycle as a function of part-load and ambient temperature.

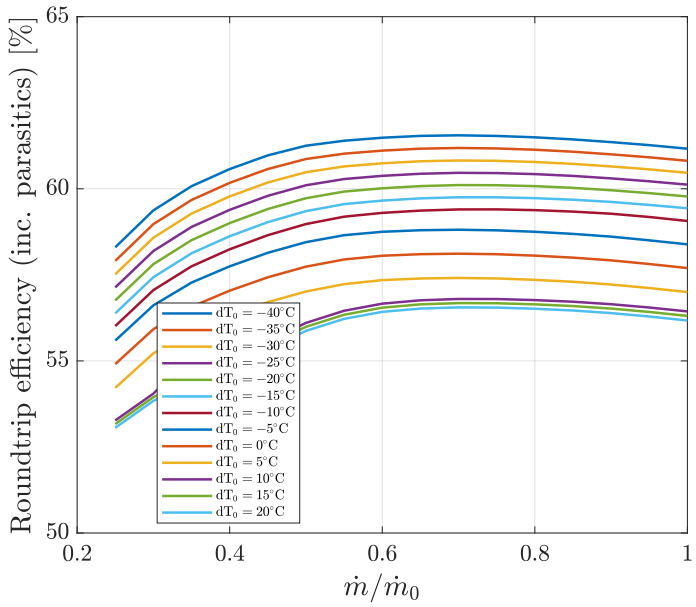

Figure 29: Round-trip efficiency of a PTES cycle as a function of part-load and ambient temperature.

5.3.2.6 Modeling of the Steam-Rankine Cycle

The off-design behavior of a steam-Rankine cycle is modeled. This is necessary to capture the off-design performance of retrofitted solar-PTES systems. The steam turbine is modeled with three stages of expansion, as shown in Figure 30 – a high pressure stage, followed by a reheat, followed by an intermediate-pressure stage and finally a low-pressure stage. The off-design model was developed with this system, although improvements to the steam turbine model are planned by increasing the number of stages to match the work of Patnode [24].

The high-pressure steam turbine stages are assumed to operate in a similar way to gas turbine stages – i.e., inlet properties are varied to keep the volumetric flow rates constant. For steam turbines, this is often modeled in terms of Stodola's ellipse which relates the mass flow coefficient and the inlet and outlet pressures relative to their design points, and may be written as:

$$\frac{\dot{m}}{\dot{m}_0}\frac{P_{\text{in},0}}{P_{\text{in}}}\sqrt{\frac{T_{\text{in}}}{T_{\text{in},0}}} = \frac{[1-(P_{\text{out}}/P_{\text{in}})^2]^{1/2}}{\left[1-\left(P_{\text{out},0}/P_{\text{in},0}\right)^2\right]^{1/2}} \tag{10}$$

Stodola's ellipse is essentially another formulation that specifies that turbomachines are constant volume flow devices, and thus it also applies to gas turbines. For gas turbines, the pressure ratio across the turbine may be kept constant by varying both the inlet and outlet pressures to the same extent. This enables gas turbines to operate over a range of operating points without affecting the pressure ratio and therefore performance. For steam turbines, the exit pressure is fixed by the condenser pressure, and is therefore also related to the cooling water supply and ambient temperatures. In this work, it is assumed that the design exit pressure is 0.08 bar but may be operated down to 0.05 bar if sufficient cooling is available. This is consistent with the design points and operational data presented in Ref. [24].

The off-design performance of the steam turbine depends on two main parameters: the inlet mass flow rate and the condenser temperature (which depends on ambient temperature and the availability of cooling from the cold storage). The off-design operation may be summarized as follows:

1. All turbine stages adhere to Stodola's ellipse
2. All stages except the final stage are operated close to their design pressure ratios [45]
3. If the inlet mass flow rate reduces:
    A. Reduce the inlet pressure to the first turbine stage proportionally. By Stodola's ellipse, the exit pressure of the first stage also reduces proportionally.
    B. As a result, the pressure ratio in the final stage decreases. The mass flow rate at the exit of the final stage is insufficient which leads to flow separation and a reduction in the stage efficiency.
    C. It is assumed that the condenser temperature is a constant and is set by the ambient temperature or availability of cooling.

4. The condenser temperature may increase or decrease depending on the ambient temperature or cooling from cold storage:
    D. The inlet pressure and mass flow rate to the first turbine stage are constant (fixed by the boiler)
    E. All turbine stages except the final stage therefore operate at their design pressure ratios
    F. If ambient temperatures are higher than the design condenser temperature then the condenser pressure increases, and the final stage pressure ratio (and efficiency) decrease – see above.
    G. If cooling is available, or ambient temperatures are lower than the design condenser temperature then the condenser pressure decreases to a minimum of 0.05 bar. From Stodola's ellipse, the mass flow through the final stage must increase slightly and this is achieved by reducing the steam extraction.

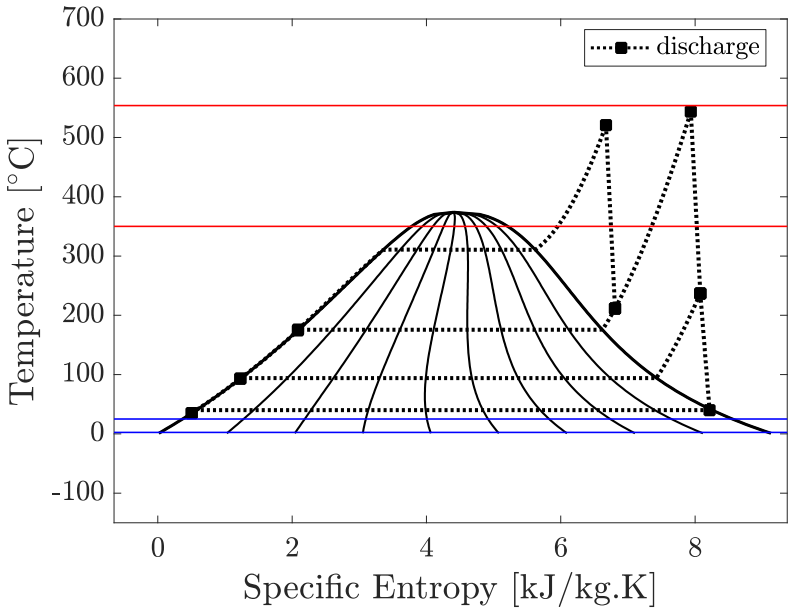

Figure 30: Temperature-entropy diagram of a steam-Rankine cycle for CSP.

5.3.2.7 Off-Design Results for Solar-PTES Cycles

In this report, the solar-PTES cycle of interest uses an ideal-gas heat pump during charge and an (existing) steam-Rankine cycle during discharge. The heat pump uses an ideal-gas Joule-Brayton cycle as described in Section 5.1.2.1. As such, part load behavior may also be managed using inventory control. One difference to the heat pumps used in PTES systems is that multiple expansion stages may be used during charge which increases the coefficient of performance (COP).

The part-load behavior of the solar-PTES system is shown in Figure 31 and Figure 32. The power output again decreases linearly with the part-load operating point. Unlike the ideal-gas Joule-Brayton cycle, the efficiency decreases at all part load points as a result of the steam

turbine behavior. The effect of ambient temperature variations are somewhat less clear, although generally lower ambient temperatures improve performance.

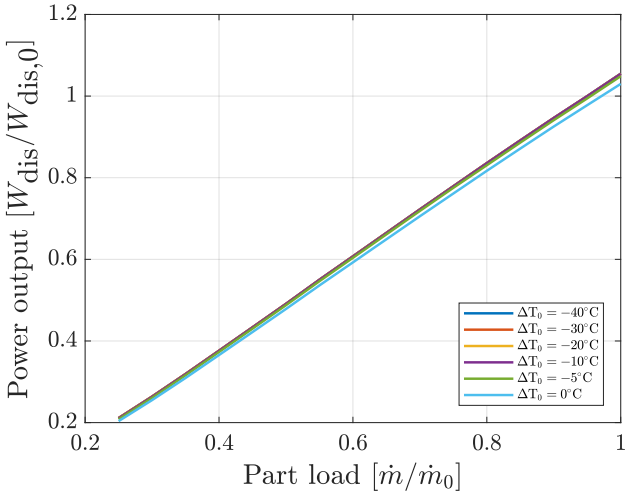

Figure 31: Power output of a discharging solar-PTES cycle as a function of part load and ambient temperature.

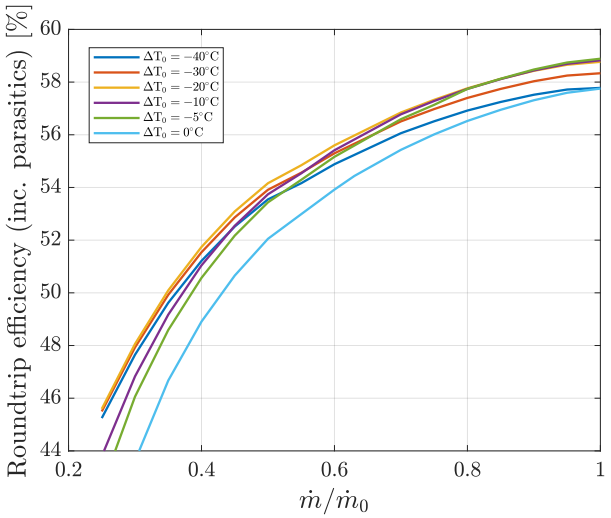

Figure 32: Round-trip efficiency of a solar-PTES cycle as a function of part load and ambient temperature.

5.3.3 Subtask 3.3: Combine Technical and Economic Models

The development of technical and economic models enables comprehensive techno-economic evaluations of PTES and solar-PTES technologies. In this section, some key techno-economic results are presented.

5.3.3.1 Ideal-Gas Joule-Brayton PTES Cycles

The heat exchanger design has a significant influence on the performance of this PTES system, since heat exchangers are required to transfer energy into and out of the storage, and also within the cycle itself. The heat exchanger is characterized by the effectiveness and fractional pressure

loss. All heat exchangers are assumed to have the same ε and f_p, with the exception of the air-cooled heat exchangers, which have fixed values of $\varepsilon = 0.9$ and $f_p = 0.1\%$.As expected, the round-trip efficiency increases monotonically with effectiveness and fractional pressure loss, as shown in Figure 33.

For a typical effectiveness of 85% the round-trip efficiency is only 40%. Reaching a round-trip efficiency over 55% requires an effectiveness greater than 95% and very low pressure losses. Such heat exchangers will require very large heat exchange areas and may present engineering challenges. The large heat exchange area leads to increased capital costs. However, Figure 33 indicates that the increased efficiency is worth the increased cost up to $\varepsilon = 0.95$ since a minimum LCOS occurs at this point. Increasing the effectiveness further leads to a sharp increase in LCOS as the limit of infinite heat exchanger area is approached at $\varepsilon = 1$. The value of ε that minimizes the LCOS will depend on project finances and projected lifetimes.

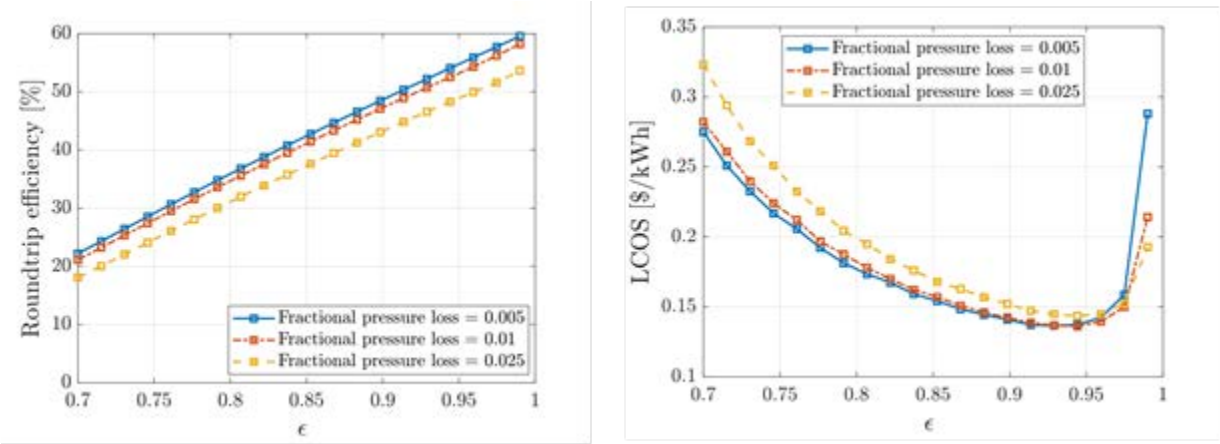

Figure 33: Influence of heat exchanger effectiveness and pressure loss on PTES round-trip efficiency and LCOS.

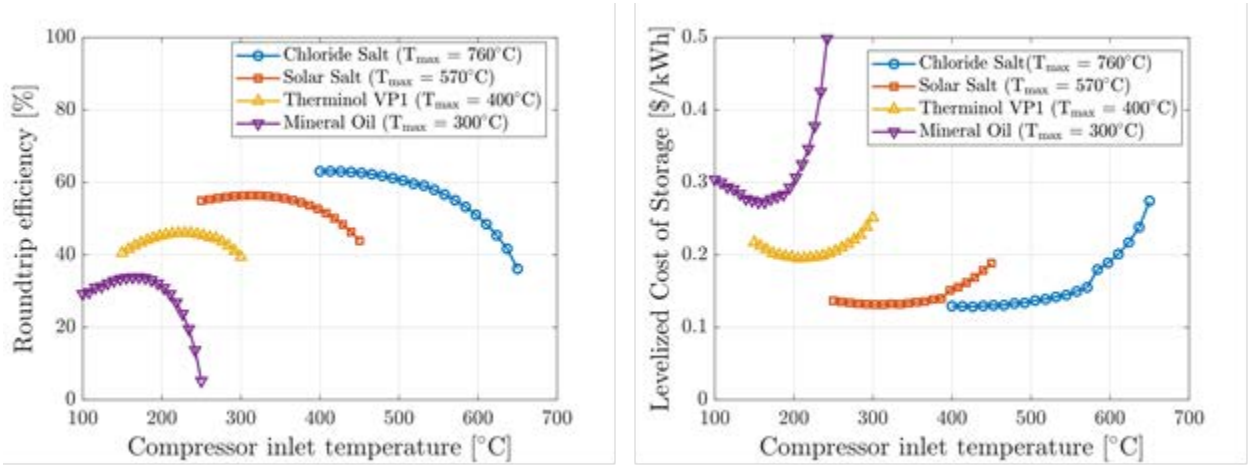

Figure 34: Effect of compressor inlet temperature on round-trip efficiency (left) and LCOS (right) for several hot storage fluids. In each case, the maximum temperature is held constant. Increasing the compressor inlet temperature reduces the pressure ratio and the temperature difference between the two hot tanks.

Another influential parameter is the maximum temperature of the cycle, which is typically constrained by the choice of storage fluid. Previous work has shown that increasing the maximum temperature of a PTES cycle leads to higher round-trip efficiencies and energy densities. However, operating at high temperatures is challenging because the yield strength of stainless steels reduces significantly above 600°C which then requires the use of more expensive materials in the heat exchangers, such as nickel alloys.

In this analysis we consider the use of four fluids for the hot storage media to examine the trade-off between efficiency and cost. Mineral oils and synthetic fluids (such as Therminol VP1) are limited to maximum temperatures of 300°C and 400°C, respectively, and carbon steels are suitable materials for systems that use these fluids. Nitrate molten salts have a maximum temperature of 560°C which requires the use of stainless steel in the hot heat exchanger between the molten salt and the power cycle. The material for the recuperator depends on the compressor inlet temperature, and stainless steels are used when this temperature is above 400°C. Carbon steels are used for the cold heat exchanger. Chloride molten salts may be operated up to 750°C, and the hot heat exchanger is therefore be constructed from nickel alloys. The recuperator is constructed from stainless steel unless the compressor inlet temperature is greater than 600°C, in which case nickel alloy is used. Carbon steel is used for the cold heat exchanger. In each case, it is assumed that the hot storage tanks are internally insulated, and that the temperature measured at the containment wall is low enough for carbon steels to be used.

The data in Figure 34 shows that, as expected, higher efficiencies can be achieved by using fluids that enable higher maximum cycle temperatures. An optimal compressor inlet temperature exists – note that this temperature is approximately equal to the lowest temperature of the hot fluid. This optimal value is primarily the result of the heat engine behavior. Typically, increasing the compressor inlet temperature increases the heat engine efficiency because heat is added at a higher average temperature. However, at very high compressor inlet temperatures, the heat engine efficiency decreases. This occurs in order to satisfy constraints on the energy storage cycle – namely to ensure that the storage fluids are returned to their original temperatures.

The LCOS captures the trade-off between cost and efficiency: higher costs increase the LCOS while higher efficiencies reduce it. It can generally be seen that increasing the compressor inlet temperature increases the LCOS; despite increasing the efficiency, higher compressor inlet temperatures lead to lower energy densities and therefore larger storage tanks and fluid volumes.

Figure 34 indicates that the relatively low efficiencies of cycles using mineral oils and synthetic oils lead to a high LCOS despite the use of lower-cost carbon steel in all heat exchangers. Using nitrate salts increases the maximum cycle temperature to 560°C and leads to large round-trip efficiencies and higher energy densities and as a result the LCOS reduces to around 0.131 ± 0.03 $/kWh$_e$ despite the use of stainless steel in the hot heat exchanger. (The ± term indicates plus or minus one standard deviation). The LCOS increases steeply above 400°C since stainless steel is used in the recuperator. Significant round-trip efficiency improvements are achieved by using chloride molten salts at 750°C rather than nitrate molten salts. However, these improvements do not translate into LCOS reductions due to the high relative cost of nickel alloys in the hot heat exchanger and recuperator, see Figure 35. In this example, the minimum LCOS is around 0.129 ± 0.03 $/kWh$_e$, although it should be noted that these results are very similar given the magnitude of the uncertainty.

These results appear to suggest that there is limited potential benefit from using chloride molten salts rather than nitrate molten salts. However, it should be noted that these cycles have not been optimized and further performance and cost enhancements may be achievable. Furthermore, the uncertainties are rather large and more detailed engineering assessments may be worthwhile.

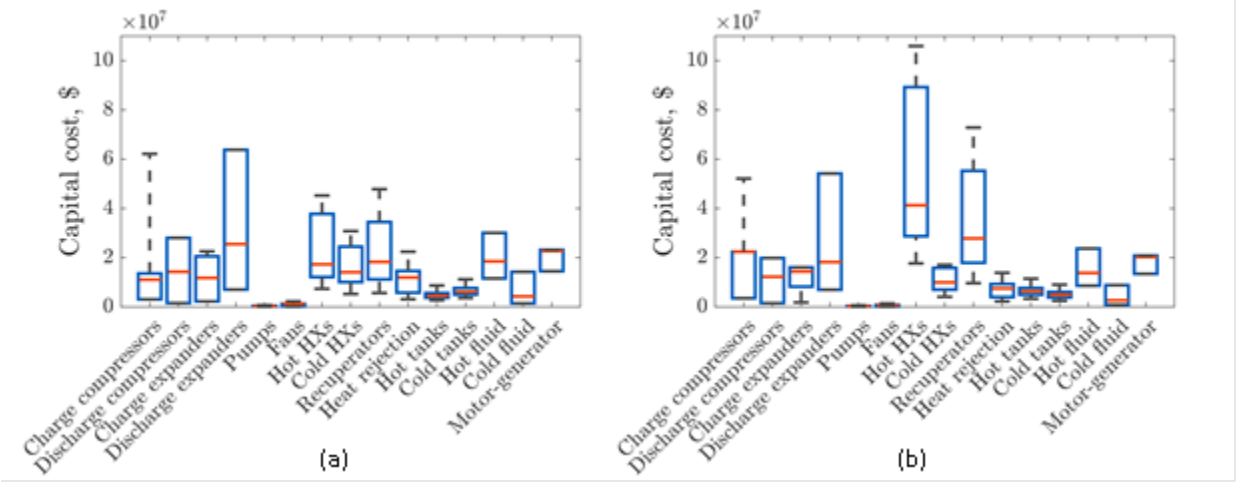

Figure 35: Distribution of component costs for ideal-gas PTES with (a) nitrate molten salt storage (b) chloride molten salt storage.

5.3.3.2 Supercritical CO_2 Joule-Brayton PTES Cycles

PTES systems that make use of recent developments in supercritical-CO_2 power cycles are also of interest. Some results for sCO_2-PTES cycles using various hot storage fluids are shown in Table 5. These results indicate that sCO_2-PTES cycles are slightly less efficient than ideal-gas PTES cycles which is primarily due to the large quantity of heat that must be recuperated within the cycle and the difficult fluid properties. A different set of cost correlations which were specifically designed for sCO_2 cycles are used, primarily based on Refs. [27,46]. The component cost distribution in Figure 37 shows that many sCO_2 components are expected to be more expensive than the corresponding ideal-gas PTES component (Figure 35). Thus, while sCO_2-PTES cycles have higher costs and LCOS than ideal-gas PTES cycles, it remains to be seen whether further developments of sCO_2 components will lead to more competitive costs.

These results again indicate that using chloride molten salts leads to efficiency gains which are outweighed by the increased heat exchanger costs leading to a higher LCOS. In this analysis, the sCO_2-PTES systems using molten salts have two recuperators and a recompressor in order to improve the heat transfer efficiency, as illustrated in Figure 36. The mineral oil system has only a single recuperator and no recompressor – the aim of this system is to reduce system cost. However, it can be seen from Table 5 that these cost reductions are limited, and the low round-trip efficiency leads to a very high LCOS. Future work on low-temperature sCO_2 cycles should concentrate on low-cost ways to increase the system efficiency, such as investigating transcritical-CO_2 cycles. Future work on high-temperature sCO_2 cycles should investigate how to optimize the recuperation and recompression stages, as well as making some predictions about how the system cost will change.

Table 5: Performance and Costs of Joule-Brayton and sCO_2 PTES Cycles Using Different Hot Fluids To Reach Different Maximum Temperatures

Data corresponds to the minimum LCOS shown in Figure 34. Costs are the mean value plus or minus the standard deviation.

		Joule-Brayton PTES			sCO_2 PTES		
Hot fluid		**Mineral Oil**	**Nitrate molten salt**	**Chloride molten salt**	**Mineral Oil**	**Nitrate molten salt**	**Chloride molten salt**
T_{max}	°C	300	570	750	300	570	750
COP	-	1.56	1.29	1.20	1.29	1.18	1.10
Heat engine efficiency	%	22.0	43.8	52.4	26.4	44.9	53.9
Round-trip efficiency	%	33.7	56.3	63.1	34.0	53.3	59.4
Cost per unit energy	$/kWh$_e$	655 ± 194	252 ± 68	268 ± 75	1549 ± 660	667 ± 280	857 ± 414
Cost per unit power	$/kW$_e$	6491 ± 1826	2522 ± 686	2673 ± 752	7766 ± 3311	5920 ± 2482	7267 ± 3513
LCOS	$/kWh$_e$	0.273 ± 0.070	0.131 ± 0.033	0.129 ± 0.033	0.515 ± 0.194	0.248 ± 0.084	0.287 ± 0.117

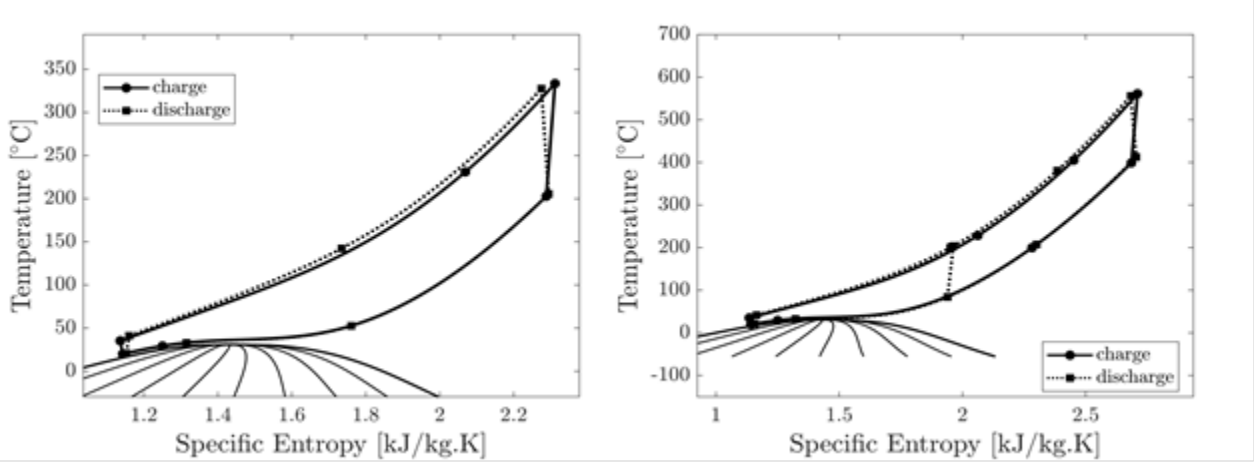

Figure 36: Temperature-entropy diagrams for sCO_2-PTES cycles. Left: system using mineral oil as the hot storage and one recuperator. Right: system using nitrate molten salts as the hot storage, two recuperators, and a recompressor.

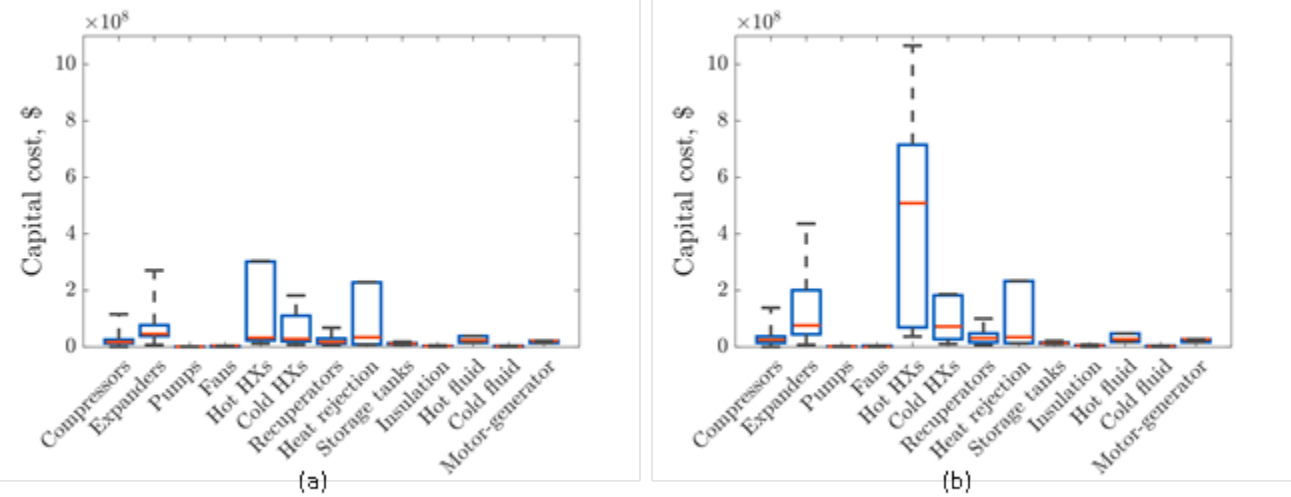

Figure 37: Distribution of component costs for sCO_2-PTES with (a) nitrate molten salt storage (b) chloride molten salt storage.

5.3.3.3 *Uncertainty of Cost Estimates*

Multiple correlations are used to estimate the cost of each component, and therefore the total capital cost and levelized cost of storage, as described in Section 5.2.1. These aggregated costs therefore follow a probability distribution, from which statistics can be obtained. Figure 38 shows the frequency distribution of the LCOS for ideal-gas and sCO_2 PTES systems which may use nitrate molten salts or chloride molten salts as the storage fluid. These distributions illustrate the range of expected values, which is generally quite broad. It is notable that sCO_2-PTES has a much wider range of expected costs than ideal-gas PTES, which illustrates the larger uncertainty of sCO_2 component costs.

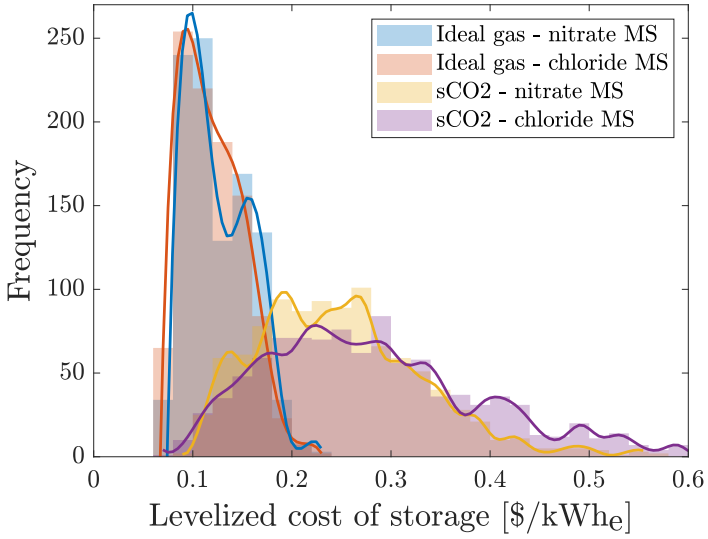

Figure 38: Distribution of LCOS estimates for ideal-gas and sCO_2 PTES systems using either nitrate molten salts or chloride molten salts.

5.3.3.4 Solar-PTES: Retrofit Steam-Rankine CSP Plant With a Joule-Brayton Heat Pump

To recap, this system comprises an existing CSP plant which includes a steam-Rankine power block and nitrate molten salt thermal storage. Preliminary results generated early in the project suggested that this system could achieve round-trip efficiencies on a similar order of magnitude to ideal-gas Joule-Brayton PTES cycles.

As described above, the thermo-economic modeling methodology was subsequently improved. A key advancement is the modeling of off-design Rankine cycle performance: when the cold storage is discharged it is used to reduce the condenser temperature and pressure. As a result, the steam turbine is operated at an off-design condition, since it is typically designed for an ambient temperature of 45°C.

Another small update is the inclusion of an "intermediate fluid loop" between the heat pump cycle and the cold storage, as shown in Figure 39. The aim is reduce the cost of the cold storage as much as possible, and therefore the most suitable fluid is water. However, the heat pump generates temperatures below the freezing point of water which could lead to ice build-up in the heat exchangers, even if the bulk of the water is not cooled to below freezing. Therefore, an intermediate fluid such as glycol is used. This fluid is cooled down by the heat pump and then this fluid cools down the water to the required temperature. Thus, ice build-up is avoided while also reducing the quantity of expensive heat transfer fluids significantly.

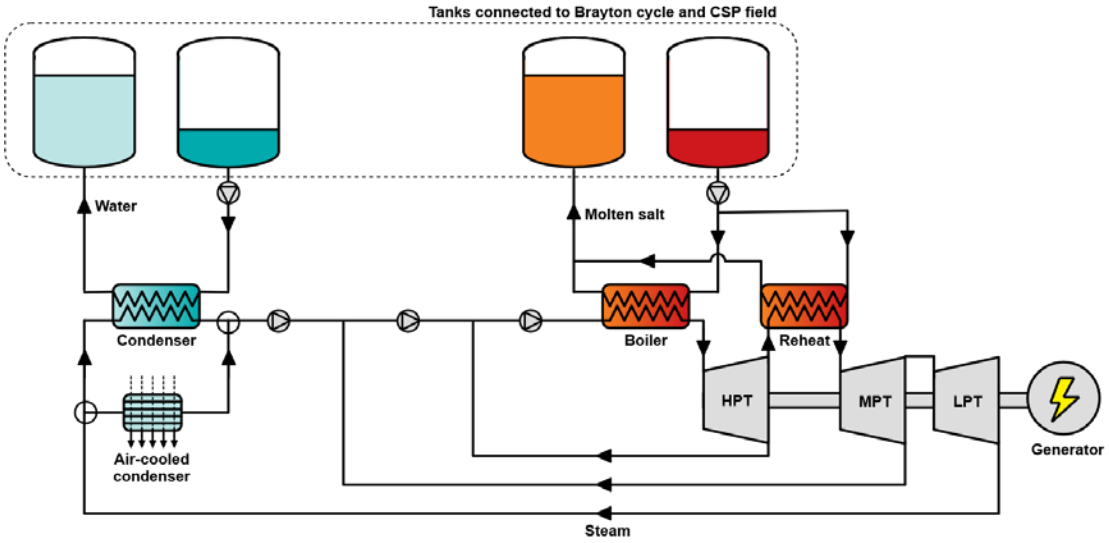

Figure 39: Schematic layout of the steam Rankine cycle. The power cycle is modified so that steam may be condensed by the cold storage tanks (if available) or by ambient air.

A major modification to the existing steam Rankine cycle is the use of cold storage during discharge to improve the power cycle performance. As shown in Figure 39, when discharging the cold storage, a second water-cooled condenser is used, since it is assumed that the existing power cycle uses an air-cooled condenser. The cold storage is typically at temperature substantially below ambient temperature. In theory, the temperature of the water-cooled condenser can be chosen. The effect of this condenser temperature – i.e., the quantity of cooling provided from the cold storage – is briefly now discussed.

Figure 40 illustrates how the round-trip efficiency of the solar-PTES system depends on the condenser temperature. Reducing the condenser temperature initially leads to an increase in round-trip efficiency because heat is rejected at lower temperatures in the power cycle. Increasing the number of expansion stages in the heat pump also improves performance, as this increases the COP and also generates less-cold temperatures in the cold storage, thereby improving heat exchange between the cold storage and the power cycle.

However, it is notable that as the condenser temperature continues to reduce, the round-trip efficiency reaches a maximum and then also reduces. This is because the cold storage is depleted before the hot storage[3]. The remaining heat from the hot storage drives the power cycle, but heat must be rejected to the environment rather than to lower temperatures. Cooling the condenser to lower temperatures requires a higher mass flow rate of cold storage fluid, therefore depleting the storage more quickly, as shown in Figure 41. Consequently, reducing the condenser temperature increases the heat engine efficiency (and thus, round-trip efficiency) while cold storage is available, but by depleting the cold storage more quickly, the average round-trip efficiency ultimately decreases. Thus, a trade-off exists in the optimal temperature of the cold storage and the rate at which it is deployed to the power cycle.

Note that in this example, the condenser temperature is allowed to decrease to low temperatures which correspond to low condenser pressures. In practice, the condenser pressure may have a lower limit – as the condenser pressure reduces the steam velocity at the turbine exit increases, leading to an "exhaust loss." Table 6 presents results for a solar-PTES system with a minimum condenser pressure of 0.05 bar. The round-trip efficiency is reasonably good considering that different power cycles are used in charge and discharge. Using multiple expansions during the charging heat pump leads to a small increase in performance. However, the capital cost also increases, and as a result, the LCOS is larger when multiple expansions are used.

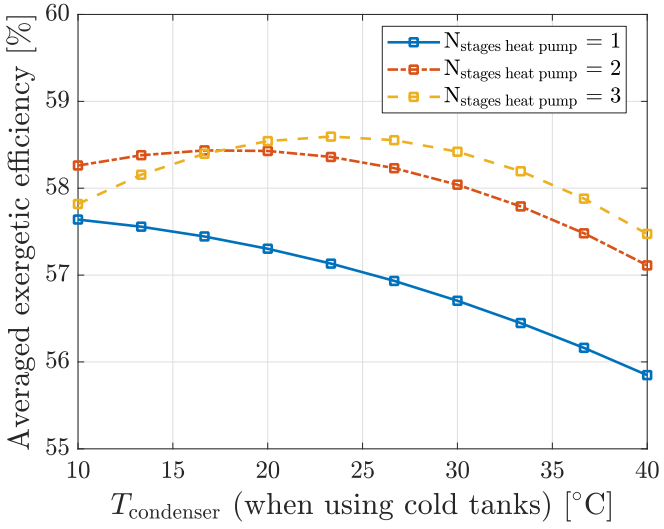

Figure 40: Round-trip efficiencies of a solar-PTES system as a function of the cooling temperature provided to the steam-Rankine cycle.

[3] This is a result of using different power cycles for charge and discharge and is not a feature of most PTES systems.

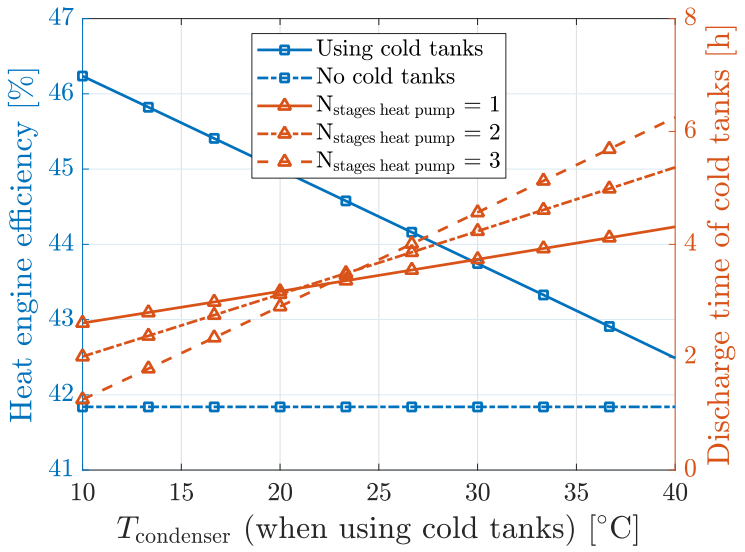

Figure 41: Effect of the condenser temperature on the efficiency of the steam turbine and the duration for which which cooling is available.

The cost and LCOS of retrofitted systems is slightly cheaper than that of stand-alone PTES systems – for instance, compare Table 6 with Table 5. This suggests that retrofitting an existing system with a heat pump could be a cost-effective approach to demonstrating PTES technology. Furthermore, this system would also have the ability to produce renewable power as a result of the concentrating mirrors. It is also interesting to evaluate the cost of a "new-build" solar-PTES system. In this case, the steam-Rankine cycle and molten salt storage also needs to be installed, as well as the heat pump and cold storage. (In assessing these costs, the solar field is not included, since only the electrical energy storage capability is being evaluated). The results in Table 6 indicate that a new build has a higher capital cost and LCOS than a stand-alone PTES cycle. PTES shares heat exchangers between the charging and discharging cycles, since the same type of power cycle is used. However, the solar-PTES system has separate power cycles for charge and discharge, as well as a slightly lower round-trip efficiency. These results suggest that PTES systems are preferable to solar-PTES systems for new-build applications. However, this does not include the potential value that the system could obtain from renewable power generation.

Table 6: Techno-Economic Results for a Solar-PTES Plant

"Retrofitted" plants do not include the cost of the molten salt storage and steam turbine, whereas "new-build" plant costs do. Results are for a 100 MWe steam plant with 10 hours discharging duration. Costs indicate the mean value and standard deviation.

			Case 1	Case 2	Case 3
Number of expansions			1	2	3
Polytropic efficiency		%	90	90	90
Heat exchanger effectiveness			0.97	0.97	0.97
Round-trip efficiency		%	55.6	57.7	57.9
Energy density		kWh_e/m^3	15.4	14.7	12.6
Capital cost	Retrofit	M$	204 ± 65	223 ± 67	288 ± 79
	New-build	M$	359 ± 90	375 ± 92	444 ± 104
Cost per unit power	Retrofit	$/$kW_e$	1934 ± 614	2107 ± 628	2757 ± 754
	New-build	$/$kW_e$	3419 ± 853	3555 ± 872	4269 ± 1004
Cost per unit energy	Retrofit	$/$kWh_e$	193 ± 61	210 ± 63	274 ± 75
	New-build	$/$kWh_e$	340 ± 85	354 ± 87	424 ± 100
Levelized cost of storage	Retrofit	$/$kWh_e$	0.124 ± 0.03	0.127 ± 0.03	0.144 ± 0.04
	New-build	$/$kWh_e$	0.165 ± 0.04	0.166 ± 0.04	0.186 ± 0.04

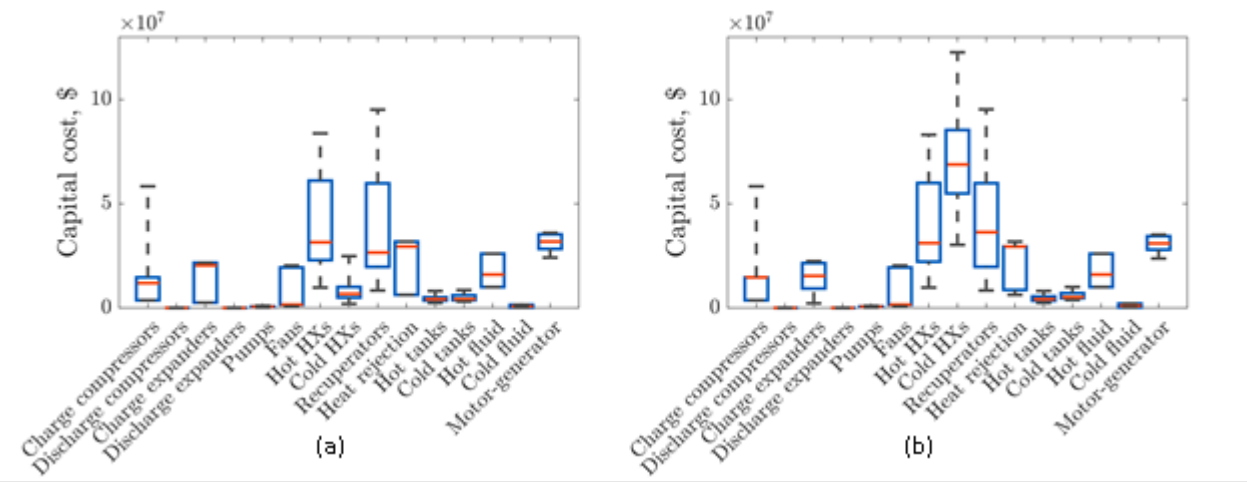

Figure 42: Distribution of component costs for solar-PTES with (a) 1 stage of expansion in the heat pump (b) 3 stages of expansion in the heat pump. (Note that the discharge compressor and discharge expander costs are zero, since the steam cycle already exists.)

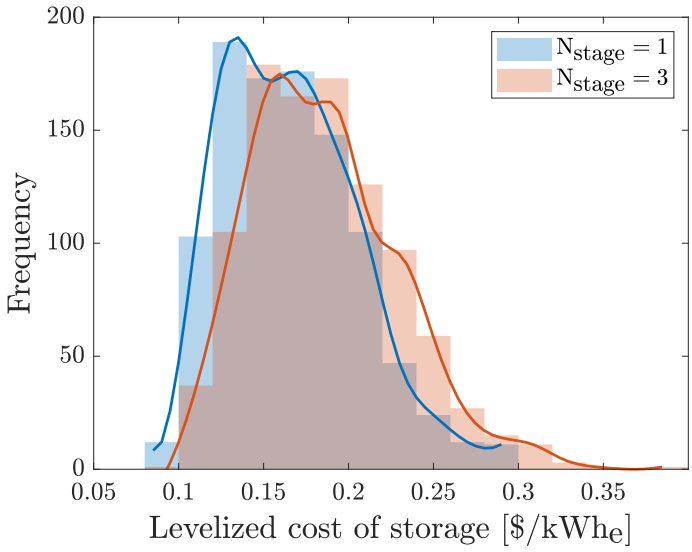

Figure 43: Distribution of LCOS estimates for solar-PTES with either one or three stages of expansion in the heat pump.

5.3.3.5 Time-Shifted Recompression sCO_2 Power Cycle

The Time-Shifted Recompression sCO_2 (TSRC-sCO_2) solar-PTES power cycle was introduced in section 5.1.2.2, as a method of conceivably retrofitting an sCO_2-recompression CSP plant. This system is a Category 3 solar-PTES[4] which requires heat from storage which is generated by both solar energy and electricity. In this concept, high temperature heat is provided by solar energy, while the heat pump charges a lower temperature storage.

While sCO_2 recompression cycles can achieve reasonably good efficiencies, it is notable that the requirement for a recompressor has a significant impact on the performance as it consumes roughly 30-40% of the work input. The recompressor could instead be used as the compressor in the charging heat pump of a PTES device. In this case, electricity at low-value periods is used to drive the heat pump and store the medium temperature thermal energy. During periods of high-value electricity, the solar heat in the molten salt storage is discharged through the sCO_2 cycle. However, the recompressor is bypassed so that the additional heat requirement for recuperation is gathered from the medium temperature storage. As a result, the net work output at high-value periods is larger than with a conventional sCO_2 recompression cycle. By changing the time at which the recompressor operates, this cycle has been dubbed the "time-shifted recompression" (TSRC) sCO_2 cycle.

Schematic cycle layouts are shown in Figure 44. The charging heat pump is a closed cycle; therefore an expander and cold storage are also required in addition to the recompressor and medium temperature storage. Unlike the above heat pumps, this cycle is not recuperated. A suitable fluid for the medium temperature storage is mineral oil, while water can be used for the cold storage. The discharging cycle is similar to an sCO_2 recompression cycle, albeit with some important differences. In a recompression cycle, the low-pressure flow splits after the low-temperature recuperator. One fraction goes through the heat rejection system, the pump and the

[4] See Section 5.1 for this definition

low-temperature recuperator, while the other fraction is re-compressed. The two fractions mix before entering the high-pressure side of the high-temperature recuperator. In the proposed cycle, all the low-pressure fluid goes through pump. The flow then splits with one fraction going through the high-pressure side of the low-temperature recuperator, and the rest being heated by the medium-temperature storage. The flows mix before entering the high-pressure side of the high-temperature recuperator. Another difference is that the flow splits before the heat rejection system. One fraction uses the atmosphere as a heat sink, while the other fraction uses the cold storage. The flows then mix before the pump. As a result, this cycle requires some modifications to the sCO_2 recompression cycle and a larger pump may be necessary.

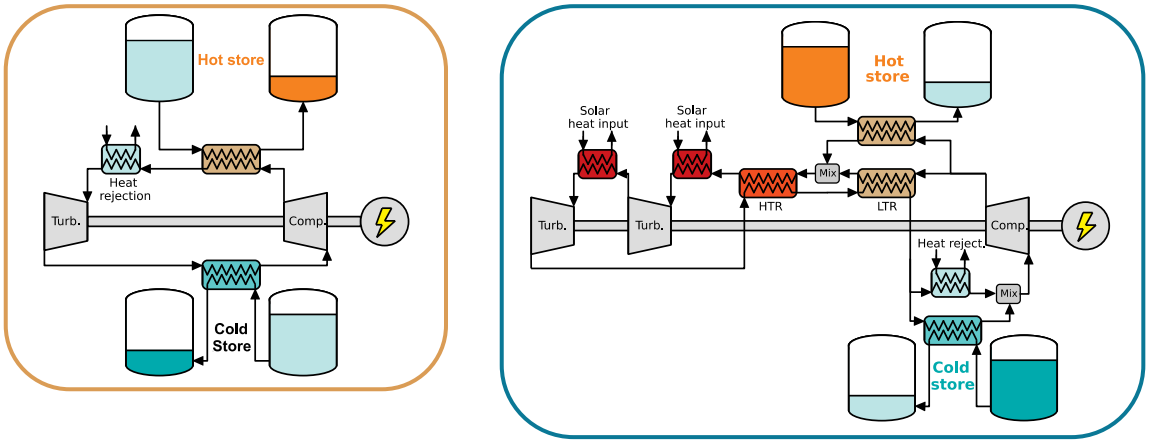

Figure 44: Schematic layout of the (a) charging and (b) discharging cycles for a time-shifted recompression sCO2 power cycle.

Additional metrics were defined for this cycle in section 5.1, and to recap, these are the exergetic efficiency and net efficiency, which are given by

$$\eta_{rt,x} = \frac{W_{\text{dis}}}{W_{\text{chg}} + \Delta \text{Ex}_{\text{solar}}} \tag{11}$$

$$\eta_{\text{net}} = \frac{W_{\text{dis}} - W_{\text{chg}}}{Q_{\text{solar}}} \tag{12}$$

The net efficiency effectively compares the storage system to a conventional solar heat engine under the assumption that the value of electricity is always constant. However, the TSRC-sCO_2 system may be able to take advantage of electricity price fluctuations as well as providing electricity storage services.

Results for a TSRC-sCO_2 cycle are compared to an equivalently sized recompression (RC) sCO_2 cycle in Table 7. These systems use nitrate molten salts for the hot storage and are therefore limited to maximum temperatures of 565°C. By avoiding the recompression during discharge, the power cycle increases the net power output during discharge by nearly 8%, which corresponds to the heat engine efficiency increasing from 45.5% to 49.0%. The TSRC-sCO_2 represents a good use of grid electricity since high values of exergetic round-trip efficiency are achieved (72.9%). On the other hand, consuming grid electricity during charge reduces the net

work dispatched to the grid over a single charge-discharge cycle. As a result, the net efficiency is somewhat lower than the conventional RC-sCO_2 cycle. This implies that the TSRC-sCO_2 cycle generates less work per unit of solar heat than the conventional cycle. Therefore, the benefit of providing electricity storage services and being able to take advantage of price fluctuations should be considered.

Economic results are also presented in Table 7. These values assume that a CSP plant has already been installed with an RC-sCO_2 power cycle and molten salt storage. Therefore, the cost only includes the cost of the medium temperature and cold storage, the charging expander, a heat rejection unit, a motor, and additional pumping during discharge. It is assumed that solar heat is stored at the same time that the charging heat pump operates: if it is economically preferable to store electricity, then it is unlikely that the discharging power cycle would dispatch electricity to the grid. As a result, the solar heat in the molten salt storage is assumed to be "free" and does not incur a cost. Thus, the energy output from the system (used in the LCOS calculation) considers all the electricity generated during discharge. Consequently, the TSRC-sCO_2 cycle achieves very low *energy storage* costs and this system appears to be competitive with other electricity storage systems.

A thorough economic assessment should also consider the cost of the CSP system, sCO_2 power block, and molten salt thermal storage, as well incorporating the renewable electricity dispatched to the grid. Calculating the *value* that this combined generation and storage system provides to the grid would provide a more meaningful evaluation of its potential than just considering the cost of the components.

Table 7: Results Comparing the Performance of a Conventional sCO_2 Recompression Cycle With a Time-Shifted Recompression sCO_2 Cycle

		sCO_2	TSRC
Charging power input, $\dot{W}_{\text{net}}^{\text{chg}}$	kJ/kg	-	15.8
Discharging power output, $\dot{W}_{\text{net}}^{\text{dis}}$	kJ/kg	100.0	107.8
Heat engine efficiency, η_{HE}	%	45.5	49.0
Exergetic roundtrip efficiency, $\eta_{rt,x}$	%	-	72.9
Net efficiency, η_{net}	%	45.5	41.8
Capital cost per unit energy discharged	$/kWh$_e$	-	100.8±30
LCOS	$/kWh$_e$	-	0.032±0.011

5.3.3.6 Comparison of Costs With Other Storage Technologies

It is challenging to assess the meaning of the LCOS without comparing the values shown here to a reference point. However, cost estimates for storage technologies vary substantially throughout the literature. Several estimates for leading technologies, such as lithium-ion batteries and pumped hydro-electric storage (PHES), are shown in Table 8. Often these costs are calculated for systems with four hours of storage. However, it is likely that PTES and solar-PTES systems are most suitable for longer durations around 10 hours. Therefore, the cost estimates shown in Table 8 are not directly comparable, especially since different duration storage systems may be used for different applications. However, this data has some value as it gives an indication as to what current storage costs are considered to be commercially competitive – especially when considering technologies that are currently being deployed such as Li-ion batteries and PHES.

Table 8: Costs for Several Energy Storage Technologies From the Literature

Technology	Storage duration, h	Storage power, MW_e	Efficiency, %	Cost, $/kW$_e$	Cost, $/kWh$_e$	LCOS, $/kWh$_e$	Refs.
PTES	5.75	2	75[a]	2990 - 6090	530 - 1080	0.20-0.65	[47]
PTES	10	1.6	52-72	-	-	0.08-0.12	[48]
JB-PTES[b]	10	100	56	1900-3100	190-310	0.10-0.16	Here.
sCO_2-PTES[b]	10	100	53	3500-8300	400-960	0.16-0.32	Here.
Solar-PTES[g]	10	100	56	1300-2500	130-250	0.09-0.15	Here.
Solar-PTES[h]	10	100	56	2600-4200	260-420	0.12-0.20	Here.
TSRC-sCO_2	10	100		700-1300	70-130	0.02-0.04	Here.
LAES	4	12	31-55	1430-2730	350-670	0.14-0.46	[47]
LAES	5	50	-	2000	400	-	[49]
Li-ion BES	4	100	87-90	1140-1810	285-453	0.204-0.298	[50]
Li-ion BES	4	100	95	3182-4922[c]	782-1231[c]	0.26-0.42[d]	[51]
Li-ion BES	10	100	95	7682-12167[c]	768-1217[c]	-	[51]
Li-ion BES	-	-	-	-	280-400[e,f]	-	[52]
V-FB	4	100	74-77	1420-2360	355-590	0.257-0.390	[50]
Zn-FB	4	100	67-70	1800-2070	450-518	0.267-0.300	[50]
PHES	4	100	76	692-1468[c]	173-367[c]	0.06-0.10[d]	[51]
PHES	10	100	76	761-1606[c]	76-160[c]	-	[51]
PHES	-	-	-	-	280[e]		[52]
AA-CAES	4	100	70	1226-1963[c]	306-491[c]	0.08-0.13[d]	[51]
AA-CAES	10	100	70	1399-2222[c]	140-222[c]	-	[51]

[a] Assumes compressor and expander efficiencies of 98% (reciprocating devices)
[b] Using nitrate molten salts for the hot storage, see Figure 34 and Table 5. Costs shown range from the mean minus one standard deviation to the mean plus one standard deviation.
[c] Calculated here based on values given in Table 6 of Ref. [51].
[d] Based on 2016 values
[e] This is the price per unit energy *capacity* rather than unit energy *discharged*
[f] Extrapolation of current costs using learning curves. Results are for "stationary storage" which encompasses Li-ion batteries and other types of large scale storage systems.
[g] Costs are for retrofitting a CSP plant with a heat pump and cold storage
[h] Costs are for a new-build solar-PTES system but do not include the cost of the solar field
Abbreviations: PTES (pumped thermal energy storage), JB (Joule-Brayton), LAES (liquid air energy storage), Li-ion BES (Lithium-ion battery energy storage), FB (flow battery), PHES (pumped hydro-electric storage), AA-CAES (advanced adiabatic compressed air energy storage).

The data indicates that the estimates made here for PTES costs are in line with other PTES estimates from the literature – some of which are higher, and some of which are lower. Notably, it was recently announced that Highview Power would deploy a 50 MW_e, 250 MWh_e liquid air energy storage (LAES) plant in the UK. LAES has many similarities with PTES, and the quoted cost figures are again in line with the estimates made here [49]. PTES costs are also comparable with other energy storage technologies.

Costs for solar-PTES systems are very competitive with other storage technologies, and values are comparable with PHES. This suggests that retrofitting existing CSP plants with a heat pump may provide the best route to demonstrate this technology on a large scale. There is also the possibility of retrofitting other power generation systems, such as coal plants, with a heat pump, although in this case the cost of the hot thermal storage should be included in the calculations.

The most optimistic Li-ion costs are based on learning curves assuming extensive deployment of this technology. It is unclear how much scope there is for JB-PTES cost reductions since these devices use technologies that have already been widely deployed such as gas turbines. However, sCO_2-type systems have not been widely deployed. Therefore, while the sCO_2-PTES costs presented here are somewhat higher than other technologies, there may be considerable scope for future cost reductions.

5.3.3.7 Annual Calculations

The off-design models allow PTES and solar-PTES systems to be modeled at part-load and with varying ambient temperatures. As a result, annual calculations are possible. Conducting annual calculations will improve estimates of the LCOS as the time-varying efficiency and true number of charge-discharge cycles will be captured. (Currently, LCOS estimates assume that the system operates at its design point and charges and discharges once per day). Furthermore, annual calculations will reveal how the system performs at different parts of the year and may lead to further improvements in system design.

To undertake annual calculations, a realistic load cycle is required, as well as the ambient temperatures at a given location. Under Subtask 5.1, the interaction of PTES and solar-PTES with the electrical grid is being investigated with the software tool PLEXOS. Correlations for PTES and solar-PTES off-design performance have been extracted from the detailed thermodynamic models and have been integrated with the PLEXOS system, as described in Section 5.5.1.

The PLEXOS models also provide other useful data such as yearly load cycles and electricity prices. These load cycles can then be "fed" back into the off-design thermodynamic models to provide another viewpoint of system performance and calculate improved estimates of the LCOS.

Some preliminary load cycles have been extracted from the PLEXOS models, and these are being used to test the operation of PTES and solar-PTES over multiple load cycles. An annual calculation requires the off-design performance of the storage system to be evaluated at each hour, requiring 8760 calculations. The performance at any given hour depends on how the system was operated in previous hours which primarily affects the state-of-charge of the storage systems, but also to a lesser extent the temperature of the storage tanks.

Conducting such a large number of calculations is computationally time-consuming. Therefore, simplifications are being investigated with the aim of decreasing the run time. In Figure 45, the performance of PTES over several load cycles is compared for two different calculation methods. The solid lines show results using the detailed models that fully captured off-design behavior (part-load and ambient temperature). The circles represent a simplified version of the model in which it is assumed that the compressors and expanders operate at their design point efficiency and pressure ratio. This is a good approximation, as the inventory control method for PTES systems leads to the compressors and expanders operating very close to their design point. The main result of this simplification is that a fewer number of iterations are required to reach converged solutions, and the computational runtime reduces significantly. As can be seen from Figure 45, there is very good agreement between these two methodologies.

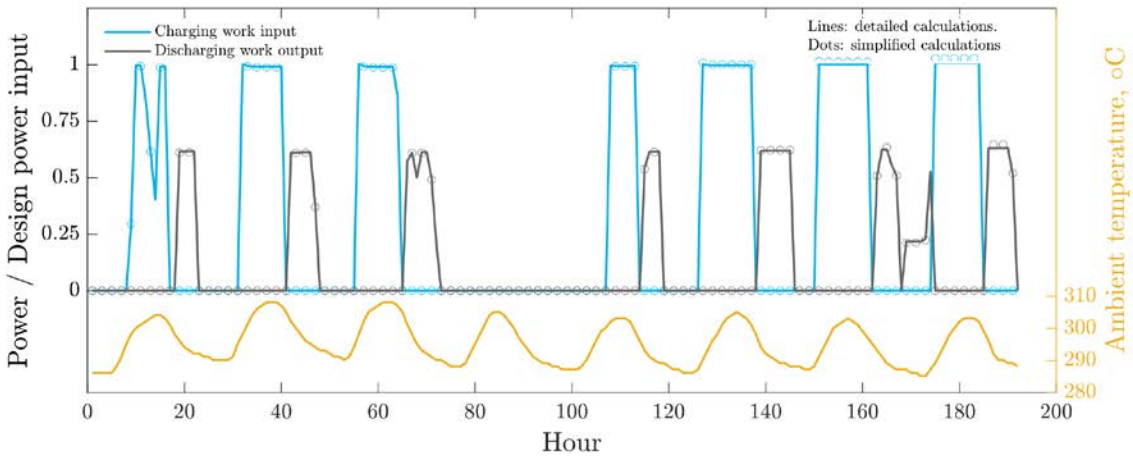

Figure 45: Charging and discharging of PTES to meet load profiles provided by PLEXOS. The figure compares two calculation methods which show good agreement.

5.3.4 Task Milestone

Milestone 4: Generate detailed, transient (time-stepping) thermal storage and power cycle models to minimize exergy losses.

The results presented above describe techno-economic models of PTES and solar-PTES systems. These models capture detailed design features of key components. A Monte-Carlo method is used to assess the uncertainty of economic results. Off-design models are also developed which enables more sophisticated analysis of system behavior.

The exergy destruction within each component can be calculated. The optimization schemes developed in subsequent tasks are used to maximize the system efficiency – i.e., minimize exergy losses.

5.4 Task 4: Multi-Objective Optimization and Future Designs of Solar-PTES Systems

The design of PTES and solar-PTES systems requires numerous design variables to be specified. Performance metrics often conflict with one another – a typical example is high efficiency designs having high capital costs. Therefore, optimization algorithms may be used to computationally find optimal system designs or reveal trade-off surfaces.

Multi-objective optimization problems (MOPs) involve minimizing or maximizing two or more objective functions subjected to constraints. Improvement on one objective may occur at the expense of the other, and hence the goal is to find the best tradeoffs between the conflicting objectives. The mathematical formulation of problems of this nature is defined as follows,

$$\begin{aligned} &\text{Minimize/ Maximise } \boldsymbol{f_m}(x_1, x_2 \ldots . x_n) \text{ Where } m = 1, 2, \ldots, M. \\ &\text{Subjected to } \boldsymbol{g_k}(x_1, x_2 \ldots . x_n) \geq 0 \text{ Where } k = 1, 2, \ldots, K \\ &\boldsymbol{h_l}(x_1, x_2 \ldots . x_n) = 0 \text{ Where } l = 1, 2, \ldots, L \\ &\boldsymbol{x_n^{\text{lower bound}}} \leq \boldsymbol{x_n} \leq \boldsymbol{x_n^{\text{upper bound}}} \; Where \; n = 1, 2, \ldots, N \end{aligned}$$

Here $\boldsymbol{f_m}$ denotes the M multi-objective functions ($f_1, f_2, \ldots, f_M$), that are subjected to K inequality constraints $\boldsymbol{g_k}$ and L equality constraints $\boldsymbol{h_l}$, bound by the minimum and maximum limits of the N independent variables $\boldsymbol{x_n}$.

MOPs can either be solved using classical deterministic algorithms such as weighted sum method and **ε**-constraint method, or stochastic algorithms such as the genetic algorithm [53,54]. Deterministic methods require a knowledge of the minimum and maximum values of objective functions and treats the multi-objective optimization as a special case of single objective optimization by constraining all but one objective. Stochastic algorithms, on the other hand, utilize randomness to search for the best tradeoffs, and converge to a set of best possible solutions known as a Pareto front or Pareto set. A more diverse set of solutions can be found by stochastic algorithms which allows the user to select the desired solution(s).

Several stochastic algorithms such as particle swarm optimization, non-dominated sorting genetic algorithm, ant colony optimization and strength pareto evolutionary algorithm exist to tackle optimization problems, each with its own characteristics [55]. Non-dominated sorting genetic algorithm (NSGA II) has been widely used in many industrial applications involving two objectives (including PTES [56]) but is less effective when there are three or more objectives [57]. Multi-objective particle swarm optimization algorithm (MOPSO) is found to be suitable for two or more objective problems and is relatively simply to execute, but a few constants in the algorithm needs to be tuned to the specific case [58].

NSGA II and MOPSO were tested on the PTES model, and both performed reasonably well. MOPSO was slightly preferred and was used for the rest of this study.

5.4.1 Multi-Objective Particle Swarm Optimization (MOPSO)

Multi-objective particle swarm optimization is a population-based approach that mimics a swarm of birds flocking and schooling in nature. Each entity in the population (a bird) is characterized by its location and velocity which are updated in each iteration based on a local best and the

group's best value of the objective functions. An algorithm based on Coello et al.'s approach that utilizes mutation and an external repository to guide the location and the velocity of the particles is implemented in this study [59]. The velocity and location of each particle in the search space is calculated as follows,

$$V^i(t+1) = W.V^i(t) + c_1 r_1\left[P^i_{\text{best}} - x^i(t)\right] + c_2 r_2\left[G^i_{\text{best}} - x^i(t)\right]$$
$$x^i(t+1) = x^i(t) + V^i(t+1)$$

Here, $V^i(t+1)\ and\ x^i(t+1)$ are the velocity and position of particle i in generation $(t+1)$. $P^i_{\text{best}}$and G^i_{best} are the local and global optimal position in the current generation. W is the inertial component whose value is taken to be 0.4. $c_1$and c_2 are personal and social acceleration coefficient that denotes the extent to which the particles are attracted towards personal and global best, respectively. In this algorithm, $c_1 = c_2 = 2$, and r_1 and r_2 are random numbers.

5.4.2 Multi-Fidelity Modeling

Optimization algorithms may require large computational resources and take a long time to converge. For instance, the MOPSO routine with a population size of 50, implemented on a PTES cycle to optimize efficiency, LCOS and capital cost took 6 hours to solve for 50 generations. To aid in faster convergence to the Pareto front, a method known as *multi-fidelity* modeling is implemented. Firstly, a simplified version of the PTES system is optimized. In this simple model, the heat exchangers' parameters are provided as an input rather than being calculated in each run. This reduces the computation time to one-fourth of what it would take to optimize a detailed PTES cycle. Optimizing the simple PTES model provides an indication as to where in the search space the optimal solutions are located. The parameters corresponding to the Pareto front from the simplified PTES model are then used to seed an initial population for the optimization of the detailed PTES model. This approach reduces the time to find optimal solutions.

5.4.3 Multi-Objective Optimization of Ideal-Gas PTES Cycles

One use of multi-objective optimization algorithms is to identify trade-off surfaces between conflicting objectives, and also to find the optimal system design. These algorithms can also be used to quantify the potential benefits from technological advances. In this section, the use of different hot storage fluids will be compared, as will the effect of placing constraints on the heat exchanger performance.

5.4.3.1 Effect of Storage Fluid on Optimal Designs

Two objectives are optimized:

1. The round-trip efficiency
2. The levelized cost of storage (LCOS)

Selecting the hot storage fluid effectively sets the maximum temperature of the power cycle. Four decision variables are considered:

1. Compressor inlet temperature
2. Discharge pressure ratio

3. Heat exchanger effectiveness
4. Heat exchanger pressure losses

These parameters were allowed to vary between the minimum and maximum limits indicated in Table 9.

Table 9: Constraints for Decision Variables in PTES Optimization

		Minimum	Maximum
Compressor inlet temperature	°C	250 (nitrates) 450 (chlorides)	450 (nitrates) 600 (chlorides)
Discharge pressure ratio		0.8	1.5
Heat exchanger effectiveness		0.7	0.99
Heat exchanger pressure loss	%	0.005	0.05

Analysis in section 5.3.3 indicated that nitrate and chloride molten salts offered significant performance and cost benefits compared to lower-temperature operating fluids. However, while chloride salts had a higher maximum temperature (and therefore round-trip efficiencies) the system cost was higher due to the use of more expensive metals in the hot heat exchanger and recuperator. As a result, the LCOS of systems using chloride salts at 750°C was very similar to that of nitrate salts at 560°C.

Figure 46 shows Pareto fronts for PTES with nitrate and chloride molten salts. The Pareto front illustrates the trade-off between conflicting objectives – it can be considered to show the optimal performance at each trade-off. For instance, at each point, it is not possible to increase the efficiency without compromising the LCOS. Nitrate salts were considered at two maximum temperatures – 560°C and 600°C. The latter represents a scenario where the thermal decomposition temperature of the salt is increased by more effectively sealing the thermal storage. This method has been demonstrated on a small scale [60]. Similarly, results are shown for chloride salts with two maximum temperatures - 650°C and 750°C. Again, the lower temperature is more achievable in the near term, whereas the upper temperature poses greater technical challenges.

The Pareto front indicates that chloride salt systems are able to achieve higher maximum round-trip efficiencies than nitrate salt systems – with maximum values over 70%. Chloride salt systems at 750°C are also able to achieve a lower LCOS than any other system, although nitrate salt systems at 600°C have very similar values. The Pareto fronts of the four cases do not overlap at any point, therefore it is possible to make the following statement:

- Chloride-salt PTES at 750°C is always preferable to:
    - Nitrate-salt PTES at 600°C which is always preferable to:
        - Nitrate-salt PTES at 560°C which is always preferable to:
            - Chloride-salt PTES at 650°C

Here, “preferable” means that for a given round-trip efficiency, the preferred technology can always achieve a lower LCOS. Conversely, for a given LCOS, a preferred technology can always achieve a higher round-trip efficiency.

These results suggest that chloride-salt PTES systems should only be developed if the salt can be operated at its maximum limits. Similarly, there appears to be a measurable benefit to increasing the maximum temperature of nitrate salts, and these technological advances should be pursued.

The second Pareto front in Figure 46 shows uncertainty bands for one nitrate and one chloride molten salt case. These uncertainty bands indicate the LCOS plus or minus one standard deviation. Clearly, the uncertainty is quite significant while the performance of the different systems is similar. It is therefore plausible that the order of the above statements could change when a more detailed engineering cost appraisal is undertaken.

The optimal decision variables for several optimized designs are given in Table 10. The chosen designs are those which obtain the highest round-trip efficiency and the lowest LCOS – essentially the most extreme points on the Pareto front. Interestingly, all designs use very high heat exchanger effectiveness, with a value of 0.95-0.96 minimizing the lifetime cost despite the high initial costs.

It may be concluded that the economic benefits of developing more advanced storage fluids are relatively limited, despite the substantial improvement in efficiency that may be achieved.

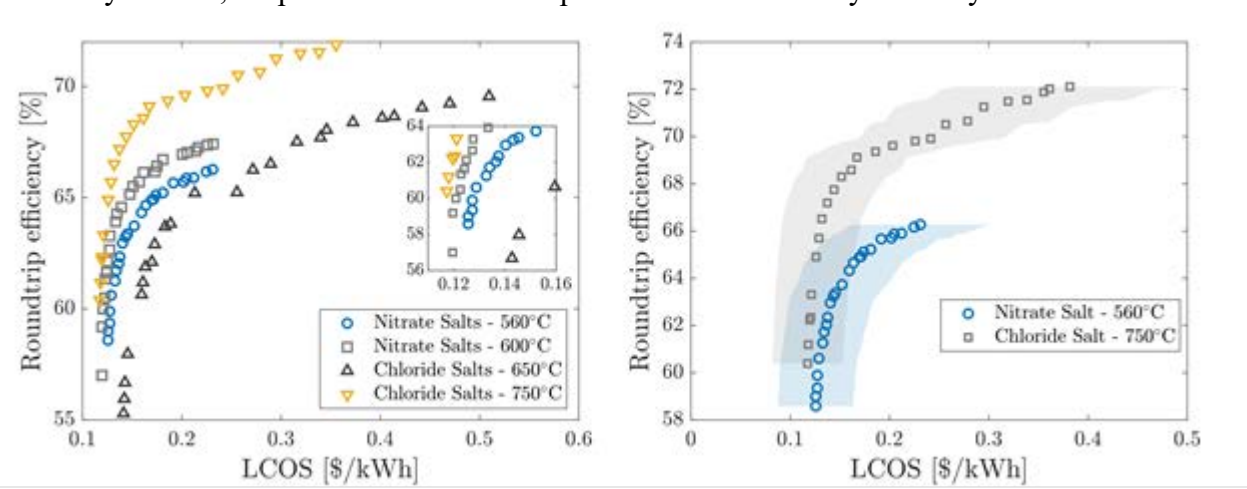

Figure 46: Pareto fronts showing the trade-off between round-trip efficiency and LCOS for PTES system with different maximum temperatures and hot storage fluids.

Table 10: Decision Variables and Results for Optimal PTES Designs With Different Maximum Temperatures and Hot Storage Fluids

		Max. round-trip efficiency		Min. LCOS	
Salt		**Nitrate**	**Chloride**	**Nitrate**	**Chloride**
Compressor inlet temp	°C	370	474	322	455
Discharge PR		1.19	1.25	1.18	1.24
Effectiveness		0.99	0.99	0.96	0.95
Pressure loss		0.005	0.005	0.006	0.012
Round-trip efficiency	%	66.3	72.1	58.6	60.4
LCOS	$/kWh	0.231	0.382	0.126	0.117

5.4.3.2 Effect of Heat Exchanger Design

One of the most important parameters in PTES design is the heat exchanger performance, which has a significant influence on both the round-trip efficiency and the cost. The previous optimization allowed heat exchangers to have a maximum effectiveness of 0.99, and the most efficient systems used this value. Those systems with the lowest LCOS still used a high effectiveness of around 0.96, as shown in Table 10. While these high values are achievable in practice, they are uncommon and are challenging to manufacture.

Several optimizations were conducted with different constraints on the maximum heat exchanger performance. In the previous optimization, the designs that minimized the LCOS still had values of effectiveness over 0.95, because the LCOS incorporates both cost and efficiency information. Therefore, the capital cost was introduced as a third objective in this section. The aim is to find a range of PTES designs, and it is assumed that PTES systems with low effectiveness heat exchangers will achieve the lowest capital costs.

Three heat exchanger scenarios are considered:

1. Heat exchangers with a maximum effectiveness of 0.85, which is typical of conventional technology
2. Heat exchangers with a maximum effectiveness of 0.99, which is the same as the first optimization run. In this case, these heat exchangers are possible but will require specialized design.
3. Heat exchangers with a maximum effectiveness of 0.99 and also have a small hydraulic diameter of 0.2 mm. This corresponds to a compact heat exchanger with microchannels that requires specialized manufacturing processes.

Pareto fronts are presented in Figure 47, and three separate graphs are shown to illustrate each trade-off between the objectives. The optimal decision variables for the extreme points on each Pareto front are presented in Table 11. As would be expected, the higher the allowable effectiveness the better the round-trip efficiency. When the effectiveness is limited to 0.85 then the maximum efficiency is just over 40%. In this case, the Pareto front is a small cluster, and Table 11 indicates that all systems use the maximum allowable effectiveness, even to minimize the LCOS and capital cost. Higher effectiveness systems lead to a lower LCOS than those that have constraints on heat exchanger performance. This suggests that developing high effectiveness heat exchangers is a worthwhile research priority.

Interestingly, it can be seen that increasing the maximum allowable effectiveness can lead to systems with lower capital costs. These PTES systems are constrained to have a discharging power output of 100 MW_e for a duration of 10 hours. When the round-trip efficiency is low the power input to the charging heat pump increases leading to higher turbomachinery costs. Storage volumes increase, and counterintuitively, the heat exchange area can also increase since more heat must be transferred to obtain the required power output.

Consequently, these results suggest that developing high effectiveness heat exchangers can lead to low upfront investment costs, as well as low lifetime costs. It should be noted that the same heat exchanger cost correlations were used in each analysis. It is likely that this is appropriate for

heat exchangers with a maximum effectiveness of 0.85 and 0.99. However, microchannel heat exchangers are likely to be more expensive due to more complicated manufacturing methods.

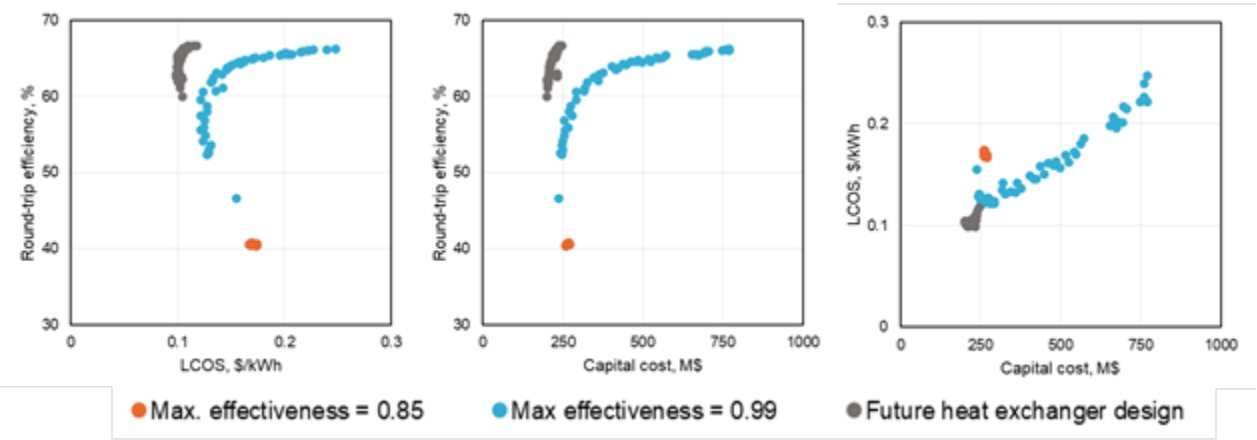

Figure 47: Pareto fronts illustrating the trade-off between round-trip efficiency, LCOS, and capital cost for PTES systems with different maximum allowable heat exchanger performance.

Table 11: Decision Variables and Results for Optimal PTES Designs That Maximize Round-Trip Efficiency, Minimize LCOS, and Minimize Capital Cost

Heat exchanger systems refer to 1: Maximum effectiveness = 0.85. 2: Maximum effectiveness = 0.99. 3: Future heat exchanger designs.

		Max. round-trip efficiency			Min. LCOS			Min capital cost		
Heat exchanger system.		1	2	3	1	2	3	1	2	3
Compressor inlet temp	°C	294	382	380	306	296	250	310	350	296
Discharge PR		0.97	1.19	1.20	0.92	1.28	1.27	0.90	0.91	1.25
Effectiveness		0.85	0.99	0.99	0.85	0.96	0.99	0.85	0.90	0.96
Pressure loss		0.01	0.005	0.005	0.01	0.006	0.005	0.01	0.07	0.005
Round-trip efficiency	%	40.7	66.3	66.7	40.5	59.6	62.6	40.3	46.6	60.0
LCOS	$/kWh	0.170	0.248	0.118	0.168	0.122	0.099	0.173	0.155	0.104
Capital cost	M$	267	770	246	263	292	232	259	239	201

5.4.4 Multi-Objective Optimization of Solar-PTES Cycles

The multi-objective optimization algorithms were also applied to the solar-PTES cycle where an existing steam-Rankine CSP plant is retrofitted with an ideal-gas heat pump. In this case, the thermal storage already exists and is assumed to be a nitrate molten salt. The remaining design variables are:

1. Compressor inlet temperature
2. Number of expansions in charging heat pump
3. Heat exchanger effectiveness
4. Heat exchanger pressure losses

The maximum and minimum values of these parameters is given in Table 12. The analysis above indicated that high-effectiveness heat exchangers were worthwhile, so the maximum allowable effectiveness is constrained to 0.99.

Table 12: Decision Variable Constraints for Solar-PTES Optimization

		Minimum	Maximum
Compressor inlet temperature	°C	250	450
Number of heat pump expansions		1	5
Heat exchanger effectiveness		0.7	0.99
Heat exchanger pressure loss	%	0.005	0.05

Two objectives were optimized: the round-trip efficiency and the LCOS, and the resulting Pareto front is shown in Figure 48. Again, the shape of the Pareto front is dominated by the heat exchanger effectiveness: high values of round-trip efficiency (over 62%) are obtained with an effectiveness greater than 0.98, whereas the lowest LCOS occurs with an effectiveness of 0.92, as indicated in Table 13. Previous analysis suggested that multiple expansion stages led to increased costs that were not justified by the improved efficiency. However, the optimized designs always had at least two expansion stages and indicates that this more complex design can lead to reduced LCOS.

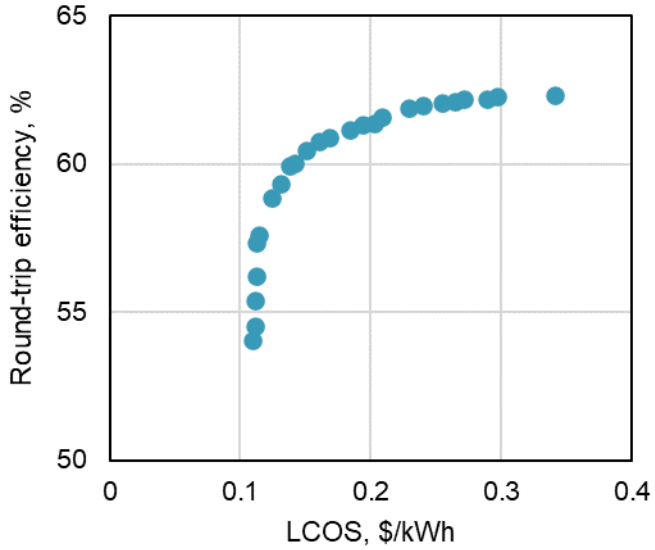

Figure 48: Pareto front for a solar-PTES system illustrating the trade-off between round-trip efficiency and LCOS.

Table 13: Design Variables and Results for Solar-PTES Systems With Maximum Round-Trip Efficiency and Minimum LCOS

		Maximum round-trip efficiency	Minimum LCOS
Compressor inlet temp.	°C	250	284
# expansions		3	2
Effectiveness		0.99	0.92
Pressure loss		0.005	0.005
Round-trip efficiency	%	62.3	54.0
LCOS	$/kWh	0.297	0.110

5.4.5 Task Milestone

Milestone 5: Optimize system design with respect to efficiency and cost.

This milestone required that optimization tools be used to determine how certain technological advances (such as reaching higher temperatures or improving heat exchanger performance) could lead to improvements in cost and performance. It has been shown that higher operating temperatures can lead to more efficient solutions at lower cost. However, the margins between different technologies are relatively small. It was found that the heat exchanger performance is a key factor. Higher effectiveness heat exchangers not only achieved higher round-trip efficiencies and lower LCOS, but in some cases could achieve lower capital costs by reducing the costs of the overall system. Developing low-cost, high effectiveness heat exchangers is a research and development priority for the successful deployment of PTES and solar-PTES.

5.5 Task 5: Assessment and Review of the Value of Solar-PTES Systems

5.5.1 Subtask 5.1: Improve Grid Analysis Models

Analysis has so far concentrated on estimating the cost and performance of PTES and solar-PTES. While the benefit of these systems can be described qualitatively – such as, reducing curtailment of renewables or providing capacity – so far, the role that they may take and the value they could provide has not been quantified.

In this analysis we use commercial production cost modeling software (PLEXOS) to determine the value of a CSP, CSP-PTES or stand-alone PTES system to the grid. Production cost models (PCMs) solve a set of optimization problems that minimize the total cost of satisfying electricity demand and ancillary services requirements by controlling commitment and dispatch schedules of an entire fleet of generators while adhering to constraints on transmission capacity and physical or operational limitations on each generator (for example, minimum and maximum load, allowable ramp rates, minimum up and down times, etc.). The annual operational value of a single entity (e.g., a CSP or PTES system) can be determined by comparing the system-wide annual production cost from simulations before and after the addition of the CSP or PTES system. In this analysis we only consider the value of the CSP or PTES system in the energy market, and do not consider any possible additional ancillary services or capacity value.

Energy value arises from *avoided* generation costs, and thus can be strongly sensitive to the location and grid scenario. Here we utilize representations of two of the interconnections in North America, and consider sub-scenarios within each model to vary photovoltaic (PV) and wind penetration. The first grid scenario describes the Western Interconnection (the synchronous grid comprising the western United States, western Canada, and a small part of Mexico near the California border). The dataset for this model is derived from an open dataset provided by the Western Electricity Coordinating Council's (WECC) Transmission Expansion Planning Policy Committee (TEPPC) 2024 Common Case database [61]. This database contains unit-specific information for approximately 4,000 generators in the Western Interconnection along with transmission network topology, and was heavily modified by NREL as part of the 2030 California Low Carbon Grid Study (LCGS) [62]. We consider placing the CSP-PTES or PTES system in a southern California location with good solar resource and high PV penetration. The second grid scenario describes the Texas Interconnection managed by the Electric Reliability Council of Texas (ERCOT). The model database includes unit-specific information for approximately 1400 generators and transmission network topology, as described in Ref. [63]. We consider a location in western Texas for the PTES system; this region is characterized by high wind resource and generation capacity, and provides significant exports to the high-load regions in the eastern section of the state.

Table 14 provides details on the grid scenarios including fuel price, CO_2 emission cost, and photovoltaic (PV) or wind penetration and curtailment. The grid scenarios and PLEXOS datasets are taken directly from pre-existing studies, with the exception of the LCGS "Higher Solar" scenario in which we simply scale up PV capacity by 20% relative to the "Target High Solar" scenario in Ref. [62]. Figure 49 and Figure 50 illustrate the annual generation mix on both a system-wide basis, and within the local region in which the CSP or CSP-PTES plant will be

placed, as well as the locational marginal price (LMP) for each the Ivanpah, CA and van Horn, TX locations. Annual simulations are carried out with a rolling 48-hour optimization horizon updated every 24 hours. Each 48-hour optimization problem is formulated as a mixed integer linear program (MILP) and solved to a gap of at most 0.075%.

We follow a similar general methodology for incorporating CSP plants in PLEXOS as that described in Refs. [64,65], but increase the level of detail in the implementation and update operational characteristics to describe the CSP-PTES or PTES systems. The model is built on an algorithm in PLEXOS generically designed for pumped-hydro systems, and is customized for the CSP-PTES or standalone PTES system via customized constraints, decision variables, and constrained sets of operational units designed to capture characteristics of the CSP-PTES system that are not easily described within the commercial software package. The hourly inflow of thermal energy to hot storage from the CSP solar field and receiver is simulated via NREL's System Advisor Model (SAM) [66]. The heat pump provides an alternative means of charging the hot storage tank from low-cost grid electricity, and simultaneously charges a cold store that can be later used for heat rejection from the heat engine, thereby increasing the heat engine efficiency during the hours in which the cold store is discharged. Operational decisions regarding the timing of cold storage discharge and the timing and levels of heat engine and heat pump operation are optimized within the production cost model solution.

Table 14: Grid Scenarios

	LCGS			**ERCOT**		
Full model geographical area	Western Interconnection			Texas Interconnection		
CSP-PTES or PTES location	Ivanpah, CA			van Horn, TX		
Weather year	2006			2012		
Annual load (TWh)[a]	1016.1 (129.3)			323.9 (22.1)		
Natural gas price ($/MMBTU)[b]	6.63 (4.54 - 8.29)			4.43 (4.30 – 4.70)		
Coal price ($/MMBTU)[b]	1.96 (0.97 - 3.18)			2.31		
Emissions cost ($/ton)[b]	29.4 (0.0 - 29.4)[c]			0.0		
Annual generation cost ($M)[d]	18770			5980		
Scenario name	**Target**	**Target High Solar**	**Higher Solar**	**Low Wind**	**Mid Wind**	**High Wind**
Annual PV penetration fraction[a]	0.082 (0.306)	0.105 (0.382)	0.115 (0.417)	0.003 (0.002)	0.003 (0.002)	0.003 (0.001)
Annual wind penetration fraction[a]	0.113 (0.175)	0.105 (0.160)	0.105 (0.153)	0.211 (0.794)	0.337 (0.867)	0.434 (0.910)
Annual PV curtailment (GWh)[a]	698 (45)	2665 (609)	6021 (1975)	0.0 (0.0)	5 (1)	21 (4)
Annual wind curtailment (GWh)[a]	191 (12.8)	567 (95)	1090 (279)	275 (91)	4956 (1974)	20286 (10200)

[a] Model-wide (region containing Ivanpah, CA or van Horn, TX)
[b] Model-wide usage-weighted average (range over geographical location and time of year)
[c] No emissions cost for locations outside of CA
[d] Annual generation cost for the LCGS "Target High Solar" and ERCOT "Mid Wind" Scenarios

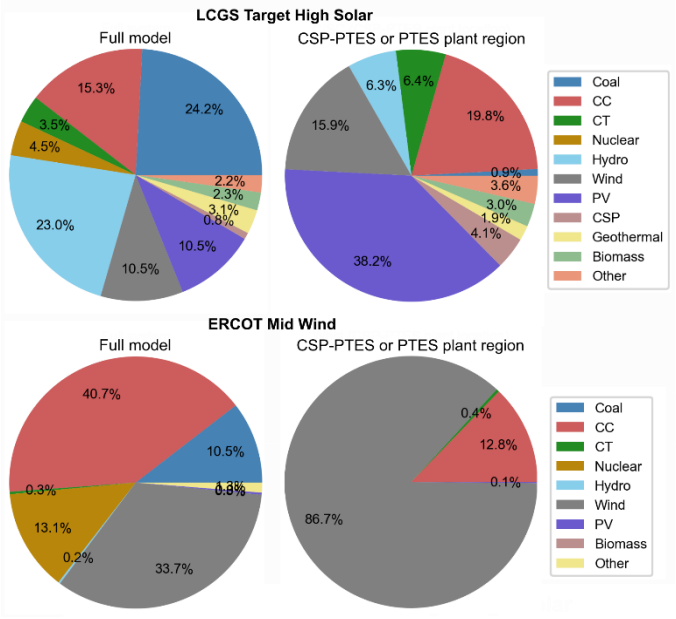

Figure 49: Annual generation mix for the LCGS Target High Solar and ERCOT Mid Wind base case grid scenarios.

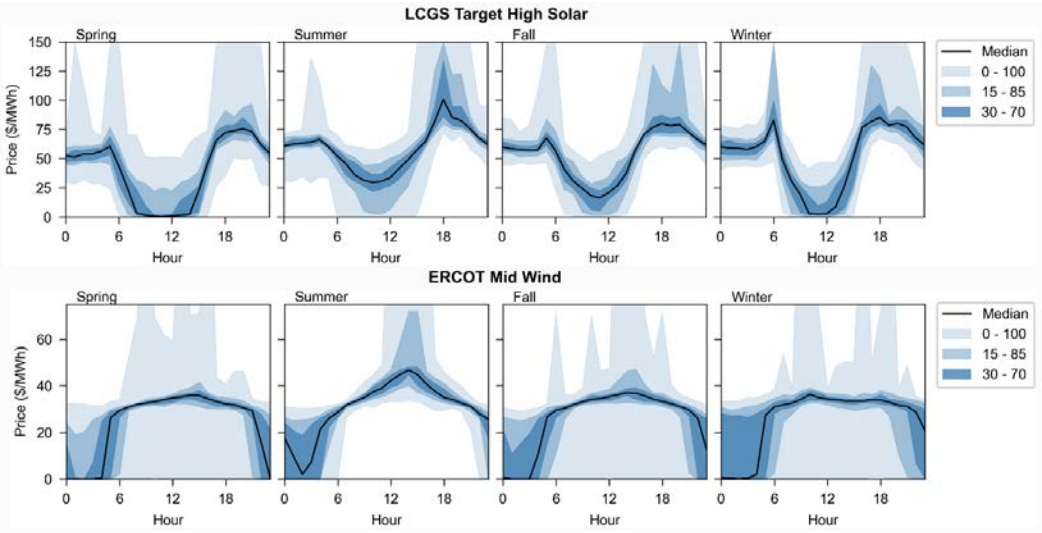

Figure 50: Locational marginal price profiles in the regions selected for addition of a CSP-PTES or PTES system.

Table 15 and Figure 51 provide the base case model input parameters describing the CSP-PTES or standalone PTES system. The large size and annual production cost of the grid scenarios requires a CSP-PTES or PTES system capacity large enough to meaningfully assess changes in production cost (and thus CSP-PTES or PTES system value) outside of the imperfect solution tolerance. The heat engine and heat pump are sized with the same fixed thermal capacity. Thus, the hourly maximum electricity generation or electricity usage varies with ambient temperature and, in the case of the CSP-PTES heat engine, whether heat is rejected to ambient vs. cold storage. Start costs for the heat engine and heat pump are unknown, but were assumed to be roughly in the range of gas combined cycle plant start costs [67] and assigned a base case value of $42/MWe/start, though this value is highly uncertain. For simplicity, the heat engine and heat

pump were assigned an identical absolute start cost based on the design point electrical capacity of the heat engine.

Figure 51 illustrates the part-load behavior of the heat engine heat rate or heat pump coefficient of performance (COP) used within the PLEXOS simulation. The heat rate is expressed relative to the full-load heat rate at design point conditions which, in the case of the CSP-PTES system, is defined with heat rejection to ambient (dashed blue line). Correspondingly, the relative heat rate when heat is rejected to cold storage (solid blue line) is less than unity over all except the smallest load fractions. A piecewise-linear representation of each part-load heat rate curve is implemented in the model given the five load points shown in Figure 51. The heat pump COP is described using an under-estimator step-wise representation (dashed lines) that matches full-load performance and captures the decrease in COP at low load. Identical part-load behavior (relative to full load) is assumed for all ambient temperature conditions. Ambient temperature variability in heat engine efficiency or heat pump COP are included via a set of pre-calculated hourly multipliers given the hourly ambient temperature conditions at the CSP-PTES location during the weather year for each grid scenario and the non-linear off-design ambient temperature behavior in Figure 51.

Table 15: CSP-PTES and PTES System Base Case Simulation Parameters

	CSP-PTES system	Standalone PTES system
Design point heat engine max electrical capacity	1000 MWe (LCGS) 500 MWe (ERCOT)	1000 MWe (LCGS) 500 MWe (ERCOT)
Heat engine min capacity	25% of max capacity	25% of max capacity
Design point heat engine full load discharge efficiency ($\eta^{HE,des}$)	0.395	0.427
Design point heat pump max electrical capacity	1815 MWe (LCGS) 908 MWe (ERCOT)	1726 MWe (LCGS) 863 MWe (ERCOT)
Heat pump min capacity	25% of max capacity	25% of max capacity
Design point full load heat pump COP	1.394	1.355
Storage capacity (hours of storage at design point full load heat engine operation)	14 hours	10 hours
Storage loss rate (% of stored energy per hour)	0.083%	0.083%
CSP solar multiple	2.0	NA
Design point ambient temperature ($T^{amb,des}$)	40°C	40°C
VO&M cost	$1.1/MWhe	$1.1/MWhe
Start cost	$42/MWe/start	$42/MWe/start
Heat engine startup energy loss	20% of rated output for 1 hr	20% of rated output for 1 hr
Rate of cold storage discharge relative to hot storage	2	1
Simultaneous heat engine and heat pump operation allowed?	Yes	No

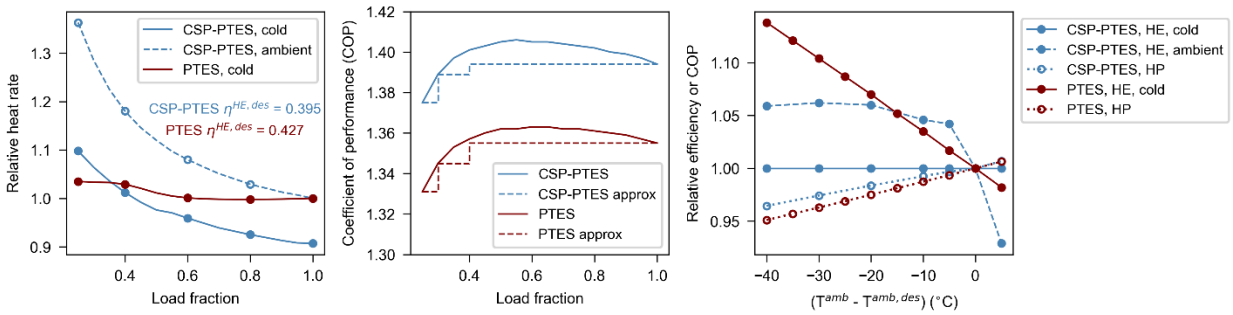

Figure 51: (a) Relative heat rates for the heat engine vs. load fraction when rejecting heat to ambient or to cold storage. (b) Heat pump coefficient of performance and step-wise approximation used in PLEXOS. (c) Ambient temperature dependence of the heat engine (HE) efficiency ($\eta(T_{amb})$ / $\eta(T_{amb,des})$) or heat pump (HP) COP ($COP(T_{amb})$ / $COP(T_{amb,des})$).

5.5.2 Task Milestone

Milestone 6: Improve solar-PTES models that can be used in grid analysis models.

Simple models of PTES and solar-PTES were initially developed for implementation in PLEXOS in Task 2. The detailed thermodynamic models developed in Task 3 enabled the off-design performance of PTES and solar-PTES to be evaluated. These off-design models have been simplified so that they can be integrated with PLEXOS as indicated by Figure 51. Thus, the representation of PTES and solar-PTES in the grid analysis models has been improved and refines estimates of the value these systems provide.

5.5.3 Grid Analysis of Ideal-Gas Joule-Brayton PTES

5.5.3.1 Start-Up Cost

The value of PTES start-up cost is uncertain since these plants have not been constructed. However, results indicate that the value is very sensitive to the start cost that is assigned. It is assumed that start costs will be similar to gas combined cycle start costs, which are estimated to be $42/MWe/start [67]. Note that both the charging and discharging cycles incur a start cost.

Reducing the start cost increases the value that PTES can provide. Figure 52 indicates PTES value including and excluding the start cost which illustrates how substantially the start cost can reduce the value. As would be expected, higher start costs reduce the number of PTES starts, which again reduces the total energy that can be stored or discharged, and reduces the value.

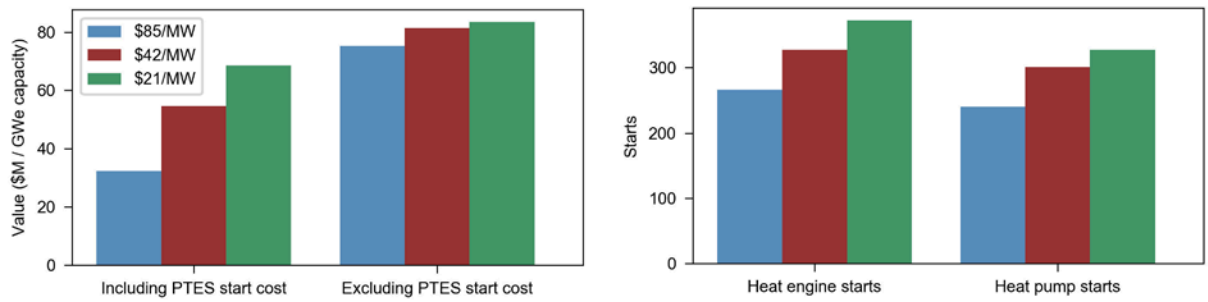

Figure 52: Effect of PTES start cost on value (left) and number of starts (right).

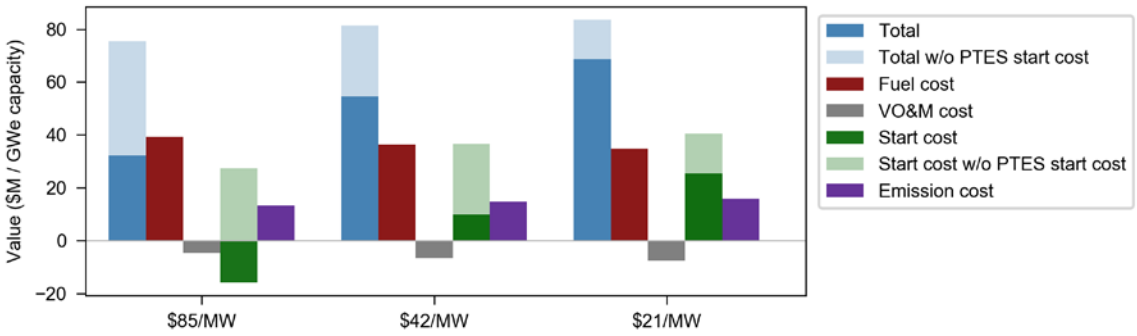

Figure 53: Bar chart showing how PTES adds value to the grid for different start costs.

Figure 53 illustrates the different components that contribute to PTES value. The main source of value is reducing fuel costs from fossil fuel power generators. In the absence of PTES start costs, it can be seen that the second major contributor is reducing the number of starts of fossil fuel plants, and therefore reducing total start costs. However, PTES start costs should be factored in. When PTES start costs are very high (85 $/MW) then the cost of PTES starts outweighs the reduction in conventional plant start-ups.

This analysis indicates that a priority should be improving estimates of PTES start costs, and also identifying methods to minimize this cost.

5.5.3.2 Renewable Penetration Scenario

Several renewable penetration scenarios are described in Table 14, and these are used to explore how the value of PTES depends on the quantity of low-value (i.e., curtailed) renewable electricity. Figure 54 indicates that the PTES value substantially increases in both the Western Interconnection and Texas Interconnection as the renewable penetration increases. The LCGS Target case has a PV penetration of ~31% in California, and the current value is around 21%. This suggests that the higher solar scenarios with 38% and 42% PV in California are not unrealistic scenarios, and that PTES could provide significant value.

In the Texas Interconnection, the current wind penetration is around 17.5% which is similar to the penetration in the low wind scenario (21%). The PTES value nearly triples if the wind penetration increases to 34% in the mid-wind scenario.

In both interconnections, the additional value is derived primarily from reducing the curtailment of renewable generation. Figure 55 shows that in the Western Interconnection, predominantly solar PV curtailment is reduced, although some wind curtailment is reduced too. The Texas Interconnection has only a small quantity of PV in these models, so wind curtailment reduction is the dominant mode. Increasing the renewable generation decreases the renewable energy that is curtailed.

The operation of PTES differs between the two interconnections, and this is again a result of when curtailed renewables are available and when demand increases. In the Texas Interconnection, PTES typically charges overnight and discharges in the middle of the day (Figure 57). Whereas, in California, charges in the middle of the day and then discharges in the evening, and occasionally in the morning (Figure 56).

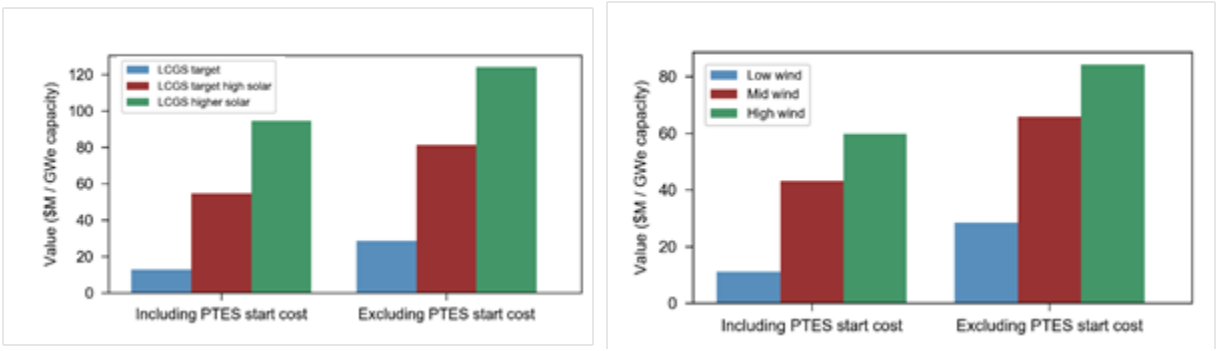

Figure 54: Value of PTES with different renewable penetrations in the Western Interconnection (left) and the Texas Interconnection (right).

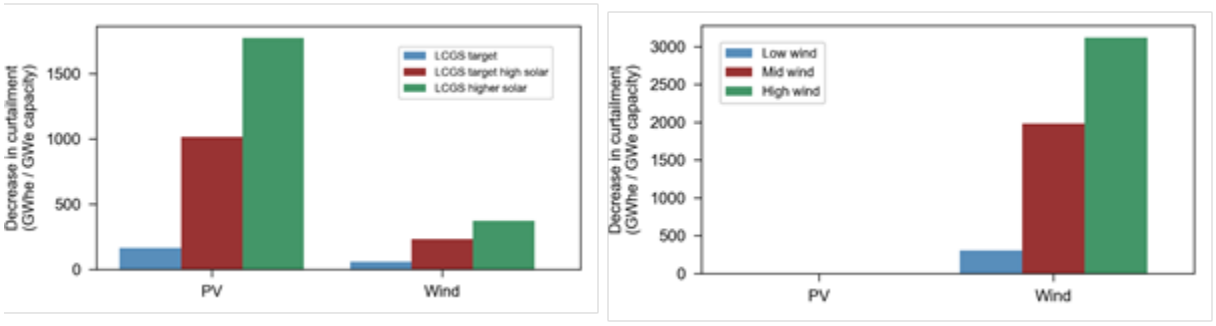

Figure 55: Change in curtailment of PV and wind when PTES is added to the grid in California (left) and Texas (right).

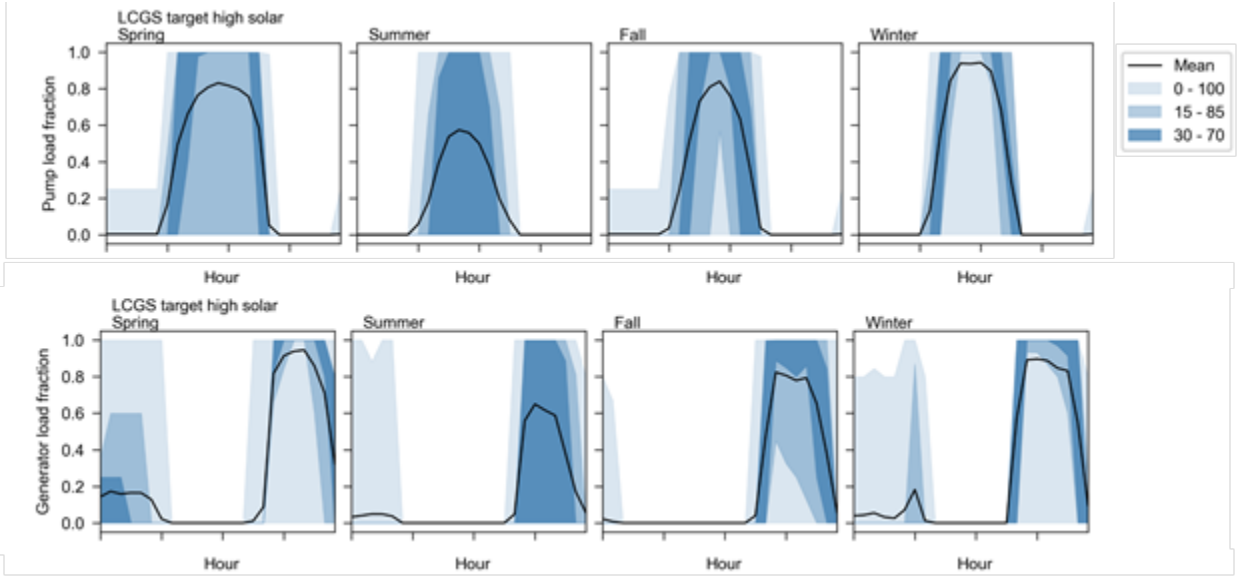

Figure 56: Average daily profiles showing periods of charging (pump load) and discharging (generator load) for the Western Interconnection.

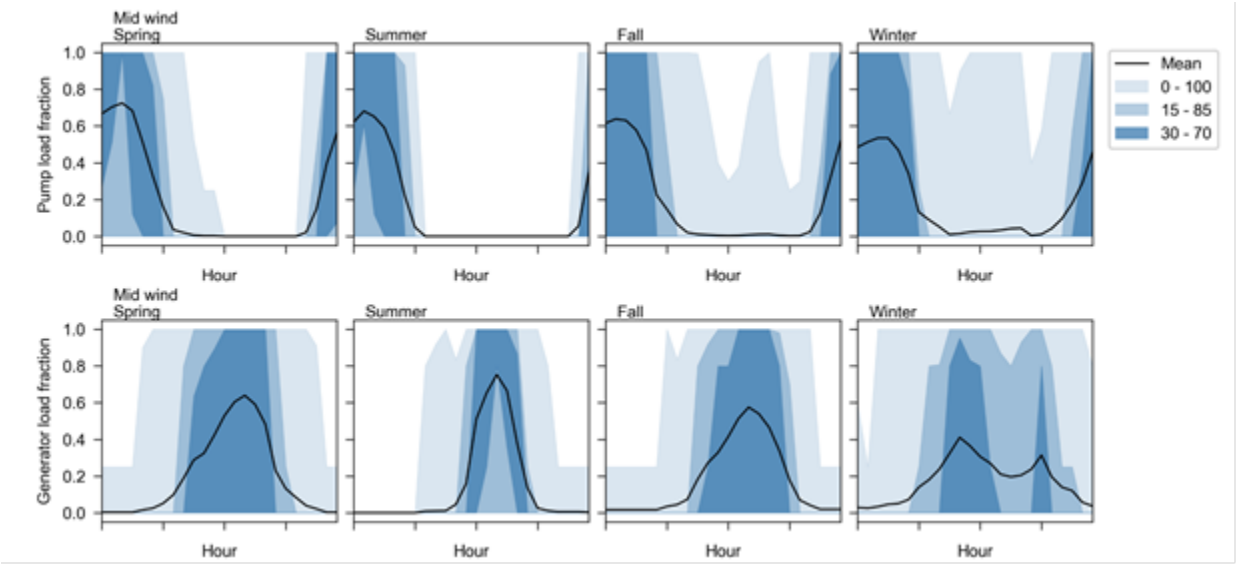

Figure 57: Average daily profiles showing periods of charging (pump load) and discharging (generator load) for the Texas Interconnection.

5.5.3.3 Thermal Storage Duration

The duration of thermal storage is varied, while the power rating is kept constant. Increasing the quantity of storage enables the system to store more curtailed energy, and consequently increases the PTES value, as shown in Figure 58. The value plateaus as the storage duration is increased further, as all curtailed energy that can reasonably be transmitted to the PTES plant is stored. It appears that the value plateaus at lower storage values in California than in Texas. The optimal duration seems to be in the range of 6-8 hours in California and 8-12 hours in Texas.

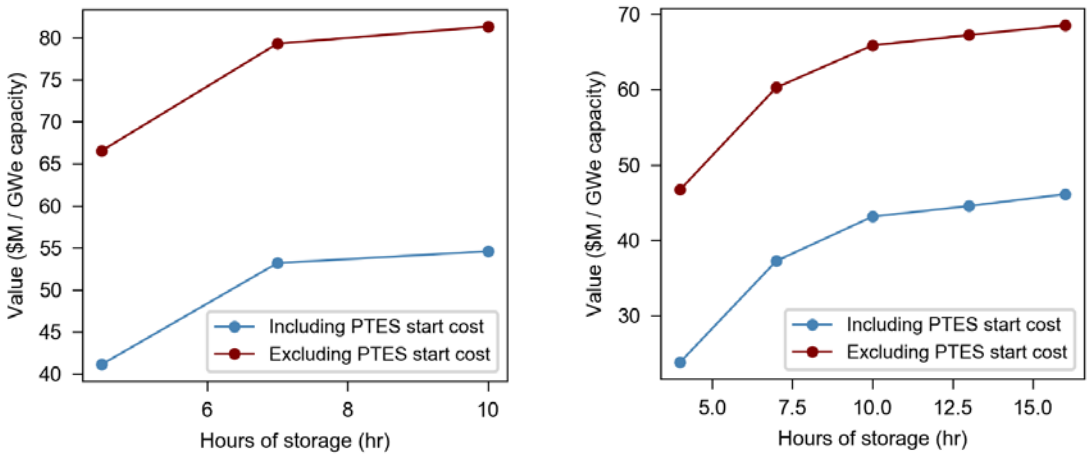

Figure 58: Effect of thermal storage duration on value of PTES on the Western Interconnection (left) and Texas Interconnection (right).

Comparing the average daily profiles of the storage state-of-charge (Figure 59 and Figure 60) provides some interesting insight into how fully the storage is used. At short storage durations, the storage is often fully charged, and the full capacity of the system is utilized. As the storage duration increases, the frequency of fully charging the system decreases. For a 10-hour system in California, the system is rarely fully charged which indicates that any additional storage is infrequently used and garners diminishing additional value. A similar trend is seen for a 16-hour system in Texas, although in this case the system may be fully charged over a wider range of hours. This probably because excess wind energy could occur at any time, whereas excess solar power is much more predictable.

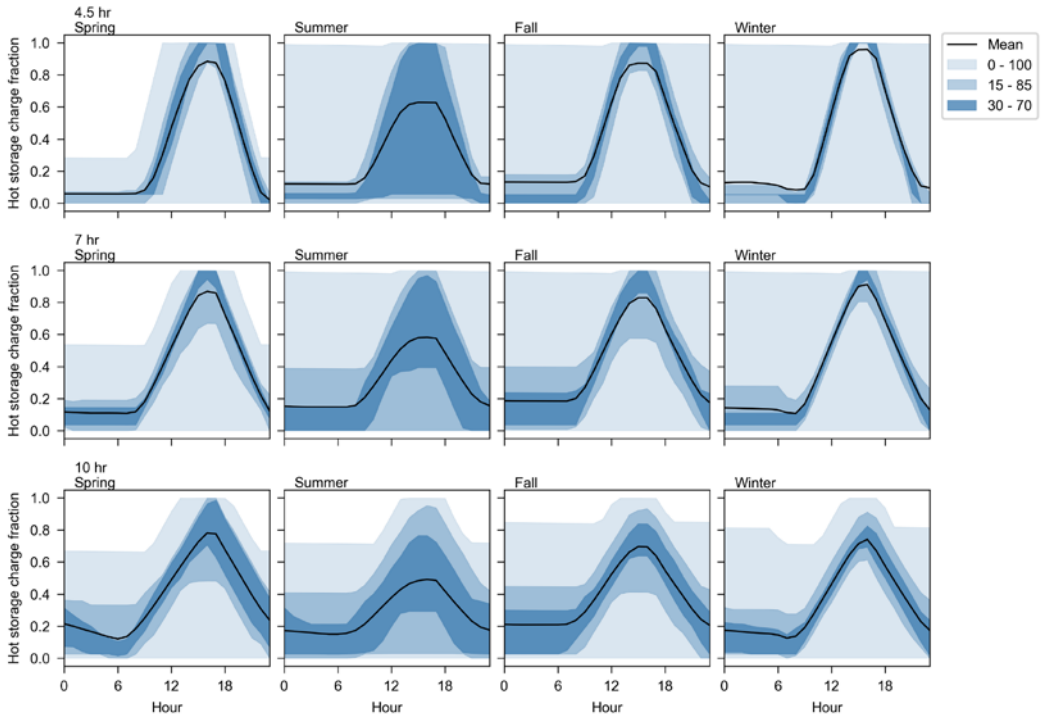

Figure 59: Average daily profiles showing the storage capacity for different storage durations in the Western Interconnection.

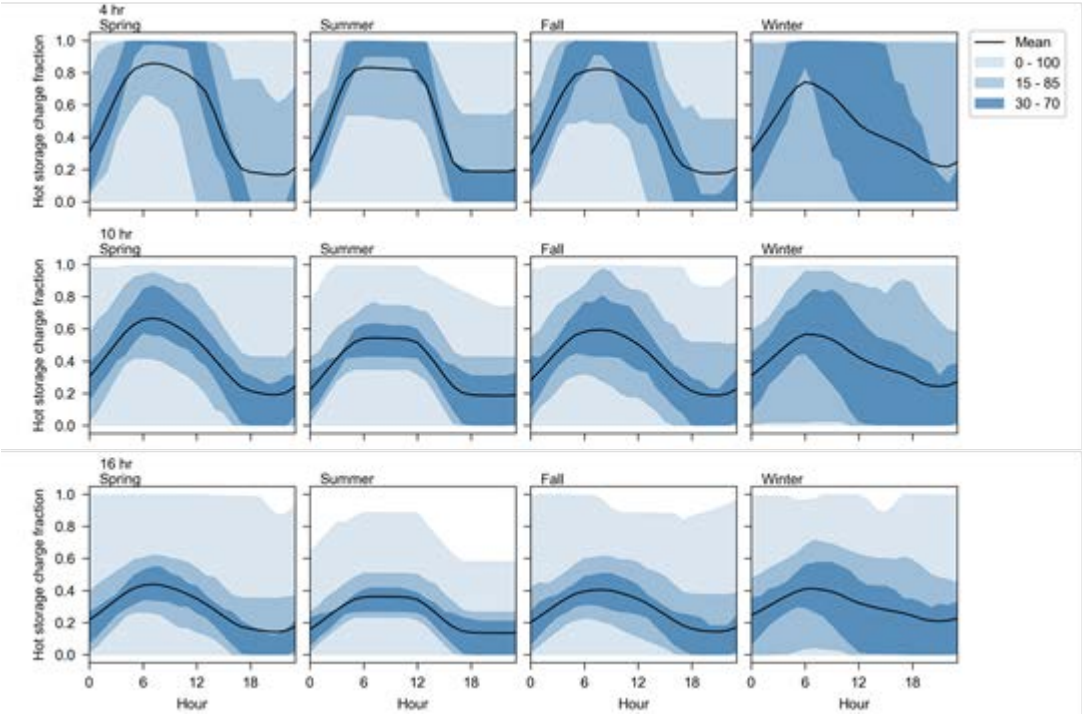

Figure 60: Average daily profiles showing the storage capacity for different storage durations in the Texas Interconnection.

5.5.3.4 Power Rating of Heat Pump

So far it has been assumed that the design durations of the charging cycle and discharging cycle are equal. As a result, the design charging power input exceeds the discharging power output. In this section, the charging power input is varied: increasing the charging power input decreases the time it takes to fully charge the system, for example.

Here, two additional scenarios are considered in addition to equal charging and discharging durations. Reducing the heat pump power to 57% of the nominal value yields a scenario where the power input to the heat pump equals the power output of the heat engine (57% is the round-trip efficiency). A second case with a high heat pump power equal to (1 / 0.57) of its nominal value is also considered. Interestingly, increasing the heat pump power rating increases the value that PTES provides to the grid (Figure 61). This suggests there are a relatively limited number of low-value hours available to charge the system, and that these low prices should be fully exploited by increasing the input power rating. These trends were seen in both California and Texas despite the different generation mixes and operating profiles of PTES.

These results present a direct trade-off with PTES capital cost. Reducing the charging power input reduces the turbomachinery size and therefore reduces the cost. However, the grid analysis results suggest that this lower-cost system would also generate less value.

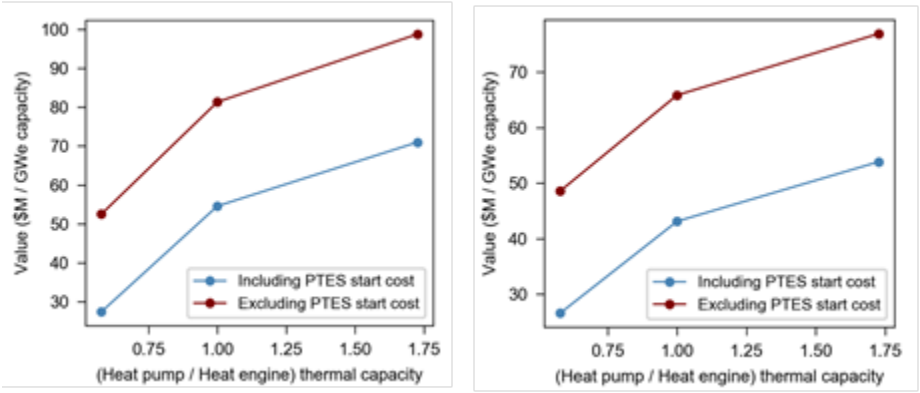

Figure 61: Effect of heat pump power rating on PTES value in the Western Interconnection (left) and the Texas Interconnection (right).

5.5.3.5 Assessment of PTES Commercial Feasibility

This analysis provides some insight into how PTES design parameters affect the value that can be provided to the grid, and also develops an understanding of how and when the system operates. The total value can also be compared to the capital cost to determine whether this energy storage system is financially viable. A simple way to do this is to consider a pay-back period that includes the annual value, as well as the operational costs and net revenue from electricity sales. The pay-back period τ_P may be expressed as

$$\tau_P = \frac{C_{\text{cap}}}{V} \tag{13}$$

where C_{cap} is the total capital cost and V is the annual value. Each of these parameters is highly uncertain, but a rough indication of the pay-back period can be useful. Here, the capital cost is assumed to be in the range of 190-300 $/kWh as indicated by the techno-economic analysis in section 5.3.3. The value is estimated by the PLEXOS grid integration model.

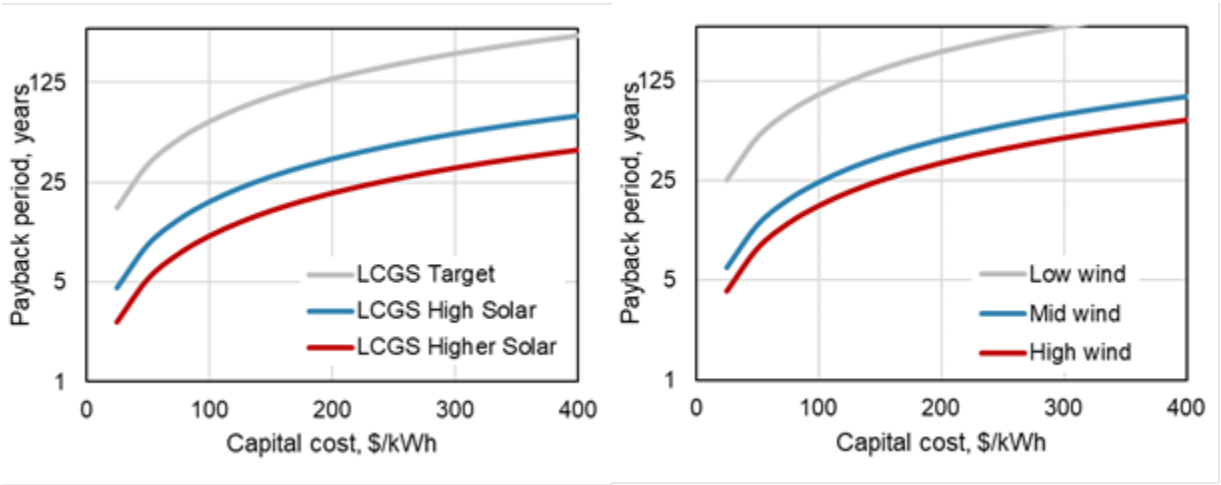

Figure 62: Pay-back periods for a 1000 MWe, 10h PTES in California (left) and Texas (right) in different renewable scenarios. (Note the base-5 logarithmic scale).

Pay-back periods are calculated for a range of PTES costs in different renewable penetration scenarios in California and Texas, as shown in Figure 62. As expected, reducing the capital cost and increasing the renewable penetration (i.e., value) leads to lower pay-back periods. For scenarios that are similar to the present day (LCGS target in CA, low wind in TX, and PTES costing around 250 $/kWh) pay-back periods are very long. In the low-wind ERCOT case, the annual income is negative and a pay-back period is not possible. However, for higher renewable penetrations the pay-back period reduces to more reasonable values. For PTES costs of 250 $/kWh the pay-back period is estimated to be around 20-35 years which is similar to the predicted lifetime of the plant. To achieve pay-back periods of less than 10 years requires large renewable penetrations and PTES costs of around 150 $/kWh. Malta Inc. currently claim cost targets of 100 $/kWh; however, this capital cost is likely to be difficult to achieve. (For comparison, it should be noted that lithium-ion batteries are expected to cost over 250 $/kWh in 2030 even with learning curve reductions [52].)

These estimates do not take into account capacity payments that would increase the annual revenue and reduce the pay-back period. Further analysis is required to assess how significant capacity payments could be on these results. PTES can provide value in other ways that are not currently captured by the grid model. For instance, PTES uses rotating machinery and can therefore provide grid inertia which reduces frequency volatility and grid stability. This feature will become increasingly important as the conventional synchronous machines found in fossil fuel power plants are displaced by renewable generation.

In summary, pay-back periods for PTES systems are likely to be a similar order of magnitude as the lifetime of the plant in scenarios with significant renewable penetrations. However, these scenarios are not unrealistic given the current rates of renewable installations. Capacity payments are likely to be a significant factor in determining whether PTES can be commercially feasible. Reductions in capital cost and O&M costs also have a significant influence on the pay-back period, but targeting costs of less than 200 $/kWh for a 10 hour system is reasonable.

5.5.4 Grid Analysis of Solar-PTES: A CSP Plant Retrofitted With an Ideal-Gas Heat Pump

As described above, a model of a Joule-Brayton heat pump which can charge the thermal storage of a CSP plant was implemented in PLEXOS. An important development was the inclusion of the cold thermal storage that can be used to boost the steam cycle power output by roughly 10%. The objective of this analysis was to evaluate the additional value that the heat pump could add to the grid compared to the stand-alone CSP plant (since the CSP plant is being retrofitted). Results were obtained for several renewable scenarios and also for various sizes of solar field and thermal storage.

The nominal system design had a solar multiple of 2 and a storage duration of 14 hours. Previous work indicated that the thermal storage tends to be charged by solar and the heat pump at the same time. If the storage is too small then there are limited opportunities to operate the heat pump since storing solar heat takes priority.

5.5.4.1 Renewable Scenarios

The solar-PTES system was located in California and the three renewable penetration scenarios detailed in Table 14 were considered.

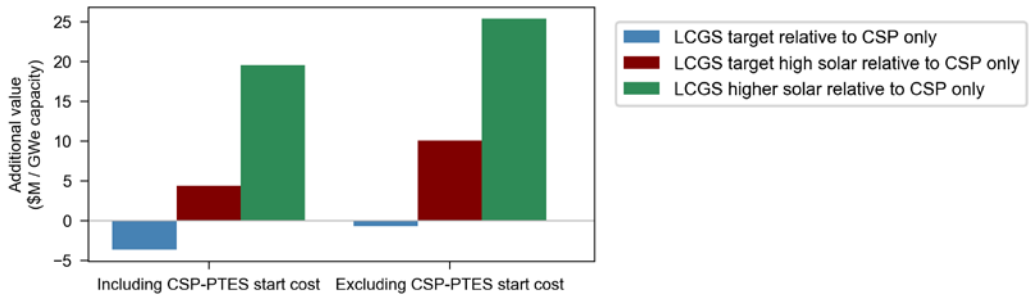

Figure 63: Additional value gained from adding a heat pump to an existing CSP plant under different renewable scenarios.

The additional value that adding a heat pump to the CSP plant is illustrated in Figure 63. The additional value is negative in the LCGS Target scenario: this is unexpected because PLEXOS has the option to not run the heat pump, so the minimum additional value should be zero which corresponds to the CSP plant operating as normal. The additional value numbers are reasonably small in the context of the entire Western Interconnection grid, so there are quite large tolerances and error bars on the results.

Increasing the renewable penetrating leads to greater value from the solar-PTES system as would be expected.

5.5.4.2 Solar Field and Thermal Storage Size

Analysis conducted under Task 2 indicated that the thermal storage was typically charged by the heat pump and solar heat during the same hours: when electricity prices are low it makes sense to store electricity and not to dispatch solar heat. Storing solar energy takes priority and this can limit the operation of the heat pump and therefore its value. Consequently, the thermal storage should be relatively large compared to how it is typically sized for CSP plants. This can be achieved in two ways, either by increasing the thermal storage duration or by reducing the solar multiple. Increasing the thermal storage capacity is the most practical when retrofitting a CSP plant. Using a low solar multiple (a “peaker” plant) may be appropriate if designing a new build system.

Two solar-PTES configurations are considered. The first solar-PTES system has a CSP plant with a solar multiple of 2 and 14 hours of storage. This is compared to a stand-alone CSP plant with either 10 or 14 hours of storage, corresponding to scenarios where additional storage is or is not added, respectively. The second solar-PTES system has a peaker CSP plant with a solar multiple of 1 and 10 hours of storage, and is compared to a stand-alone CSP plant with a solar multiple of 1 and with 6 or 10 hours of storage.

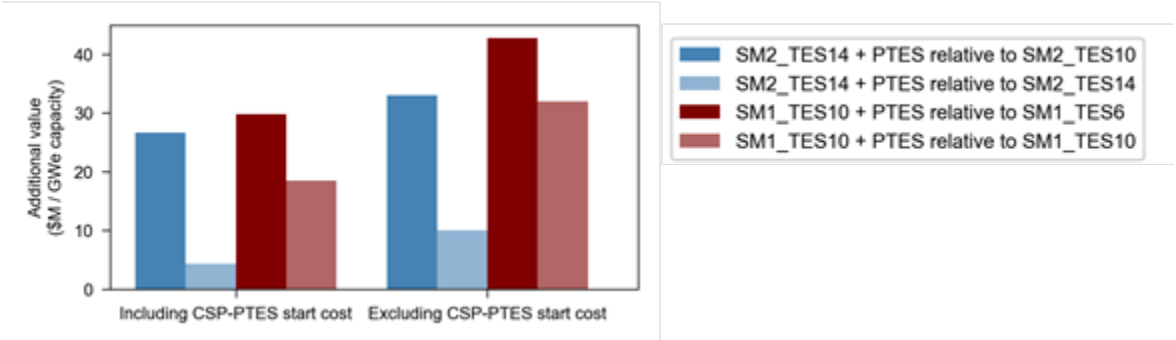

Figure 64: Effect of solar multiple and thermal storage duration on solar-PTES grid value.

When no additional storage is added to the system, the additional value provided by the heat pump is very small, as shown in Figure 64. However, adding four hours of storage increases the value by roughly a factor of 5 for the system with a solar multiple of 2. The heat pump provides a significant benefit to the peaker CSP plant (solar multiple of 1). This can be attributed to the thermal storage being large compared to the available solar heat, which provides more opportunities to run the heat pump and store energy. Figure 65 illustrates that the heat pump runs more frequently and at higher loads in this system than with the more conventional system that has a solar multiple of 2.

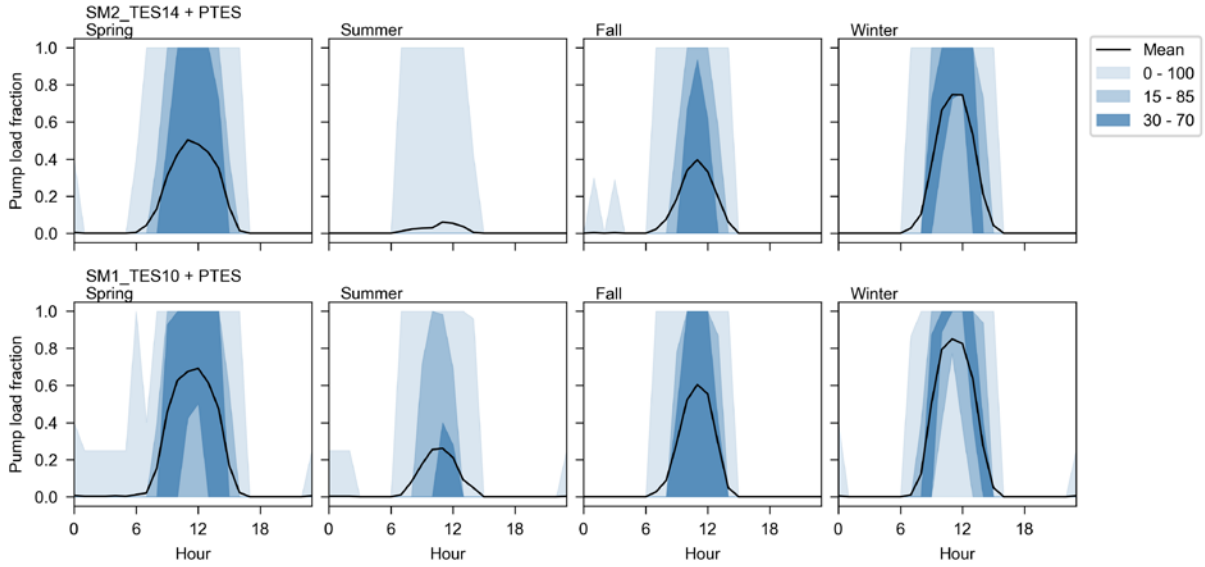

Figure 65: Average daily profiles showing the heat pump load for solar-PTES systems.

5.5.4.3 Comparison With an Electrically Charged System

A simple alternative to retrofitting a CSP plant with a heat pump is to use an electrical heater to charge the molten salt storage. The electrical heater is relatively cheap compared to a heat pump, but it has a low efficiency, with a COP of 1. As a result, the overall round-trip efficiency will be the same as the steam Rankine cycle efficiency. The electrical heater also does not create a cold store and cannot therefore improve the steam cycle power output.

The heat pump model was modified to represent an electrical heater. The COP was set to 1, cold storage was not implemented, and start costs for the charging cycle were reduced to 20 $/MW

since the electrical heater is a less complicated device. Results are shown in Figure 66 for a CSP plant with a solar multiple of 2. Surprisingly, the electrical heater system provides *more* additional value than the more efficient heat pump system. This is due to the higher start costs of the heat pump which reduce the total value – it can be seen that when start costs are not included, the heat pump produces more additional value. Thus, it is important to accurately estimate the start cost of the heat pump and electrical heater. As with the previous results, the additional value is considerably larger when extra thermal storage is included.

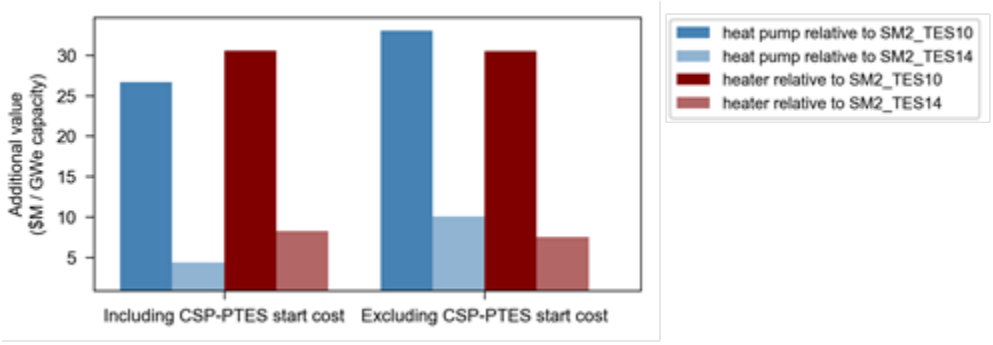

Figure 66: Additional value provided by solar-PTES: comparing charging with a heat pump to an electrical heater.

5.5.4.4 Commercial Feasibility of Solar-PTES

A simple method of evaluating the commercial feasibility of solar-PTES is to estimate the pay-back period as described above. In Figure 67 the payback period of a heat pump solar-PTES system and an electrical heater solar-PTES system are compared in the LCGS Target High Solar scenario with a CSP field with a solar multiple of 2 and with 14 hours of storage. For a given system cost, the payback period of the heat pump system is slightly higher than the electrical heater because the electrical heater provides more value to the grid (due to lower start costs). The heat pump system is likely to be considerably more expensive than the electrical heater. Estimates in Section 5.3.3 suggested the retrofitted cost of the heat pump would be in the range of 130-250 $/kWh which leads to pay-back periods over 25 years. On the other hand, electrical heaters are relatively cheap (potentially in the range of 75-150 $/kW$_e$), and the full cost of the electrical heater plus storage could be less than 50 $/kWh, which leads to pay-back periods of around 10 years.

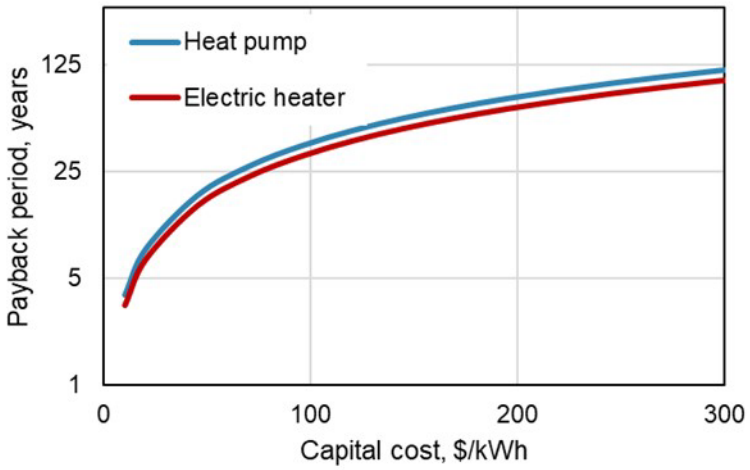

Figure 67: Pay-back periods for a solar-PTES system in California. A CSP field with solar multiple of 2 and storage duration of 10 hours is retrofitted with either a heat pump or an electrical heater, and an additional 10 hours of storage. (Note the base-5 logarithmic scale.)

5.5.5 Task Milestone

Milestone 7: Assess net value of PTES and solar-PTES by undertaking grid analysis studies using updated system performance curves and cost correlations.

This milestone required that PTES adds value to the grid and that solar-PTES adds more value than a stand-alone CSP plant. Both of these objectives were met although these is considerable uncertainty around the value of several parameters, such as start costs, that have a significant influence on the results. Estimates of these parameters should be improved. PTES and solar-PTES may also provide other services, such as grid inertia and capacity, which are not currently included in the PLEXOS models but could provide significant value.

5.5.6 Subtask 5.2: Feedback From Experts

In this task, feedback on solar-PTES systems was requested from industrial and academic experts. The objective was to identify key technological barriers and evaluate the feasibility of solar-PTES. Feedback was received from three individuals who had experience in industry and academia relating to Carnot Batteries, power plants, CSP, and technology development. Discussions with these individuals concentrated on the feasibility of retrofitting a CSP plant with a Joule-Brayton heat pump. The feedback has been compiled into several key points described below:

1. Cost is more important that round-trip efficiency. Electric heaters are likely to be more promising than heat pumps.
2. The combined solar-PTES system is relatively complex, especially when considering the integration of the cold storage. Integrating an electrical heater would be simpler, cheaper, and is a more mature technology.
3. The economics of PTES-type systems can be improved if thermal energy is also a useful output. For PTES this could be hot or cold energy. Solar process heat systems may provide a better opportunity for the integration of PTES.

4. The complexity of system control should be considered. The hot and cold tanks can be discharged independently. This theoretically can improve performance – for instance, if the power boost from cold tanks is saved for the most valuable time periods or highest ambient temperatures. However, the tank inventories have to be carefully managed.
5. Transient modeling of the system is necessary, especially when considering the complexity of the system.
6. An off-the-shelf heat exchanger will have an effectiveness of around 80-85%, but analysis indicates that values of 90-95% are necessary. While obtaining a high effectiveness can be achieved it substantially increases costs. This is not just due to additional heat exchanger surface area. It is more difficult for a manufacturer to be able to guarantee the required performance if the effectiveness is very high due to imperfections such as cross-flow.
7. The system involves a lot of heat transfer, so reducing heat exchanger costs is important.
8. The analysis suggests that increasing the heat pump pressure is desirable because it reduces volumetric flows and therefore the turbomachinery cost. However, the heat exchangers (and pipework) have to be pressurized which may impact the type of heat exchanger that can be used (and its cost). For example, printed circuit heat exchangers can operate at high pressures, but have high manufacturing costs.
9. Important to consider all pressure losses in pipes and valves around the system since these could be significant.
10. Changing turbomachinery operating points away from what is conventionally used in gas turbines will require the development of new turbomachinery which can take several years. In some cases, existing machinery could be modified.
11. It may be challenging to convince a turbomachinery manufacturer to develop new turbomachinery unless it is clear that a sufficient market exists. A similar issue may exist for the development of high effectiveness heat exchangers.
12. These types of heat pumps may have various applications, and these should be explored as it may provide more opportunities for these technologies and therefore increase the market size and likelihood of development.
13. Retrofitting an existing plant is lower risk than developing a new, stand-alone Carnot Battery, and has the advantage that a grid connection already exists and reduces permitting issues.
14. However, a retrofit will require the cooperation of several parties, such as power plant operator, utility, component manufacturers and financing.
15. There may be a limited number of suitable CSP installations, but a similar concept is applicable at coal plants. The integration of cold storage into a coal plant which already has a cooling tower would be simpler than in a CSP plant with an air-cooled condenser.

In summary, several recommendations for future research priorities may be made:

1. Heat exchangers dominate the performance and cost of PTES and solar-PTES, which therefore requires the development of low-cost, high effectiveness heat exchangers.

2. The trade-off between simple, low-cost electrical heaters and expensive, efficient, complex heat pumps should be explored. Electrical heaters could be the first step in demonstrating these concepts in a low-risk fashion.
3. Transient modeling of PTES and solar-PTES would answer questions about ramp rates, time to switch between charging and discharging, and the impact of variable operation the system performance and control
4. A significant challenge for PTES and solar-PTES is convincing manufacturers to develop new technologies when the market is not yet proven. Market studies, policies, and alliances of interested parties could help.

5.5.7 Task Milestone

Milestone 8: Assess the commercial viability of solar-PTES concept.

In this project, techno-economic models have been developed to evaluate the performance and cost of PTES and solar-PTES. A PLEXOS grid analysis model was implemented to estimate the value these systems could provide to the grid. By comparing the capital cost to the value, it is possible to obtain a rough estimate for pay-back periods and identify scenarios that enable sufficiently low pay-back periods. Academic and industry experts provided feedback on the solar-PTES concept and identified key issues that should be addressed.

In summary, necessary conditions for PTES and solar-PTES to achieve reasonable pay-back periods include (1) scenarios with increased (but realistic) renewable penetrations compared to current values (2) low capital costs of <250 $/kWh for PTES and <100 $/kWh for solar-PTES. The commercial viability will be improved if capacity payments are included, but the extent of improvements needs to be investigated. PTES and solar-PTES can provide grid inertia which will be an increasingly valuable service to the grid as renewable penetrations increase, and the value of this service also needs to be evaluated. The magnitude of start costs is uncertain and estimates should be improved. Using an electrical heat is likely to be considerably cheaper than a heat pump when retrofitting a CSP plant, and this system has the lowest pay-back periods despite the lower round-trip efficiencies.

Expert feedback suggested that retrofitted solar-PTES had several merits such as reduced risk and good performance. However, they are relatively complex and expensive, especially when compared with electrical heaters. Coal plants provide a greater number of suitable locations than CSP plants. Further research and manufacturer collaboration is required to develop the high efficiency heat exchangers and novel turbomachinery that are necessary for this system.

6 Conclusions

Pumped thermal energy storage (PTES) is a storage system that stores electricity in thermal reservoirs. In this project, methods of integrating PTES with concentrating solar power (CSP) systems were investigated. Techno-economic models were developed of PTES and solar-PTES devices and used to assess their performance, cost, and commercial viability. Systems were optimized using multi-objective optimization techniques. The value that these storage devices provide to the grid were estimated using a production cost model. In this report, these tasks and results are described in detail and illustrate that the project milestones were satisfied.

Results are presented for PTES systems that use ideal-gas Joule-Brayton cycles and supercritical CO_2 Joule-Brayton cycles. It was found that ideal-gas systems typically achieved higher round-trip efficiencies and lower levelized cost of storage (LCOS). Heat exchangers are a key component for achieving good performance. For a typical effectiveness of 85%, the ideal-gas PTES has a round-trip efficiency of 40%. Reaching round-trip efficiencies greater than 55% requires an effectiveness of over 95%. While high effectiveness heat exchangers have high costs, it was found that the substantial benefit to the round-trip efficiency leads to minimum lifetime costs (LCOS) when the effectiveness is around 95%.

Increasing the maximum temperature of PTES also improves the round-trip efficiency. However, maximum temperatures are constrained by the operational limits of the storage fluids. Several fluids were compared, including nitrate molten salts and novel chloride molten salts. Chloride salts can operate at higher temperatures than nitrate salts and therefore improve the system efficiency. However, higher temperatures require more expensive materials in the heat exchangers which leads to larger capital costs.

Multi-objective optimization of PTES showed that chloride-salt systems typically outperformed nitrate-salt systems. For instance, the maximum efficiency was 72.1% and 66.3%, while the minimum LCOS was 0.117 ± 0.03 \$/kWh$_e$ and 0.126 ± 0.03 \$/kWh$_e$ for chloride salts and nitrate salts, respectively. However, the minimum LCOS for both fluids is very similar and suggests there may be little benefit to using more complicated, higher-temperature systems. Future work should consider the use of alternative storage systems, such as particles or packed beds, which have fewer constraints and lower media cost. PTES costs were compared with alternative storage technologies and were shown to be competitive with predicted costs of Lithium-ion batteries.

Off-design models of PTES were developed, and a control method known as “inventory control” was implemented. This approach confers a unique feature on PTES in that the system can operate down to around 40% part-load without significantly compromising the round-trip efficiency. This suggests that this storage system may be able to operate flexibly under a variety of conditions.

Several solar-PTES concepts were explored. One of the most feasible retrofits an existing CSP plant with a Joule-Brayton heat pump. The heat pump can be used to charge the extant molten salt storage at the CSP plant, and also creates a cold storage that can be used to reduce the condenser temperature in the discharging steam cycle, thereby improving performance. Optimization studies indicated that the most efficient systems had a round-trip efficiency of 62% while the lowest costs systems had an LCOS of 0.117 ± 0.03 \$/kWh$_e$. Retrofitting a CSP plant

reduces the number of new components, and therefore solar-PTES was found to have a lower capital cost than stand-alone PTES and the LCOS was slightly lower. However, if a new solar-PTES system was constructed, the system would be more expensive than PTES, as well as having a lower round-trip efficiency. On the other hand, the hybrid solar-PTES device would be able to provide both flexible renewable power generation as well as electricity storage services.

The value that PTES and solar-PTES can provide to the electrical grid was investigated with the grid analysis model PLEXOS. These systems derive value from reducing the curtailment of renewable generation, and thus displacing fossil fuel generation and reducing fuel and start-up costs. As would be expected, PTES and solar-PTES value increases as the renewable penetration is increased. PTES was considered in both California and Texas, and was found to operate at different times due to the different generation mixes and demand profiles. For example, California has larger solar generation so PTES was primarily charged during the day and discharged at night, whereas Texas has a large wind deployment which meant that PTES could be charged at any time, but particularly at night and during the winter. These results have implications for the design, control, and operation of PTES in different regions.

An approximate method of assessing the commercial viability of these systems is to estimate a pay-back period based on the upfront capital cost and the annual value and operations cost. Renewable penetrations need to increase in order for PTES to have reasonable payback periods of less than 25 years, although the simulated renewable penetrations are not unrealistic scenarios. This result is based on estimated PTES capital costs of 250 $/kWh$_e$ for a 100 MW$_e$, 10 hour system. Reducing the capital cost to 150 $/kWh$_e$ would reduce payback periods to 10-15 years and would require technological innovation.

It should be noted that there is considerable uncertainty in combining the capital cost estimates with the grid value, and several influential parameters, such as the PTES start cost, are unknown and require refinement. Furthermore, PLEXOS does not evaluate other sources of value that PTES may provide, such as capacity and grid inertia, which could further reduce the pay-back period.

It was found that adding a heat pump to a CSP plant increased the value that the system provided to the grid. This value is reasonably small if only the existing hot storage at the CSP plant is used, since the thermal storage can often be largely charged by solar energy leaving limited opportunities for the heat pump to run. The additional value can be substantially increased by adding a few additional hours of hot thermal storage. Solar-PTES was compared to a CSP plant which could use an electrical heater to charge the storage instead of the heat pump. The electrical heater could provide mode additional value than the heat pump due to lower start costs. As a result, the estimated pay-back periods for when using a heat pump are around 25 years, and decrease to fewer than 10 years if an electrical heater is used. The electrical heater system is also cheaper and less complex and may provide the most suitable method of creating a solar-PTES system.

Experts from the storage and CSP industry were contacted, and they provided feedback on solar-PTES design, performance, and limitations. The general consensus was that solar-PTES systems have some merits, but are complex and expensive when compared to electrical heating.

Key areas where additional research could help advance PTES and solar-PTES development include:

- Development of high-efficiency, low-cost heat exchangers
- Transient modeling of power cycles to understand operational limits
- Refined grid analysis research that includes some of the unique services PTES can provide, such as grid inertia and capacity
- Investigate other opportunities for these types of devices – e.g., improving economics by providing other outputs such as heat and cold
- Market research to demonstrate the extent to which these systems could be deployed

Acknowledgements

This work was authored in part by the National Renewable Energy Laboratory, operated by Alliance for Sustainable Energy, LLC, for the U.S. Department of Energy (DOE) under Contract No. DE-AC36-08GO28308. Funding provided by U.S. Department of Energy Office of Energy Efficiency and Renewable Energy Solar Energy Technologies Office. The views expressed in the article do not necessarily represent the views of the DOE or the U.S. Government. The U.S. Government retains and the publisher, by accepting the article for publication, acknowledges that the U.S. Government retains a nonexclusive, paid-up, irrevocable, worldwide license to publish or reproduce the published form of this work, or allow others to do so, for U.S. Government purposes.

References

[1] A. V Olympios, J.D. McTigue, P. Farres-Antunez, A. Tafone, A. Romagnoli, Y. Li, Y. Ding, W.-D. Steinmann, L. Wang, H. Chen, C.N. Markides, Progress and prospects of thermo-mechanical energy storage—a critical review, Prog. Energy. 3 (2021) 022001. https://doi.org/10.1088/2516-1083/abdbba.

[2] A. White, G. Parks, C.N. Markides, Thermodynamic analysis of pumped thermal electricity storage, Appl. Therm. Eng. 53 (2013) 291–298. https://doi.org/10.1016/j.applthermaleng.2012.03.030.

[3] J. McTigue, Analysis and optimisation of thermal energy storage, University of Cambridge, 2016. https://doi.org/10.17863/CAM.7084.

[4] M. Mercangöz, J. Hemrle, L. Kaufmann, A. Z'Graggen, C. Ohler, Electrothermal energy storage with transcritical CO2 cycles, Energy. 45 (2012) 407–415. https://doi.org/10.1016/j.energy.2012.03.013.

[5] S.A. Wright, C.S. Davidson, W.O. Scammell, Bulk Energy Storage using a Supercritical CO 2 Waste Heat Recovery Power Plant, in: 4th Int. Symp. - Supercrit. CO2 Power Cycles, 2014.

[6] W.D. Steinmann, The CHEST (Compressed Heat Energy STorage) concept for facility scale thermo mechanical energy storage, Energy. 69 (2014) 543–552. https://doi.org/10.1016/j.energy.2014.03.049.

[7] J.D. McTigue, A.J. White, C.N. Markides, Parametric studies and optimisation of pumped thermal electricity storage, Appl. Energy. 137 (2015) 800–811. https://doi.org/10.1016/j.apenergy.2014.08.039.

[8] A.J. White, J.D. McTigue, C.N. Markides, Analysis and optimisation of packed-bed thermal reservoirs for electricity storage applications, Proc. Inst. Mech. Eng. Part A J. Power Energy. 230 (2016) 739–754.

[9] J.D. McTigue, A.J. White, Segmented packed beds for improved thermal energy storage performance, IET Renew. Power Gener. 10 (2016) 1498–1505.

[10] T. Desrues, J. Ruer, P. Marty, J.F. Fourmigué, A thermal energy storage process for large scale electric applications, Appl. Therm. Eng. 30 (2010) 425–432. https://doi.org/10.1016/j.applthermaleng.2009.10.002.

[11] P. Farrés-Antúnez, H. Xue, A.J. White, Thermodynamic analysis and optimisation of a combined liquid air and pumped thermal energy storage cycle, J. Energy Storage. 18 (2018) 90–102. https://doi.org/10.1016/j.est.2018.04.016.

[12] R.B. Laughlin, Pumped thermal grid storage with heat exchange, J. Renew. Sustain. Energy. 9 (2017). https://doi.org/10.1063/1.4994054.

[13] Y.M. Kim, D.G. Shin, S.Y. Lee, D. Favrat, Isothermal transcritical CO2 cycles with TES (thermal energy storage) for electricity storage, Energy. 49 (2013) 484–501. https://doi.org/10.1016/j.energy.2012.09.057.

[14] M. Morandin, M. Mercangöz, J. Hemrle, F. Maréchal, D. Favrat, Thermoeconomic design optimization of a thermo-electric energy storage system based on transcritical CO2 cycles, Energy. 58 (2013) 571–587. https://doi.org/10.1016/j.energy.2013.05.038.

[15] J. Howes, Concept and Development of a Pumped Heat Electricity Storage Device, Proc. IEEE. 100 (2012) 493–503. https://doi.org/10.1109/JPROC.2011.2174529.

[16] M. Abarr, B. Geels, J. Hertzberg, L.D. Montoya, Pumped thermal energy storage and bottoming system part A: Concept and model, Energy. (2016) 1–12. https://doi.org/10.1016/j.energy.2016.11.089.

[17] G.F. Frate, M. Antonelli, U. Desideri, A novel Pumped Thermal Electricity Storage (PTES) system with thermal integration, Appl. Therm. Eng. 121 (2017) 1051–1058. https://doi.org/10.1016/j.applthermaleng.2017.04.127.

[18] S.D. Garvey, A.J. Pimm, J.A. Buck, S. Woolhead, K.W. Liew, B. Kantharaj, J.E. Garvey, B.D. Brewster, Analysis of a Wind Turbine Power Transmission System with Intrinsic Energy Storage Capability, Wind Eng. 39 (2015) 149–173. https://doi.org/10.1260/0309-524X.39.2.149.

[19] P. Vinnemeier, M. Wirsum, D. Malpiece, R. Bove, Integration of heat pumps into thermal plants for creation of large-scale electricity storage capacities, Appl. Energy. 184 (2016) 506–522. https://doi.org/10.1016/j.apenergy.2016.10.045.

[20] A. Benato, Performance and cost evaluation of an innovative Pumped Thermal Electricity Storage power system, Energy. (2017). https://doi.org/10.1016/j.energy.2017.07.066.

[21] J.D. McTigue, P. Farres-Antunez, C.N. Markides, A.J. White, Integration of heat pumps with solar thermal systems for energy storage, in: Encycl. Energy Storage, Elsevier, 2022. https://doi.org/10.1016/B978-0-12-819723-3.00131-1.

[22] P. Farrés-Antúnez, Modelling and development of thermo-mechanical energy storage, University of Cambirdge, 2018. https://doi.org/https://doi.org/10.17863/CAM.38056.

[23] SimTech, Process Simulation Environment (IPSEpro), (2017). http://www.simtechnology.com/CMS/index.php/ipsepro.

[24] A.M. Patnode, Simulation and performance evaluation of parabolic trough solar power plants, 2006. http://www.minds.wisconsin.edu/handle/1793/7590.

[25] J.D. McTigue, N. Kincaid, G. Zhu, D. Wendt, J. Gunderson, K. Kitz, Solar-Driven Steam Topping Cycle for a Binary Geothermal Power Plant Solar-Driven Steam Topping Cycle for a Binary Geothermal Power Plant, NREL/TP-5500-71793. (2018). https://www.nrel.gov/docs/fy19osti/71793.pdf.

[26] J. Couper, W.R. Penney, J. Fair, S. Walas, Chemical Process Equipment: Selection and Design, 3rd Editio, 2012.

[27] N.T. Weiland, B.W. Lance, S.R. Pidaparti, SCO2 Power Cycle Component Cost Correlations from DOE Data Spanning Multiple Scales and Applications, Proc. ASME Turbo Expo 2019. (2019).

[28] W. Seider, D. Lewin, J.D. Seader, S. Widagdo, R. Gani, K.M. Ng, Product and Process Ddesign Principles: Synthesis, Analysis, and Evaluation, 4th Editio, Wiley, 2017.

[29] J. Lyons, C.W. White, Process Equipment Cost Estimation Final Report, 2002.

[30] M.S. Peters, K.D. Timmerhaus, Plant design and economics for chemical engineers, McGraw-Hill, Inc., 1990.

[31] A.S. Nagorny, N. V. Dravid, R.H. Jansen, B.H. Kenny, Design aspects of a high speed permanent magnet synchronous motor / generator for flywheel applications, 2005 IEEE Int. Conf. Electr. Mach. Drives. (2005) 635–641. https://doi.org/10.1109/iemdc.2005.195790.

[32] I.H. Bell, J. Wronski, S. Quoilin, V. Lemort, Pure and Pseudo-pure Fluid Thermophysical Property Evaluation and the Open-Source Thermophysical Property Library CoolProp, Ind. Eng. Chem. Res. 53 (2014) 2498–2508. https://doi.org/10.1021/ie4033999.

[33] J.D. McTigue, P. Farres-Antunez, K. Sundarnath J, C.N. Markides, A.J. White, Techno-economic analysis of recuperated Joule-Brayton pumped thermal energy storage, Energy Convers. Manag. 252 (2022). https://doi.org/10.1016/j.enconman.2021.115016.

[34] D.E. Beasley, C. Ramanarayanan, H. Torab, Thermal response of a packed bed of spheres containing a phase-change material, Int. J. Energy Res. 13 (1989) 253–265.

[35] A.J. White, Loss analysis of thermal reservoirs for electrical energy storage schemes, Appl. Energy. 88 (2011) 4150–4159. https://doi.org/10.1016/j.apenergy.2011.04.030.

[36] M. Cascetta, F. Serra, G. Cau, P. Puddu, Comparison between experimental and numerical results of a packed-bed thermal energy storage system in continuous operation, Energy Procedia. 148 (2018) 234–241. https://doi.org/10.1016/j.egypro.2018.08.073.

[37] S. Loem, T. Deethayat, A. Asanakham, T. Kiatsiriroat, Thermal characteristics on melting/solidification of low temperature PCM balls packed bed with air charging/discharging, Case Stud. Therm. Eng. 14 (2019) 100431. https://doi.org/10.1016/J.CSITE.2019.100431.

[38] G. Nellis, S. Klein, Heat Transfer, Cambridge University Press, 2008.

[39] F. Incropera, D. DeWitt, T. Bergman, A. Lavine, Fundamentals of Heat and Mass Transfer, 7th Editio, John Wiley and Sons, 2011.

[40] K. Hoopes, D. Sánchez, F. Crespi, A New Method for Modelling Off-Design Performance of sCO2 Heat Exchangers Without Specifying Detailed Geometry, 5th Int. Symp. - Supercrit. CO2 Power Cycles. 1 (2016) 1–14.

[41] A. Sciacovelli, Y. Li, H. Chen, Y. Wu, J. Wang, S. Garvey, Y. Ding, Dynamic simulation of Adiabatic Compressed Air Energy Storage (A-CAES) plant with integrated thermal storage – Link between components performance and plant performance, Appl. Energy. 185 (2017) 16–28. https://doi.org/10.1016/j.apenergy.2016.10.058.

[42] L.S. Dixon, C.A. Hall, Fluid Mechanics and Thermodynamics of Turbomachinery, Elsevier Science, 2010.

[43] N. Zhang, R. Cai, Analytical solutions and typical characteristics of part-load performances of single shaft gas turbine and its cogeneration, Energy Convers. Manag. 43 (2002) 1323–1337. https://doi.org/10.1016/S0196-8904(02)00018-3.

[44] J.J. Dyreby, Modeling the Supercritical Carbon Dioxide Brayton Cycle with Recompression, (2014).

[45] D.H. Cooke, On Prediction of Off-Design Multistage Turbine Pressures by Stodola's Ellipse, J. Eng. Gas Turbines Power. 107 (1985) 596–606.

[46] M.D. Carlson, B.M. Middleton, C.K. Ho, Cycles Using Component Cost Models Baselined With Vendor Data, Proc. ASME 2017 Power Energy Conf. (2017) 1–7.

[47] S. Georgiou, N. Shah, C.N. Markides, A thermo-economic analysis and comparison of pumped-thermal and liquid-air electricity storage systems, Appl. Energy. in press (2018) 1119–1133. https://doi.org/10.1016/j.apenergy.2018.04.128.

[48] A. Smallbone, V. Jülch, R. Wardle, A.P. Roskilly, Levelised Cost of Storage for Pumped Heat Energy Storage in comparison with other energy storage technologies, Energy Convers. Manag. 152 (2017) 221–228. https://doi.org/10.1016/j.enconman.2017.09.047.

[49] D. Carrington, Climate emission killer: construction begins on world's biggest liquid air battery, Guard. (2020). https://www.theguardian.com/environment/2020/jun/18/worlds-biggest-liquid-air-battery-starts-construction-in-uk (accessed June 18, 2020).

[50] Lazard, Lazard's Levelized Cost of Storage Analysis - Version 4.0, (2018).

[51] V. Jülch, Comparison of electricity storage options using levelized cost of storage (LCOS) method, Appl. Energy. 183 (2016) 1594–1606. https://doi.org/10.1016/j.apenergy.2016.08.165.

[52] O. Schmidt, A. Hawkes, A. Gambhir, I. Staffell, The future cost of electrical energy storage based on experience rates, Nat. Energy. 2 (2017) 1–8. https://doi.org/10.1038/nenergy.2017.110.

[53] M. Hennen, P. Voll, A. Bardow, An Adaptive Normal Constraint Method for Bi-Objective

Optimal Synthesis of Energy Systems, in: J.J. Klemeš, P.S. Varbanov, P.Y.B.T.-C.A.C.E. Liew (Eds.), 24 Eur. Symp. Comput. Aided Process Eng., Elsevier, 2014: pp. 1279–1284. https://doi.org/https://doi.org/10.1016/B978-0-444-63455-9.50048-9.

[54] N. Gunantara, A review of multi-objective optimization: Methods and its applications, Cogent Eng. 5 (2018) 1–16. https://doi.org/10.1080/23311916.2018.1502242.

[55] M.T.M. Emmerich, A.H. Deutz, A tutorial on multiobjective optimization: fundamentals and evolutionary methods, Nat. Comput. 17 (2018) 585–609. https://doi.org/10.1007/s11047-018-9685-y.

[56] J.D. McTigue, A.J. White, C.N. Markides, Parametric studies and optimisation of pumped thermal electricity storage, Appl. Energy. 137 (2015). https://doi.org/10.1016/j.apenergy.2014.08.039.

[57] G. Campos Ciro, F. Dugardin, F. Yalaoui, R. Kelly, A NSGA-II and NSGA-III comparison for solving an open shop scheduling problem with resource constraints, IFAC-PapersOnLine. 49 (2016) 1272–1277. https://doi.org/10.1016/j.ifacol.2016.07.690.

[58] S. Cheng, H. Lu, X. Lei, Y. Shi, A quarter century of particle swarm optimization, Complex Intell. Syst. 4 (2018) 227–239. https://doi.org/10.1007/s40747-018-0071-2.

[59] C.A. Coello Coello, G. Toscano Pulido, M. Salazar Lechuga, Handling multiple objectives with particle swarm optimization, IEEE Trans. Evol. Comput. 8 (2004) 282–290. https://doi.org/10.4018/ijmfmp.2015010104.

[60] A. Bonk, M. Braun, V.A. Sötz, T. Bauer, Solar Salt – Pushing an old material for energy storage to a new limit, Appl. Energy. 262 (2020) 114535. https://doi.org/10.1016/j.apenergy.2020.114535.

[61] Western Electricity Coordinating Council (WECC)., TEPPC Study Report – 2024 PC1 Common Case and Release Notes for WECC 2024 Common Case Version 1.1, 2015.

[62] G. Brinkman, J. Jorgenson, A. Ehlen, J. Caldwell, Low Carbon Grid Study: Analysis of a 50% Emission Reduction in California, NREL Tech. Rep. - NREL/TP-6A20-64884. (2016).

[63] B.A. Frew, G. Brinkman, P. Denholm, V. Narwade, G. Stephen, A. Bloom, J. Lau, Impact of operating reserve rules on electricity prices with high penetrations of wind, Under Rev. (n.d.).

[64] J. Martinek, J. Jorgenson, M. Mehos, P. Denholm, A comparison of price-taker and production cost models for determining system value, revenue and scheduling of concentrating solar power plants., Appl. Energy. 231 (2018) 854–865.

[65] J. Jorgenson, M.O. Connell, P. Denholm, J. Martinek, M. Mehos, A Guide to Implementing Concentrating Solar Power in Production Cost Models, 2018.

[66] NREL, System Advisor Model (SAM), (2017). https://sam.nrel.gov/.

[67] N. Kumar, P. Besuner, S. Lefton, D. Agan, D. Hilleman, Power Plant Cycling Costs, NREL Subcontract Rep. NREL/SR-5500-55433. 27 (1978) 245–248.